Integrated regional hydrogeophysical conceptualisation of the Musgrave Province, South Australia

Tim Munday, Andrew Taylor, Matthias Raiber, Camilla Soerensen, Luk Peeters, Carmen Krapf, Tao Cui, Kevin Cahill, Brady Flinchum, Nick Smolanko, Jorge Martinez, Tania Ibrahimi, Mat Gilfedder

Goyder Institute for Water Research
Technical Report Series No. 20/04

www.goyderinstitute.org

Goyder Institute for Water Research Technical Report Series ISSN: 1839-2725

The Goyder Institute for Water Research is a partnership between the South Australian Government through the Department for Environment and Water, CSIRO, Flinders University, the University of Adelaide, and the University of South Australia. The Institute enhances the South Australian Government's capacity to develop and deliver science-based policy solutions in water management. It brings together the best scientists and researchers across Australia to provide expert and independent scientific advice to inform good government water policy and identify future threats and opportunities to water security.

Enquires should be addressed to: Goyder Institute for Water Research
Level 4, Rundle Mall Plaza, 50 Rundle Mall,
Adelaide, SA 5000
tel: 08 8313 5020
e-mail: enquiries@goyderinstitute.org

Citation

Munday, T., Taylor, A., Raiber, M., Soerensen, C., Peeters, L., Krapf, C., Cui, T., Cahill, K., Flinchum, B., Smolanko, N., Martinez, J., Ibrahimi, T. and Gilfedder, M. (2020) *Integrated regional hydrogeophysical conceptualisation of the Musgrave Province, South Australia.* Goyder Institute for Water Research Technical Report Series No. 20/04.

Disclaimer

The CSIRO, as a project partner, advises that the information contained in this publication comprises general statements based on scientific research and does not warrant or represent the completeness of any information or material in this publication. The project partners do not warrant or make any representation regarding the use, or results of the use, of the information contained herein about to its correctness, accuracy, reliability, currency or otherwise and expressly disclaim all liability or responsibility to any person using the information or advice. Information contained in this document is, to the knowledge of the project partners, correct at the time of writing.

Contents

Figures

Tables

Executive summary

Water is a critical resource in ensuring a healthy population and maintaining a vibrant agricultural sector but it is also an integral raw material for mineral exploration, mining and processing. The identification, characterisation and access to suitable water resources for exploration and processing is essential for the minerals and energy resources sector and sits at the heart of many of the relationships between the minerals industry and communities. The Department for Environment and Water Finding Long-term Outback Water Solutions (FLOWS) Initiative seeks to address an essential step on the critical path to delivering State Economic Priority 1: Unlocking the full potential of South Australia's resources, energy and renewable assets. This G-Flows Stage-3 project has supported the South Australian Government's FLOWS initiative to locate, define and quantify groundwater resources in key areas of the state including priority mineral prospective zones as identified in the South Australian Regional Mining and Infrastructure Plan 2014.

The G-Flows Stage-3 project has delivered new data and information into the location and extent of groundwater resources in the Musgrave Province. It aims to reduce the risks faced when developing projects allowing for more informed decision-making and robust feasibility studies by potential developers and investors. The work program was driven by advances made though previous Goyder Institute research and integrates with the South Australian Government's Plan for Accelerating Exploration (PACE) initiative, and the ongoing research and collaborative efforts of the Geological Survey of South Australia (GSSA), particularly in the utilisation of regional geophysical surveys for exploration under deep cover, data integration and 3D and 4D geological modelling.

This report summarises the acquisition and interpretation of new geophysical data across the Musgrave Province, which has been combined with the collation and review of existing groundwater salinity, groundwater yield, groundwater level and groundwater environmental tracer and chemistry data to improve current estimates of interpolated groundwater levels and groundwater recharge and flow across the province. The integration of these datasets underpinned:

1) the development of a revised hydrogeological framework of the Musgrave Province, and
2) a refined conceptual model of groundwater recharge and flow.

Hydrogeological framework

A revised hydrogeological framework map is a key output from the G-Flows Stage-3 Project. The processed airborne electromagnetic (AEM) survey data reveals the palaeovalley network in detail (Figure 1-1). The figure shows the deepest part of the palaeovalley network (thalweg; indicated as black lines) which provide a key target for water resource exploration.

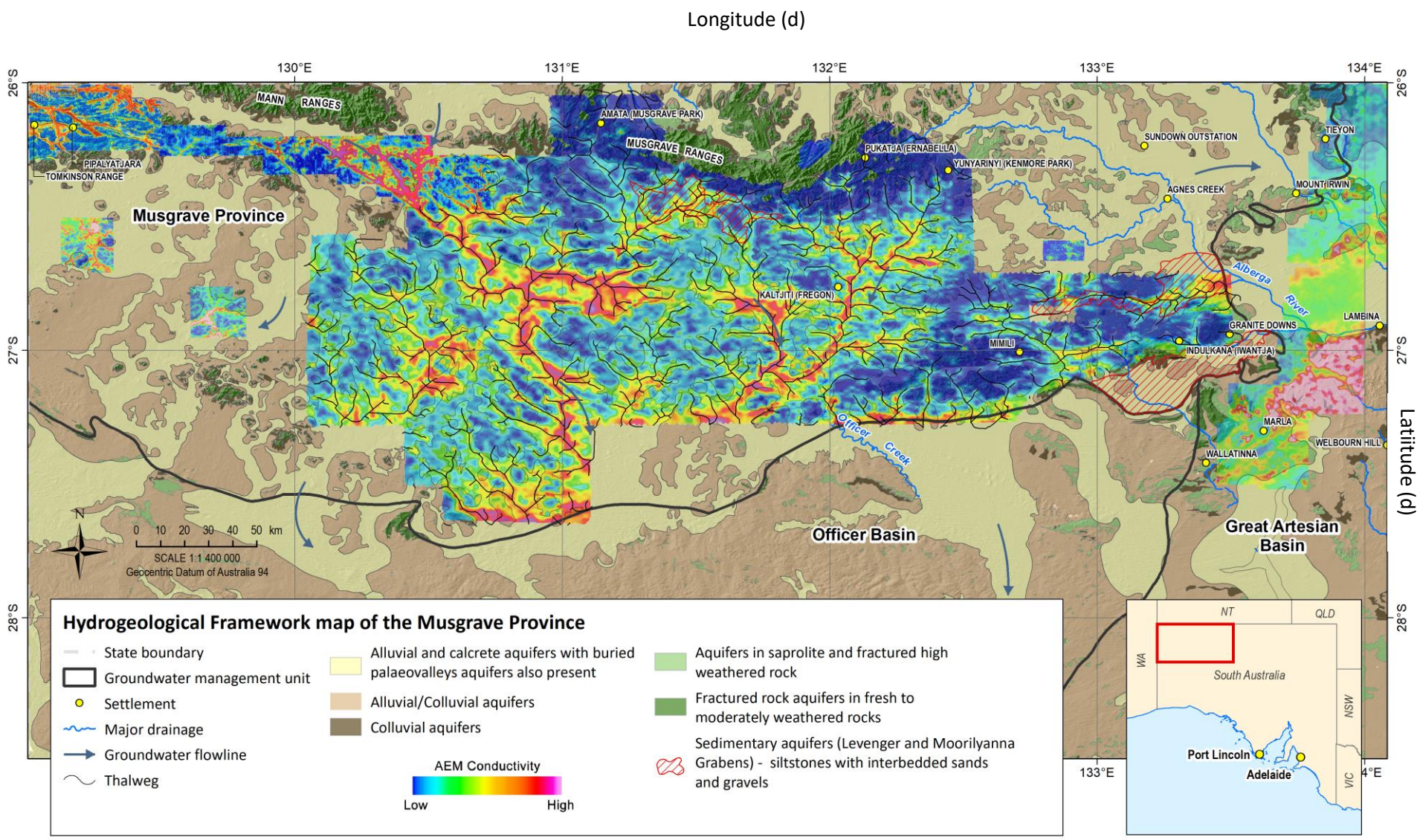

Figure 1-1. Hydrogeological framework map of the Musgrave Province.

Conceptual model of groundwater recharge and flow

The combined geophysics and groundwater hydrology work in G-Flows Stage-3 builds on the earlier work outlined above, and confirms, in broad terms, some of the previous conceptual understanding of aquifers in the arid Musgrave Province. The conceptualisation of both the geology and hydrogeology have been previously presented in conceptual schematics by Munday et al. (2013) and more recently by Gogoll (2016). In this study we have also considered findings from some localised work by Parsekian et al. (2014), and more recently by Munday et al. (2016), Krapf et al. (2019), and Costar et al. (2019), and then coupled them with findings in this study to subsequently adapt and refine conceptual schematics from Munday et al. (2013) and Gogoll (2016) as shown in Figure 1-2.

The key hydrogeological processes include:

- Highly episodic runoff from the outcropping Musgrave, Mann and Tomkinson ranges;
- Highly episodic groundwater recharge predominantly at the ranges, where bedrock aquifers outcrop, but episodic recharge fluxes are also possible through ephemeral drainage lines traversing surficial alluvium and colluvium away from the ranges;
- Alluvial/colluvial and bedrock aquifers are hydraulically interconnected via localised bedrock discharge recharging the alluvium/colluvium surrounding the ranges and via throughflow from the alluvium/colluvium recharging underlying palaeovalley and compartmentialised bedrock aquifers;
- Intermediate to regional groundwater flow is 'generally' from north to south in both alluvial/colluvial and palaeovalley aquifers;
- Groundwater flow is controlled by highly episodic and low recharge fluxes occurring predominantly around the Musgrave and Mann ranges in the north of the province with flow proceeding and diminishing south towards the Officer Basin given very low hydraulic gradients;
- Intermediate to regional groundwater flow in alluvial/colluvial and palaeovally aquifers is also controlled by bedrock topography where small outcrops and shallow subcrops of crystalline basement sporadically interupt and create more tortuous flow paths from north to south;
- Structure compartmentalises the alluvial/colluvial fill in the palaeovalleys which may also influence the groundwater flow paths;
- The flow paths may also be interrupted by netectonic activity resulting from the reactivation of basement structures and the formation of hydraulic barriers in the overlying sediment package;
- Groundwater discharge in alluvial/colluvial aquifers occurs via a combination of evapotransitaion and throughflow to both underlying palaeovally and bedrock aquifers, as well as southerly flow towards the Officer Basin;
- Groundwater discharge in bedrock aquifers occurs as evapotranspiration in aquifer outcrops and throughflow to adjacent alluvial/colluvial aquifers at the foot of the ranges;
- There is no hydraulic or hydrogeochemical evidence to support a hypothesis for intermediate to regional groundwater flow in bedrock aquifers in such a data sparse region. Evidence from airborne geophysics, lithological and stratigraphic logs, geological modelling, regional magnetics and high variability in both bore yields and groundwater salinity suggests the bedrock aquifers are highly compartmentalised but hydraulically interconnected at locations where they are overlain with palaeovalley and alluvial/colluvial aquifers.

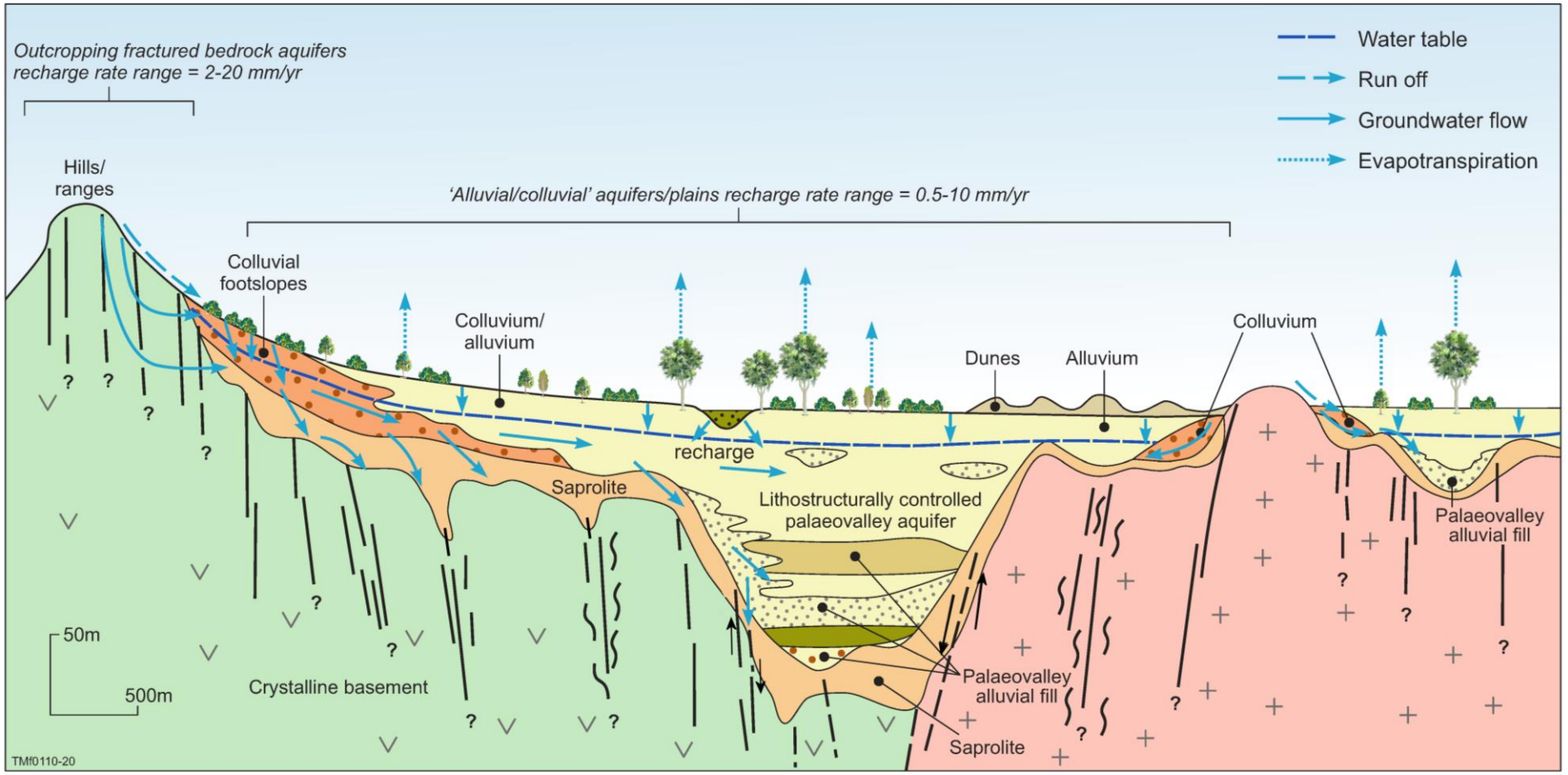

Figure 1-2. Schematic hydrogeological conceptual model showing a typical palaeovalley drainage system in the Musgraves. Figure adapted from Munday et al. (2013, 2020) and Gogoll (2016).

Acknowledgments

This study was carried out as part of the G-Flows Stage-3 Project. This project was funded jointly by the Goyder Institute for Water Research, and its partner organisations, including: Department for Environment and Water (DEW), Commonwealth Scientific and Industrial Research Organisation (CSIRO), Flinders University, South Australia (FUSA). The South Australian Department of Energy and Mines (DEM) is also acknowledged for their support in the co-funding of the regional AEM survey that formed the foundation for the work reported here and for supporting its acquisition through Geoscience Australia. We specifically acknowledge the work and support of Miles Davis, Steve Hill and Rian Dutch in helping make this happen. Linked to the project was work undertaken by Mark Keppel, Adrian Costar and Kent Inverarity of DEW, and Carmen Krapf of DEM who planned and initiated and interpreted the drilling and borehole geophysics that was instrumental in helping validate the airborne EM component of the work. Mats Gulbrandsen from iGIS provided invaluable support in the application of the Smart Interpretation method employed on SkyTEM data in the eastern Musgrave Province.

We acknowledge the support of CSIRO's Deep Earth Imaging Future Science Platform in undertaking this research.

We acknowledge the traditional owners of the Anangu Pitjantjatjara Yankunytjatjara (APY) Lands, the Pitjantjatjara, Yankunytjatjara and Ngaanyatjarra people. We would also like to thank the APY General Manager and the entire APY Executive Board who were supportive of the G-Flows Stage-3 project.

We thank the Goyder Institute Research Advisory Committee members: Kane Aldridge (Goyder Institute), Justin Brookes (The University of Adelaide), Jennie Fluin (DEW), Jim Cox (SARDI), Dirk Mallants (CSIRO), Neil Power (DEW), Darryl Day (ICE WaRM), Craig Simmons (Flinders University), Jacqueline Frizenschaf (SA Water), and Peter Teasdale (UniSA).

We are extremely grateful for the support of a wide range of people, organisations, companies, and departments who all provided assistance to help undertake and complete this project.

Thank you also to the broader project team for their hard work in undertaking, presenting, and writing up the many aspects of work completed as part of G-Flows Stage-3.

1 Introduction and overview

1.1 Introduction

Groundwater resources in remote arid areas of South Australia such as the Musgrave Province are the only available water resources to support the livelihood of communities as well as economic development. However, the arid climate of the province combined with a geological setting dominated by crystalline basement at shallow depths presents a hydrogeological environment where both groundwater recharge and storage are low. For this reason, over the past two decades several important geological and hydrogeological studies varying from desktop analyses, drilling investigations, geophysical surveys and groundwater quality and resource assessments have taken place. These studies, while varying in nature, have all contributed to evaluating the opportunities and risks for future groundwater resource development in either isolated parts of the province or across extensive areas. However, given the remoteness, groundwater resources in large parts of the province remain poorly mapped and characterised, while demand for community water supplies is ongoing.

1.2 Previous studies

Some of the earliest work was conducted by Fitzgerald et al. (2000) and focussed primarily on the quality of groundwater in aquifers where concerns about faecal contamination and poor-quality groundwater being supplied to Indigenous communities had been raised. Subsequent work by Dodds et al. (2001) focussed more on quantifying groundwater supplies to better evaluate the future suitability and sustainability of existing community groundwater supplies at nine communities. The findings by Dodds et al. (2001) highlighted the immediate need for establishing a regional water management plan across the province. The water plan was first initiated a year later in 2002 (APYWMP, 2002) which also included the establishment of the Anangu Pitjantjatjara Yankunytjatjara Water Management Council (APYWMC).

Following work by Dodds et al. (2001), Australian Groundwater Technologies (AGT) was commissioned by the state water utility (SA Water) to undertake two groundwater supply sustainability assessments at key Indigenous communities initially in 2003 (AGT, 2003) and then a broader assessment in 2008 (AGT, 2008). Both assessments were desktop analyses combining groundwater level monitoring, metered groundwater use and climate data to assess the sustainability of individual community production bores. The key findings from AGT (2008) were that some of the community groundwater production bores that supported key northern communities (Amata and Pukatja) were under stress and alternative groundwater supplies needed to be sourced for use in the future.

The sustainability assessments by AGT led to further extensive desktop studies across the entire Musgrave Province, as well as geophysical surveys, drilling and multiple groundwater resource assessments at the regional scale to improve the understanding of groundwater resources across the entire province. The Government of South Australia in 2009 established its 'Water for Good' plan which included the monitoring and management of non-prescribed groundwater resources to ensure their future sustainable use. Under this plan Watt and Berens (2011) produced the most comprehensive (at that time) desktop evaluation of groundwater resources in the Musgrave Province. They concluded that the key knowledge gaps included estimates of groundwater storage, evaluations of potential groundwater yield rates, estimates of volumes of groundwater for abstraction and an understanding of the nature and volumes of groundwater recharge.

The evaluation by Watt and Berens (2011) led to the initiation of some key field studies by Leaney et al. (2013), Ley-Cooper and Munday (2013), Munday et al. (2013) and Kretschmer and Wohling (2014) that aimed to improve the understanding of important groundwater processes. The study by Ley-Cooper and Munday (2013) and Munday et al. (2013) provided much improved hydrogeological mapping across the province by collating and reinterpreting existing airborne geophysics and using this to develop an improved hydrogeological map of the province. The studies by Leaney et al. (2013) and Kretschmer and Wohling (2014) involved targeted groundwater sampling for environmental tracers and chemistry which identified the

presence of a regional-scale groundwater flow system, as well as mapping and quantifying groundwater recharge and flow. In addition, two honours studies were undertaken into the sustainability (Craven, 2012), and the hydrogeochemistry (Custance, 2012) of regolith-hosted aquifers in the region.

Since these regional scale studies, the search for alternative and sustainable community water supplies has continued with the new regional-scale hydrogeological mapping by Munday et al. (2013) underpinning further targeted local-scale work. In 2014, Parsekian et al. (2014) successfully validated the improved hydrogeological mapping by Munday et al. (2013) to identify and better map a local-scale aquifer for one of the indigenous communities using near-surface geophysics. In 2015, Howles et al. (2017) successfully used the airborne geophysics from additional interpretations of the regional aeromagnetic data undertaken by Munday to undertake targeted drilling of the fractured and weathered bedrock aquifers which resulted in 18 new production wells being drilled and installed at seven Indigenous communities. The most recent work which from a hydrogeology perspective will be summarised in this report has involved the acquisition of a new large-scale airborne electromagnetic (AEM) survey (Soerensen et al. 2018), as well as some targeted drilling in part of a key palaeovalley (Costar et al., 2019). The AEM survey summarised in Soerensen et al. (2018) now fills the large gaps between existing AEM surveys which when combined cover almost the entire Musgrave Province. In 2018, drilling of the eastern side of the Lindsay East Palaeovalley (Costar et al., 2019) was undertaken to characterise the depth, nature and hydrological connectivity of aquifers within palaeovalley fill.

1.3 Overview and aim

The aim of this report is to summarise the acquisition and interpretation of new geophysical data (airborne, near-surface and down-hole) that when combined with existing data assists in mapping and conceptualising the hydrogeology across almost the entire Musgrave Province. In addition, the interpretation of this new geophysical data has been combined with the collation and review of existing groundwater salinity, groundwater yield, groundwater level and groundwater environmental tracer and chemistry data to improve current estimates of interpolated groundwater levels and groundwater recharge and flow across the province. The integration of these datasets underpins the development of:

i. a revised hydrogeological map of the province,
ii. a refined conceptual model of groundwater recharge and flow, and
iii. a revised recharge component of the water balance for key aquifers across the province.

1.4 Palaeovalleys vs. palaeochannels

The terms valley and channel fill deposits are a commonly referenced feature of the Australian landscape and of considerable significance, as they are host to both groundwater and mineral resources (Clarke, 2009). To-date the nomenclature used in reference to these systems has been has both inconsistent and potentially confusing. For example, in the South Australian context, the terms 'palaeovalley' and 'palaeochannel' have been employed interchangeably by, for example, Tewkesbury and Dodds (1997), Hou et al. (2003a, b), and Hou et al. (2007) for features in the Musgrave Province and Gawler Craton. For the purposes of clarity, we define the nomenclature used in this report. It is important to note that we are primarily concerned with using airborne geophysical methods, particularly airborne electromagnetic methods to map the extent and thickness of palaeovalley fill sequences, and to describe the varying petrophysical properties (reflected as varying electrical conductivities) of the materials (sediments and groundwater) that make up this fill. Consequently, we have chosen to ascribe to the nomenclature of Clarke (2009) when discussing how this sedimentary fill evolved and what it is like in the contemporary landscape.

Specifically, we employ the terms 'palaeoriver' to describe the ancient fluvial system responsible for developing some of the palaeovalleys; 'palaeodrainage' for the network of palaeorivers that may have been present in the ancient landscape; 'palaeochannel' for the channel formed by palaeorivers; 'palaeochannel deposits' for the sediments that infill the Palaeochannels; and 'palaeovalleys' for valleys incised by these 'palaeorivers' (cf. Clarke 2009). Our use of the term "palaeovalley" is consistent with the nomenclature used by Magee (2009), Lewis et al. (2010), Watt and Berens (2011) and the more recent publications which address aspects relating to the Musgrave Province palaeovalleys by Krapf et al. (2019), and Costar et al. (2019).

2 Study area

2.1 Geography

The South Australian Musgrave Province forms part of a crystalline basement terrain that extends across the common borders of South Australian, Western Australian and Northern Territory. The topography and drainage of the Musgrave region is shown in Figure 2-1. The northern part of the region is occupied by the rugged hilly terrain of the Mann and the Musgrave ranges with Mt Woodroffe reaching an elevation of 1435 m AHD (Australian Height Datum). The Birksgate and the Everard ranges occur to the south. The topographical elevations decrease to around 350–400 m AHD towards the south and the southeast of the area where wide calcrete plains occur covered by aeolian deposits. The Great Victoria Desert to the south of the northern ranges is covered by sand plains and dune fields (Watt and Berens, 2011).

2.2 Climate

Climate for the study area is semi-arid to arid with a hot, dry desert climate, short cool to cold winters and low, unreliable rainfall (Watt and Berens, 2011). The mean temperature ranges from 32°C to 36°C in the summer and drops to a mean of around 20°C in winter. Rainfall patterns are spatially variable, with average annual rainfall ranges from around 150–225 mm, although rainfall is unpredictable, and averages can be misleading. Rainfall occurrence and intensity is episodic. Average annual evaporation exceeds 3500 mm, resulting in the rapid evaporation of surface water runoff. Perennial surface water and connected drainage systems are absent.

2.3 Geology

The geology of the Musgrave Province is complex, and for the area of interest to the G-Flows study it has been summarised by Pawley and Krapf (2016), a precis of which is reproduced here. The Province comprises a region of crystalline basement consisting mainly of the amphibolite and granulite facies gneisses intruded by mafic – ultramafic dykes and granitoids, and swarms of dolerite dykes. The oldest exposed rocks belong to the undifferentiated Birksgate Complex (Figure 2-2) and consist of amphibolite to granulite facies, felsic and minor mafic gneisses with igneous intrusive, volcanic, volcaniclastic and, less commonly, sedimentary precursors (Edgoose et al., 2004; Major and Conor, 1993; Wade et al., 2006; Wade et al., 2008). A metasedimentary cover sequence is interpreted to unconformably overlie the protoliths of the Birksgate Complex in the eastern Musgrave Province (Wade et al., 2008). These metasedimentary rocks are interlayered with felsic, mafic, and calc-silicate gneisses, and have been interpreted as a metavolcanic sequence (Conor, 2004). The extent of this package is unknown. During the province-wide Musgravian Orogeny (Edgoose et al., 2004; Major and Conor, 1993; Smithies et al.,2010) the rocks of the Musgrave province were deformed and metamorphosed at amphibolite to granulite facies Large volumes of predominantly felsic magma, which have been grouped into the Pitjantjatjara Supersuite were intruded during and immediately following the Musgravian Orogeny (Edgoose et al., 2004; Howard et al., 2011; Smithies et al., 2011).

The Musgravian Orogeny was followed by the Giles Event and igneous rocks of this event includes the variably deformed, mafic-ultramafic layered intrusions of the Giles Complex, bimodal volcanic rocks and associated rift sediments of the Bentley Supergroup, the Tjauwata Group, the Alcurra Dolerite dyke suite, and minor granitic intrusions and felsic dykes (Close et al., 2003; Edgoose et al., 2004; Evins et al., 2010; Glikson et al., 1995; Glikson et al., 1996; Howard et al., 2011; Woodhouse and Gum, 2003). Following the Giles Event, the Musgrave Province was intruded by a number of dolerite suites. The 570-530 Ma Petermann Orogeny was a major intracratonic event that resulted in the reactivation of several crustal scale, east-west trending shears, faults and thrusts and the development of widespread mylonitic shear fabrics, that characterise the Province and are clearly defined in regional aeromagnetic data (Figure 2-3).

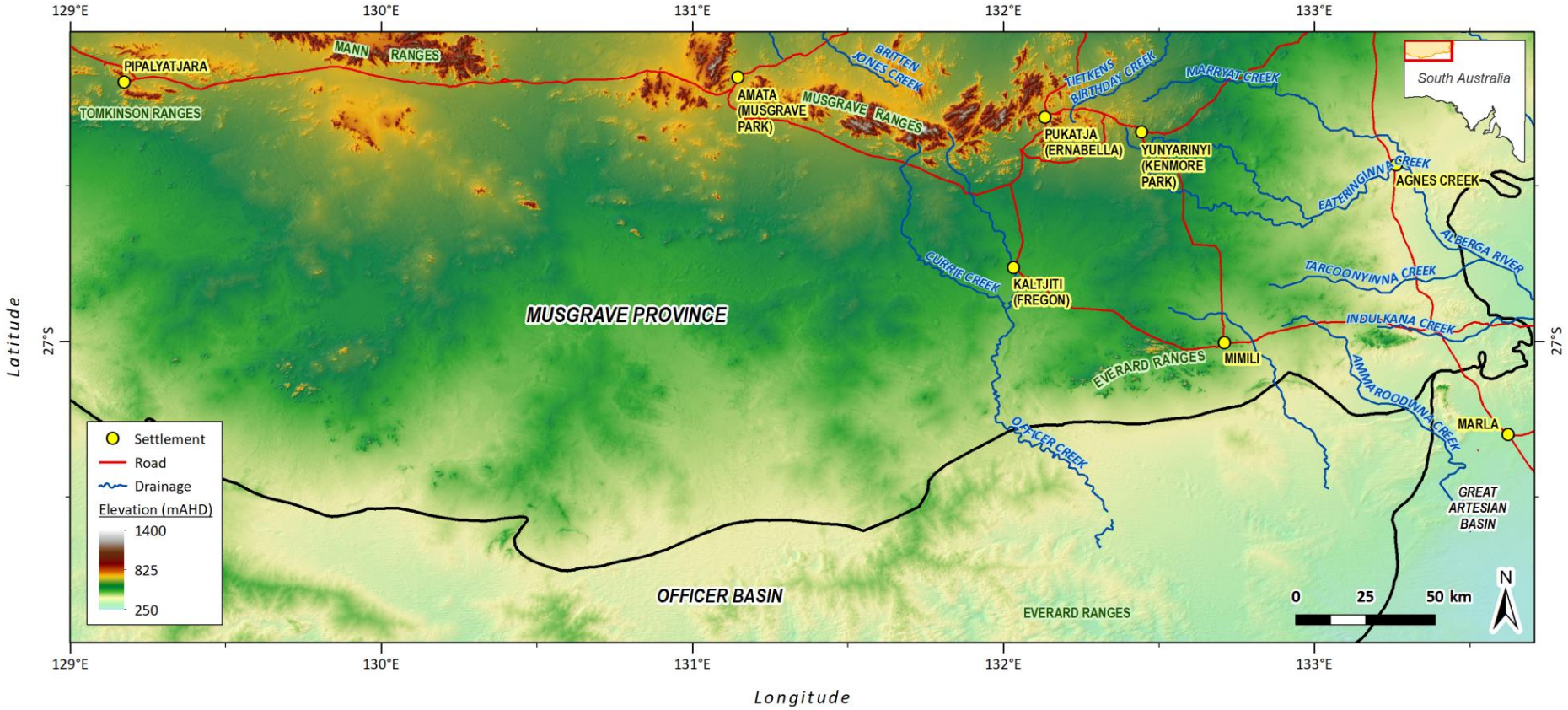

Figure 2-1. Musgrave Province study area location.

Coeval with the Petermann Orogeny was the development of the Levenger and Moorliyanna grabens, which are strike-slip basins that were infilled with clastic sediments derived from the locally exposed Musgrave Province basement (Coats, 1962).

Sediments of the intracratonic Officer Basin have been deposited during the Neoproterozoic to Late Devonian and crop out in a linear belt south of the Musgrave Block, marking the northern limit of the basin (Figure 2-3). The Musgrave Province has undergone at least one phase of intensive deep weathering and erosion prior to the deposition of clastic sediments of the Mesozoic Eromanga Basin (part of the Great Artesian Basin) along its eastern margin (Cotton et al., 2006; Krieg and Rogers, 1995). Sediments of the Eromanga Basin, which is part of the Great Artesian Basin, occur on the south-east margin of the Anangu Pitjantjatjara Yankunytjatjara (APY) Lands. They were deposited between ~150–100 Ma and include important aquifers.

Intense chemical weathering of the Mesozoic sedimentary rocks as well as basement rocks occurred at several periods during the late Cretaceous and Tertiary and resulted in deep weathering profiles that can reach up to 90 m below the present-day land surface. The typically composite weathering profiles are characterised by kaolinisation and mottled or varicoloured, pallid, ferruginous or siliceous zones. Multiple phases of post-Mesozoic, dominantly siliceous and ferruginous induration, led to the formation of widespread silcrete and ferruginous duricrust.

During the Neogene, rivers, that had their headwaters in the Musgrave and Mann Ranges and drained southwards into the Eucla Basin, incised up to 70 m into the underlying weathered rocks. These palaeodrainage systems formed wide, deep valleys that were subsequently filled with clastic sediments during a warm and wet subtropical to tropical climate. This infill, which included the Lindsay and Serpentine palaeodrainage system as well as the Hamilton Basin (Lewis et al., 2010; Magee, 2009; Rogers, 1995) was extensive. The lacustrine Mangatitja Formation, which crops out extensively throughout the Musgrave Province, is a remnant of this event (Rogers, 1995). These comprise clastic sediments mostly composed of clay, sandy clay and minor lenses of coarse sand and gravel and are commonly associated with near surface calcrete deposits. In the Quaternary, with the onset of aridity, episodes of alluvial and aeolian activity, resulted in today's landscape with the formation of an extensive cover (Figure 2 4) of alluvial plains, sand plains and aeolian dunes and dunefields (Figure 2 5). The modern sand dunes and sand spreads of the Great Victoria Desert mantle the lowlands and the southern region of the Province.

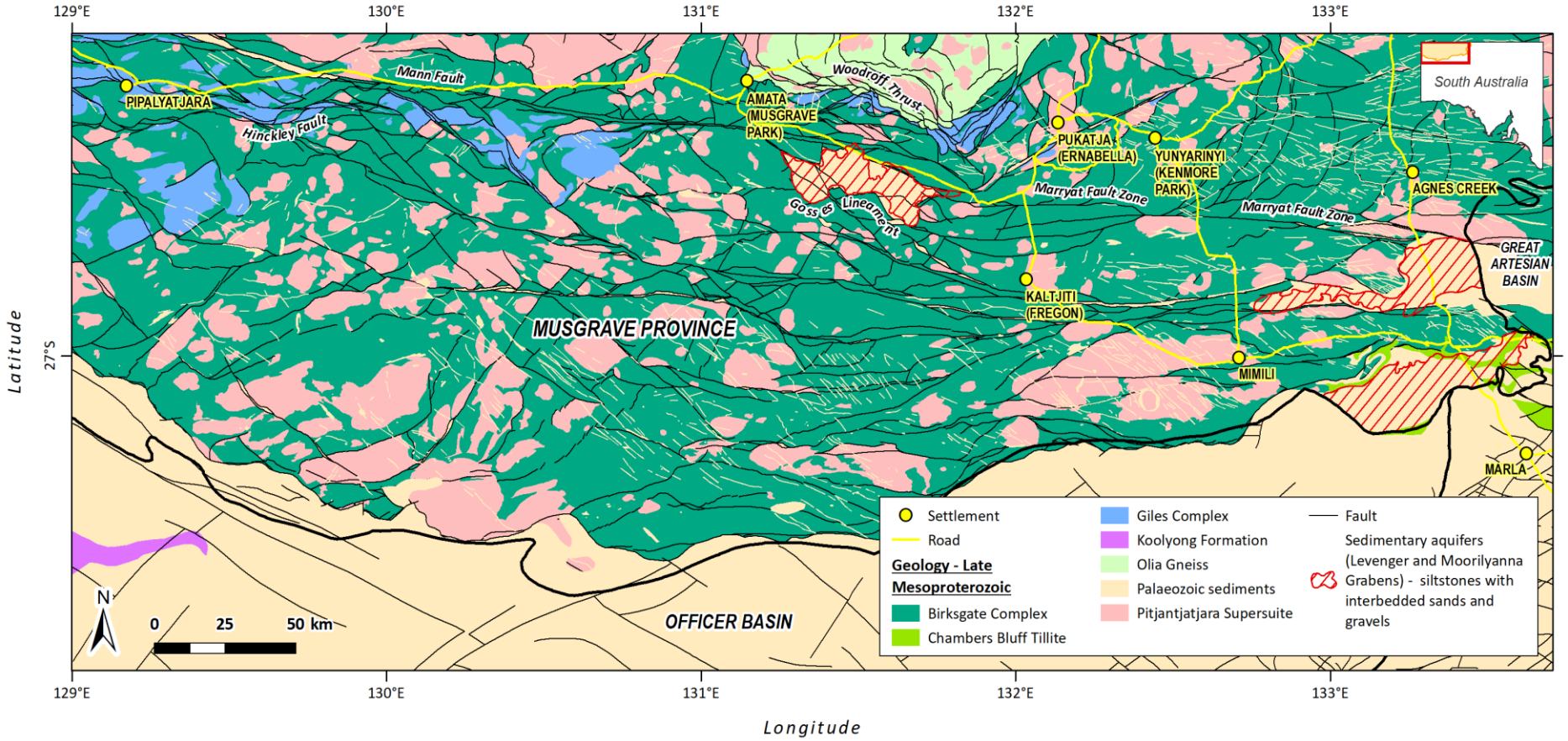

Figure 2-2. Basement geology of the Musgrave Province in South Australia.

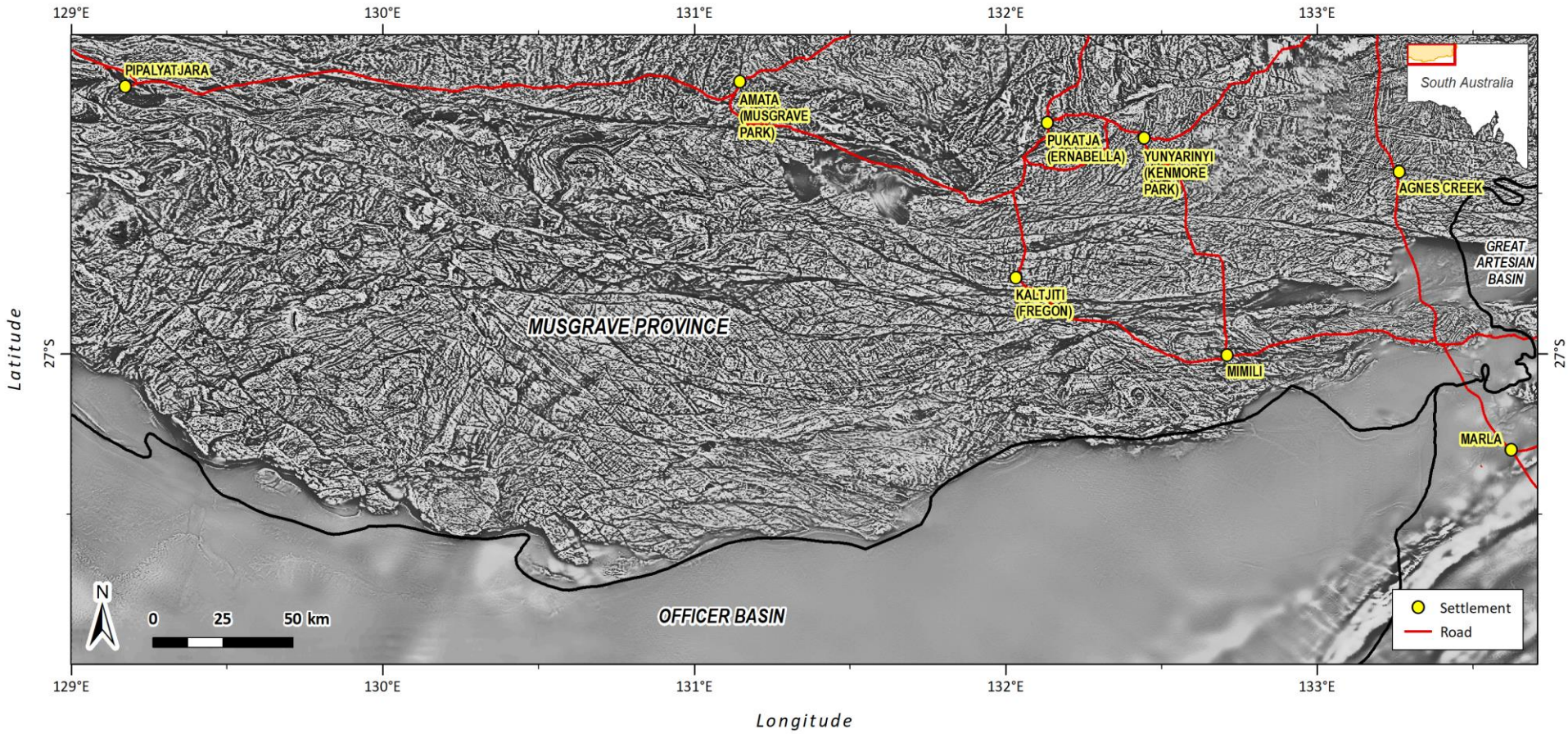

Figure 2-3. Regional airborne magnetics – first vertical derivative (1st VD), showing extensive network of east-west oriented shears and faults in the Musgrave Province.

2.4 Hydrogeology

While basement outcrops as isolated hills and ranges, much of it is covered by regolith. Surface flow across the area is limited to intense rainfall events and primarily confined to outcropping rock and to a limited number of channels that drain across adjacent flat country (Tewkesbury and Dodds, 1997). Surface flow tends to occur for a short period and over small stream sections based on the location and intensity of the rainfall event. Groundwater is present in the weathered and fractured sections of the basement, in buried palaeovalleys filled with sands, silts and clays, and in calcretes and surficial sediments consisting of alluvial, fluvial and aeolian deposits (Watt and Berens, 2011). Groundwater recharge is variable and linked to episodic rainfall events. Work by Cresswell et al. (2002) indicated that immediately adjacent to the ranges it is relatively high (~30 mm/yr), and lower elsewhere (1-10 mm/yr). Updated details on the rates of groundwater recharge are provided in later sections of this report. Groundwater salinity throughout the region is highly variable, ranging from 100 mg/L to >20,000 mg/L with higher salinities observed in sediments of the palaeovalleys.

The pre-Pliocene palaeovalley system, incised into Musgrave Province, is known to be present from limited exploratory drilling, and has been postulated to contain a significant groundwater resource (Dodds and Sampson, 2000). However, as mentioned earlier, their geometry and extent remain largely hidden from view by a valley fill of Pliocene to Pleistocene sediments and overlying Quaternary sand dunes of the Great Victoria Desert (Lewis et al., 2010). Their evolution is postulated to be similar to that described for the palaeodrainage systems located on the margins of the Gawler Craton (see Hou et al., 2003a).

Lewis et al. (2010) considered the palaeovalleys to be the best targets for groundwater supply, however they suggested their internal lithological heterogeneity could affect groundwater flow and hence make them a less prospective groundwater target.

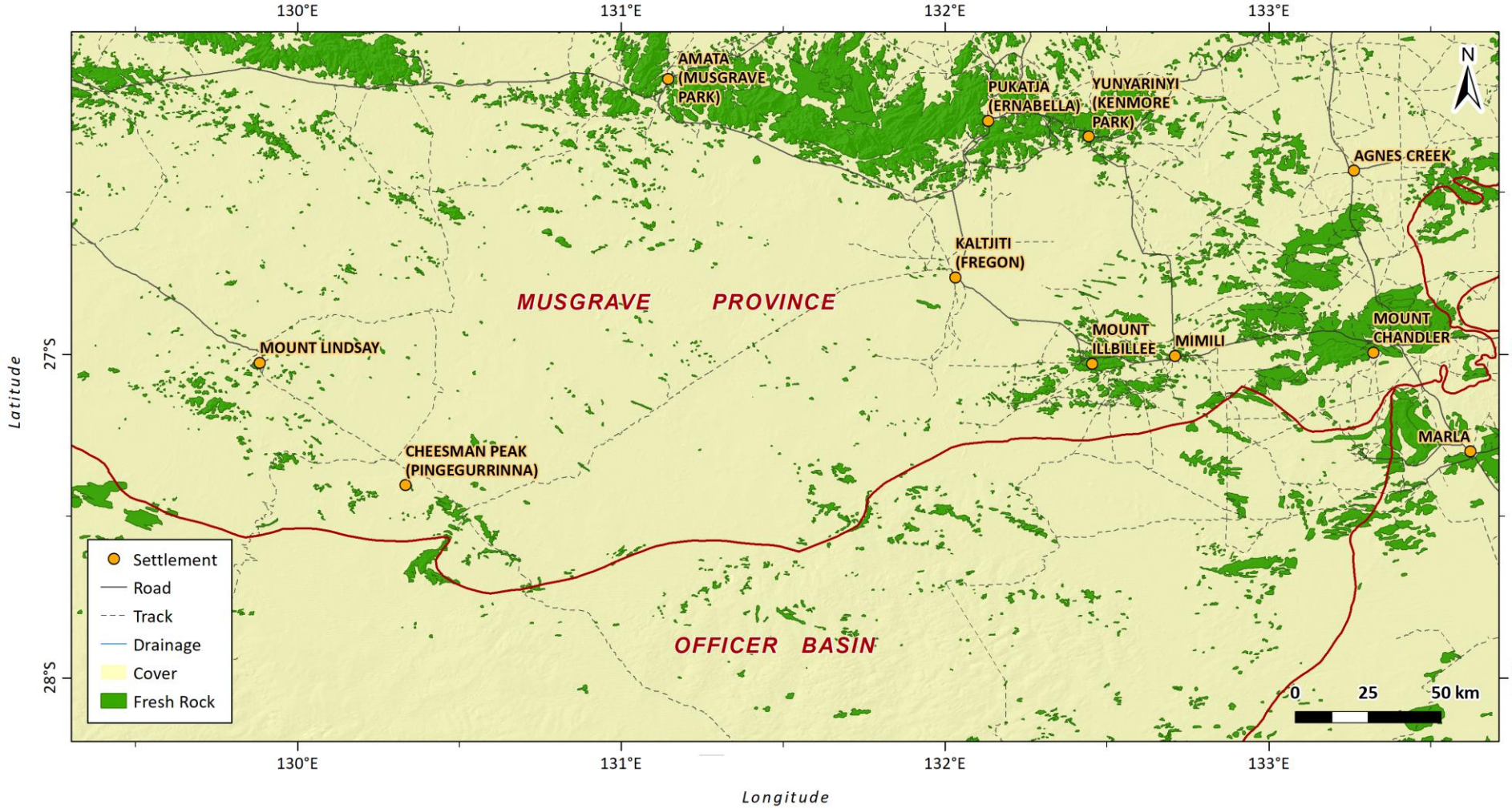

Figure 2-4. The distribution of cover (transported and *in-situ* regolith) across the Musgrave Province.

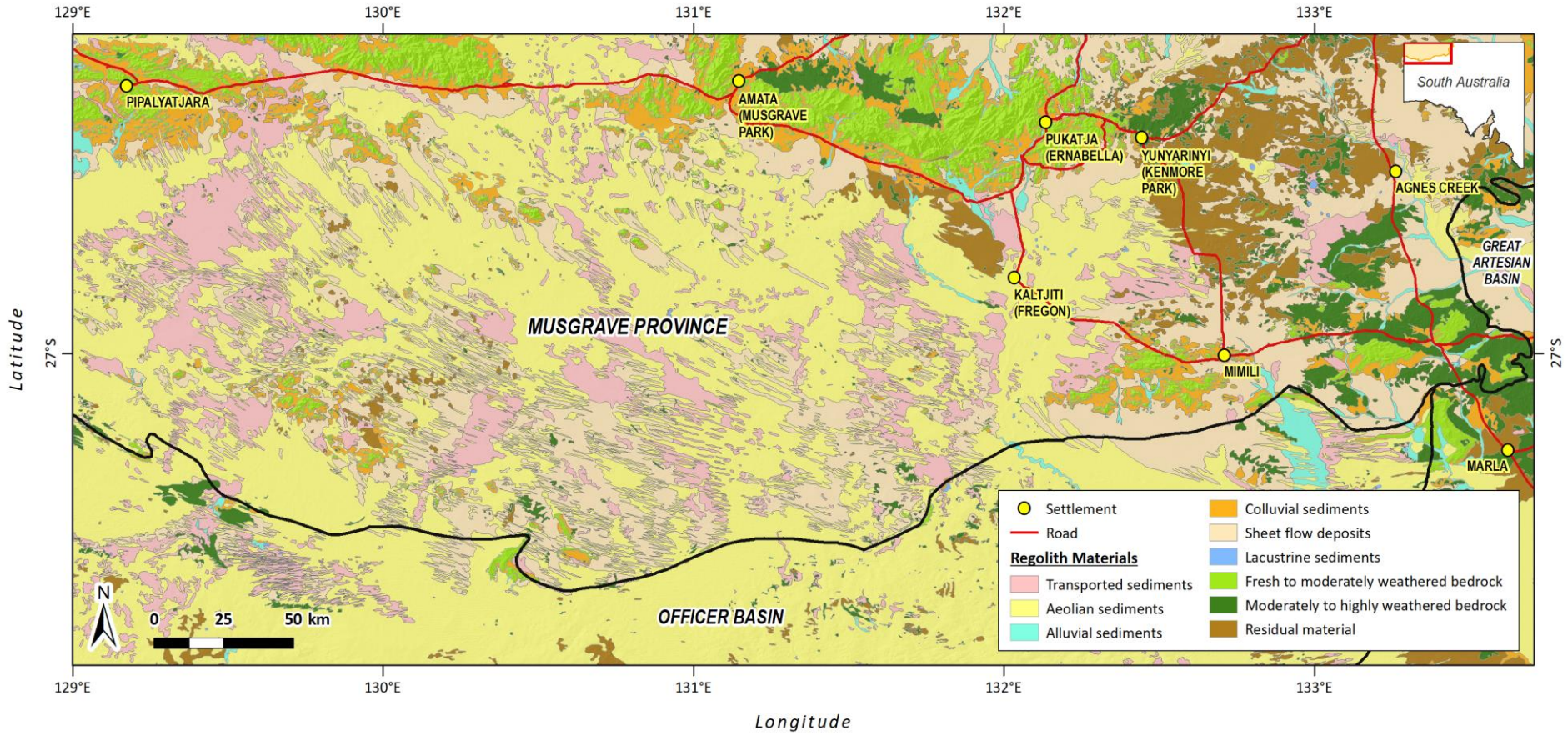

Figure 2-5. Simplified regolith materials map for the Musgrave Province adapted from Krapf et al. (2012).

3 Methods

3.1 Hydrogeological Framework

The presence of a thick and complex regolith cover across the Musgrave Province, whilst an impediment to effective and efficient minerals exploration, represents an opportunity from a water resource perspective. As mentioned previously, the incision and subsequent infilling of palaeovalley systems in the basement rocks, which are known from limited drilling through the region (Dodds and Sampson, 2000, Watt and Berens, 2011), but also from previous geophysical surveys (see, for example, Wightman, 1973; Dodds and Clarke, 2003; Munday et al., 2013; Parsekian et al., 2014), have been postulated to contain a significant groundwater resource. However, until recently their geometry and extent, the nature of the aquifer materials and the water resources they may contain have remained relatively undetermined.

Initial work in the G-Flows Stage-1 project developed a physical hydrogeological framework map of the Province (Figure 3-1), drawing on links between contemporary topography, geological structure (from regional magnetics) and limited coverage of airborne electromagnetic data which identified the presence of a conductive, often structurally controlled, palaeovalley fill (Figure 3-2).

3.1.1 THREE-DIMENSIONAL GEOLOGICAL MODELLING

A three-dimensional (3D) geological model of the Musgrave Province has been developed using AEM conductivity-depth slices from the inversion models presented in previous sections and Shuttle Radar Topographic Mission (SRTM) digital elevation data using SKUA-GOCAD® 3D geological modelling software. The conductivity-depth slices of the 10 m intervals were imported into the 3D geological modelling software framework, to assess the spatial patterns of subsurface conductivity at varying depth intervals below the ground surface.

Conductivities above a cut-off value of 45 Ohm were removed to determine the lateral extent of palaeovalleys at each depth conductivity slice. From this, an interface between palaeovalleys and underlying bedrock was picked and a surface representing the base of the palaeovalley system was generated. This surface was then used to build a volumetric 3D geological model using SKUA's Structure & Stratigraphy (S&S) workflow. The resulting 3D geological model was compared with additional geological datasets such as geological structures to identify relationships between palaeovalley evolution and faults.

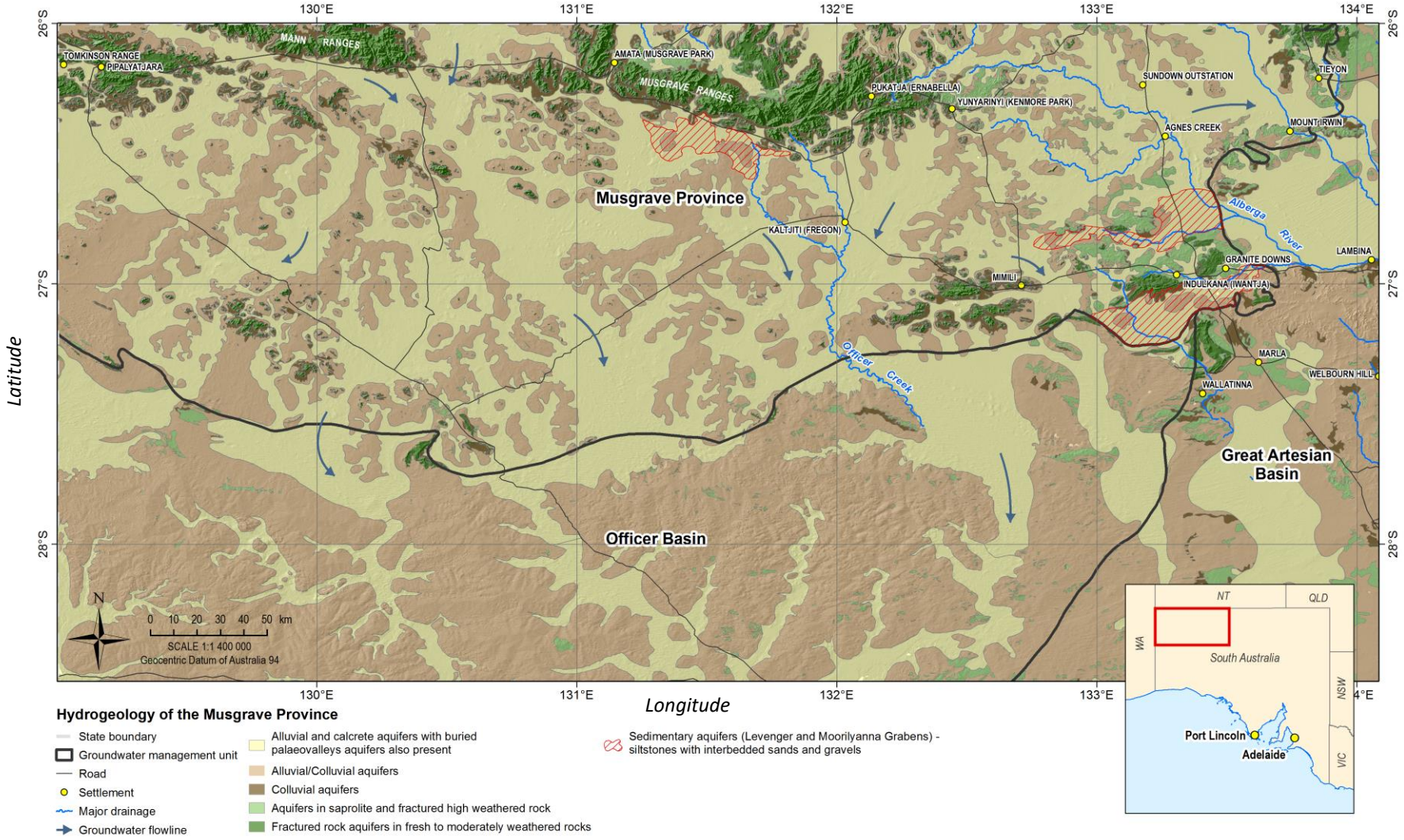

Figure 3-1. G-Flows Stage-1 - Physical hydrogeological framework map of the Musgrave Province (from Munday et al. 2013).

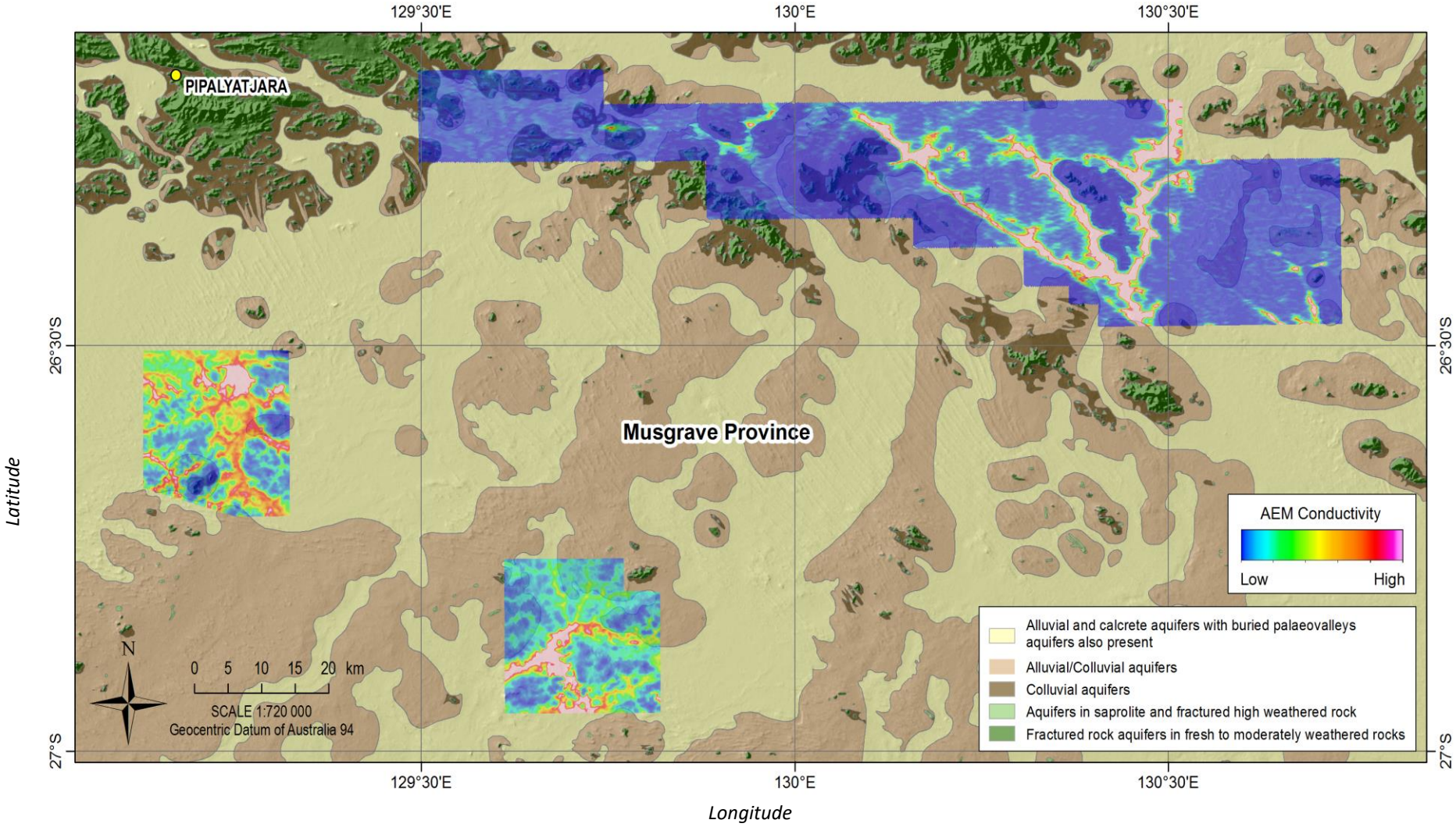

Figure 3-2. Subset of the physical hydrogeology framework map for the Musgrave Province overlain by interval conductivity images from airborne electromagnetic surveys acquired as part of mineral exploration programs undertaken in the region. Areas of high conductivity coincide with a palaeovalley fill of Pliocene to Pleistocene sediments overlain by Quaternary sand dunes of the Great Victoria Desert.

3.2 Geophysical data – processing and interpretation

The Goyder Institute's Facilitating Long-Term Outback Water Solutions Stage 3 (G-Flows Stage-3) Project sought to validate the regional hydrogeological framework and methodology mentioned above (see also Munday et al. 2013). It also sought to extend that framework to provide a regional groundwater resource assessment in a data poor area through the integration of regional geophysical and geological data coupled with targeted hydrogeological data acquisition (principally through drilling). In part, this was achieved through the extended acquisition of regional-scale airborne electromagnetic (AEM) survey data set acquired by the Geological Survey of South Australia, and supported by the Goyder Institute and the Department for Environment and Water. This data set was key to furthering our understanding of the character, thickness and variability of cover materials across the Musgrave Province.

3.2.1 MUSGRAVE PROVINCE AIRBORNE ELECTROMAGNETIC SURVEYS

For the State Government regional AEM data acquisition, two different AEM surveys were planned with a relatively wide line spacing of 2 km, wide enough to cover a large region, whilst being close enough to provide useful information about the variability of cover, including the location and geometry of the major palaeovalley systems known to be present in the area. Both surveys were flown with a line spacing of 2 km in a north-south direction. The western survey was flown with the TEMPEST high moment (HM) system, and the eastern part with the SkyTEM312FAST system (Figure 8). Both systems are time domain airborne EM systems, one being of a fixed wing configuration (TEMPEST), the other being helicopter borne (SkyTEM). The orientation of the survey boundaries and their extent was defined in consultation with key stakeholders in the region, including state government departments, the community and industry.

Acquisition, quality assurance and quality control of the two AEM surveys was managed by Geoscience Australia (GA) on behalf of the Geological Survey of South Australia (GSSA) and CSIRO using their standard protocols. Survey specifications (system type, line orientation and spacing) was determined through discussion between the GSSA, the Department of Environment, Water and Natural Resources (DEWNR), CSIRO, and GA, guided by a desire to resolve regolith thickness and understand regional variations in regolith stratigraphy.

The survey area was divided into two separate parts with a small overlap – one overlapping line where the surveys join. Both surveys were flown with a line spacing of 2 km in a north-south direction. The 8595 line kilometres of TEMPEST HM data were acquired between the 18th of August and 17th of September 2016 by CGG Aviation Pty. Ltd., while the 8412 line kilometres of SkyTEM312 data were acquired between 9th September and 13th of October 2016. In addition to the 2 km line spacing, SkyTEM data were also acquired in smaller infill areas where the line spacing was reduced to 250 m and 500 m to map finer details in these areas (Figure 3-3).

3.2.2 INVERSION MODEL

The Musgrave AEM surveys were inverted using a smooth layer model as described in Soerensen et al. (2018). This type of model typically consists of 15–30 layers with fixed thicknesses, often increasing with depth. The amount the conductivity of one layer can vary to the next is defined by a vertical constraint. The large number of layers and the gradual change in conductivity in this type of model makes the resulting conductivity models appear continuous.

For the purposes of this study, a 30-layer model was used for the inversion of both the TEMPEST and the SkyTEM datasets, although alternative approaches including a blocky or few-layer model and a sharp inversion were also considered. The merits of these are discussed in a later section. The first layer thickness of the smooth model was chosen to be 3 m with logarithmically increasing thicknesses to a depth of 300 m which is the depth of the last layer boundary. The starting model was a homogenous half space with an auto calculated conductivity, which is calculated as the mean of the apparent resistivity for each sounding. The

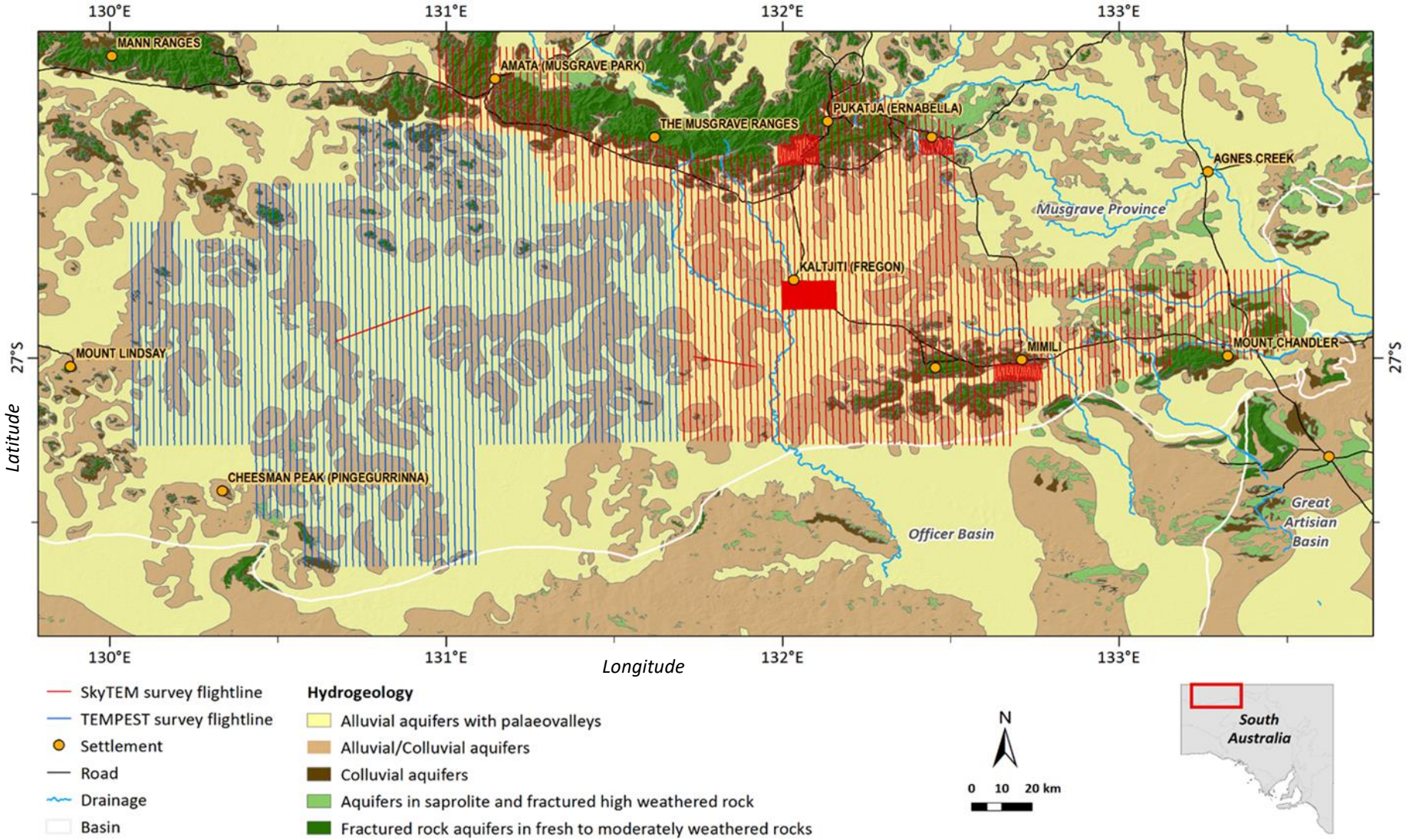

Figure 3-3. The flight line orientation map for the Musgrave Province airborne electromagnetic survey. Flight lines are overlain on a hydrogeological framework map for the region.

regularisation constraints (smoothness constraints) were set to a vertical constraint of 3, a value which allows some vertical structure, without introducing artefacts caused by overfitting the data. The horizontal constraint was set to 1.8 for all layer intervals.

Laterally *constrained* inversion (LCI)

Both the regional SkyTEM and TEMPEST datasets were inverted separately using the laterally constrained inversion (LCI) methodology (Auken and Christiansen, 2004; Auken et al., 2005). The spatial constraints, which are defined for adjacent soundings, allow prior information (e.g. the expected geological variability of the area) to migrate along the flight lines. The use of constraints along lines enhances the connection of layer parameters between adjacent soundings. In the context of the Musgrave Province this approach encourages the definition of laterally continuous conductive layers which is an aid to target definition and geological interpretation.

Spatially *constrained* inversion (SCI)

The SkyTEM312FAST data for the infill areas adjacent to the towns of Kaltjiti, Mimili, Yunyarinyi and Pukatja were inverted using the Spatially Constrained Inversion (SCI) methodology described by Viezzoli et al. (2009). The SCI is a quasi 3D inversion methodology, based on a 1D forward response, with 3D spatial constraints. The spatial constraints allow prior information (e.g. expected geological variability) to migrate along/through the entire dataset. This type of inversion uses constraints along lines and across lines, which means that layer parameters are connected between adjacent soundings.

The constraints for the SCI are set in a Delaunay Triangulation, where the connection is made to the nearest neighbour. The advantage of using a spatially constrained inversion is seen in less striped inversion results as the geological information from one line to another is carried across. The output models balance the information present locally within the individual TEM soundings with the ones carried by the constraints, in this case from adjacent soundings. The SCI has a demonstrated applicability in semi-layered environments including those encountered in the palaeovalley sediment packages of the Musgrave Province.

Airborne electromagnetic-derived ground conductivity structure

Conductivity-depth intervals or interval conductivities were generated from the inversion results of both the regional TEMPEST and the SkyTEM surveys, in 10 m intervals from surface to 200 m depth. Displaying inversion results as conductivity-depth images is a common way to visualise the spatial distribution of the conductivity within a survey area. In areas with large topographical variations it can be beneficial to display conductivities not only with depth but also as elevation intervals, accounting for variations caused by the topography. Example interval conductivities for the two regional surveys are shown overlaid on the regional hydrogeological framework map developed as part of G-Flows Stage-1 (Figure 3-4 and Figure 3-5), and a 1st vertical derivative (1VD) of airborne magnetic data map (Figure 3-6 and Figure 3-7). The intervals were gridded using kriging with a cell size of 400 m. Similar maps for each of the infill areas flown in the Eastern part of the Musgrave Province were also generated.

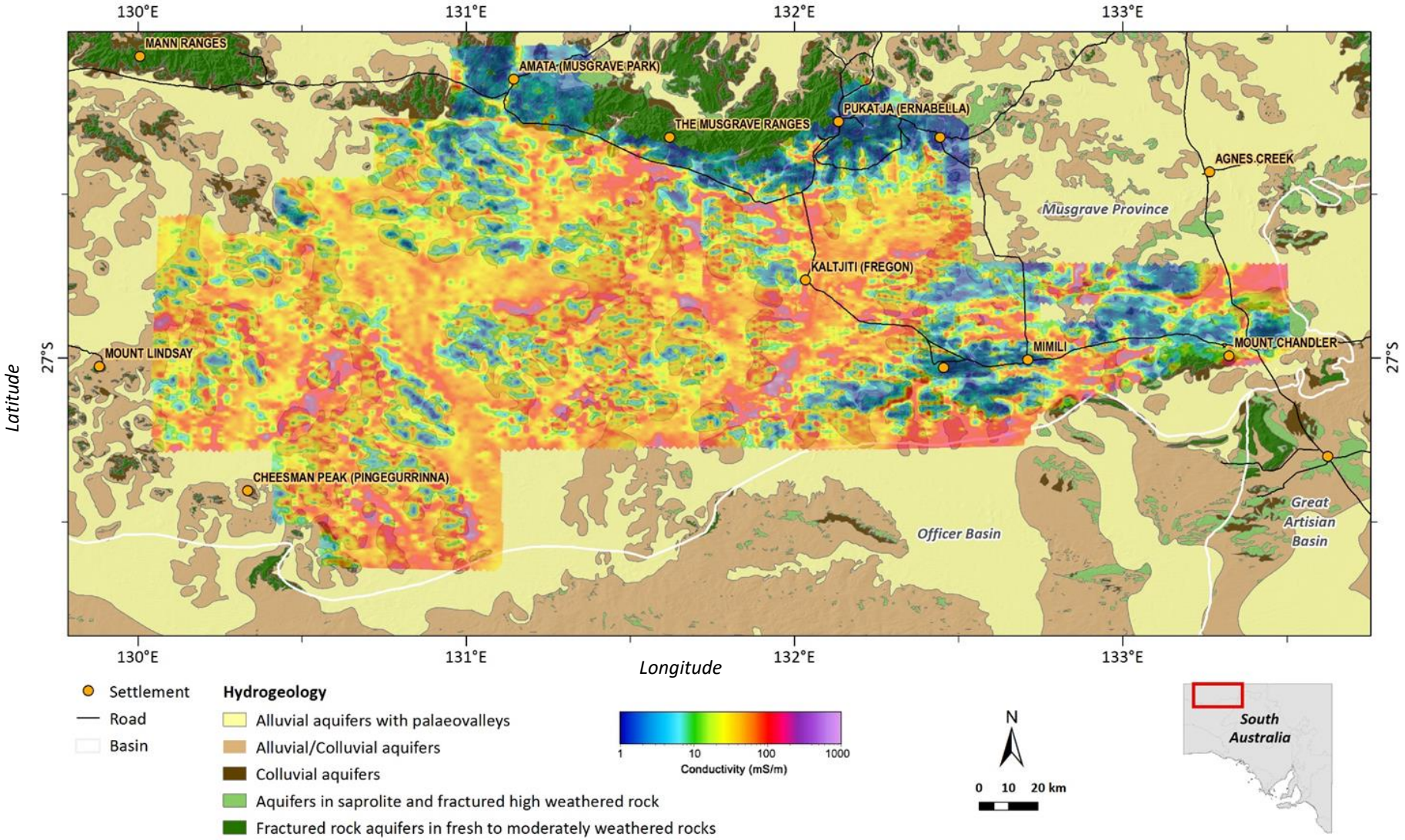

Figure 3-4. Interval conductivity (10-20 m) depth slice overlain on the hydrogeological framework map.

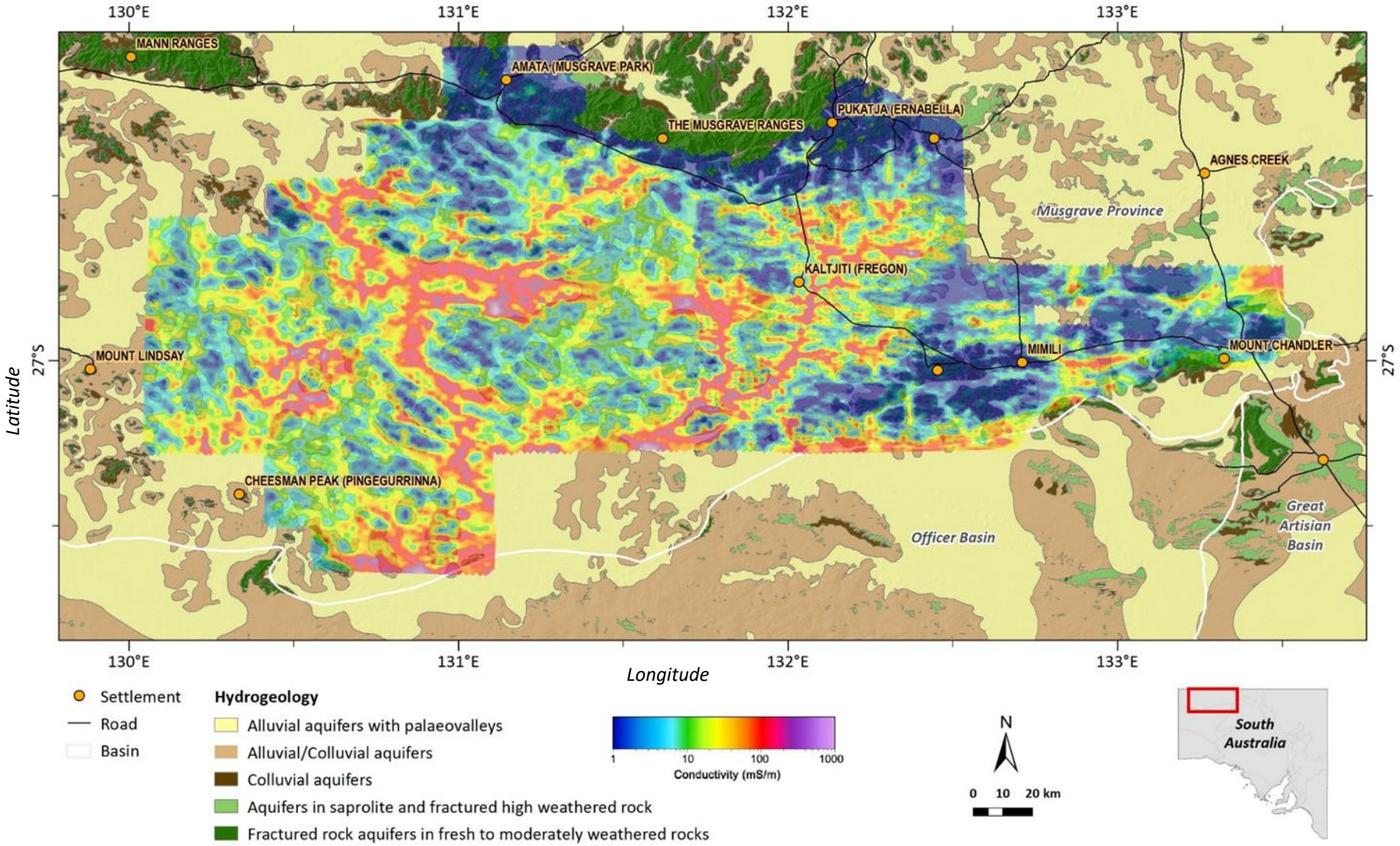

Figure 3-5. Interval conductivity (90–100 m) depth slice overlain on the hydrogeological framework map.

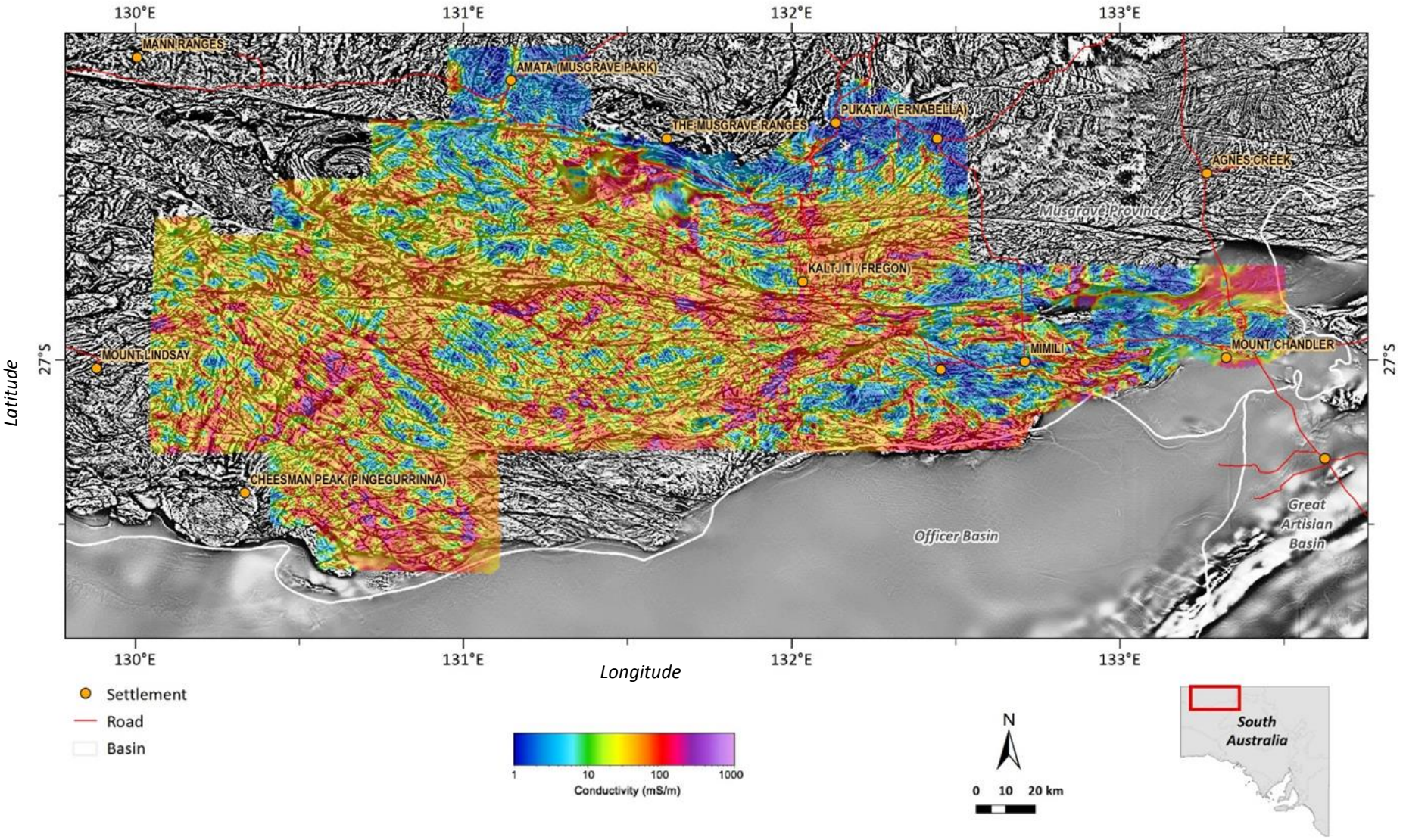

Figure 3-6. Pseudocoloured conductivity depth interval (10–20 m below ground surface) overlain on panchromatic 1st vertical derivative (1VD) airborne magnetics image.

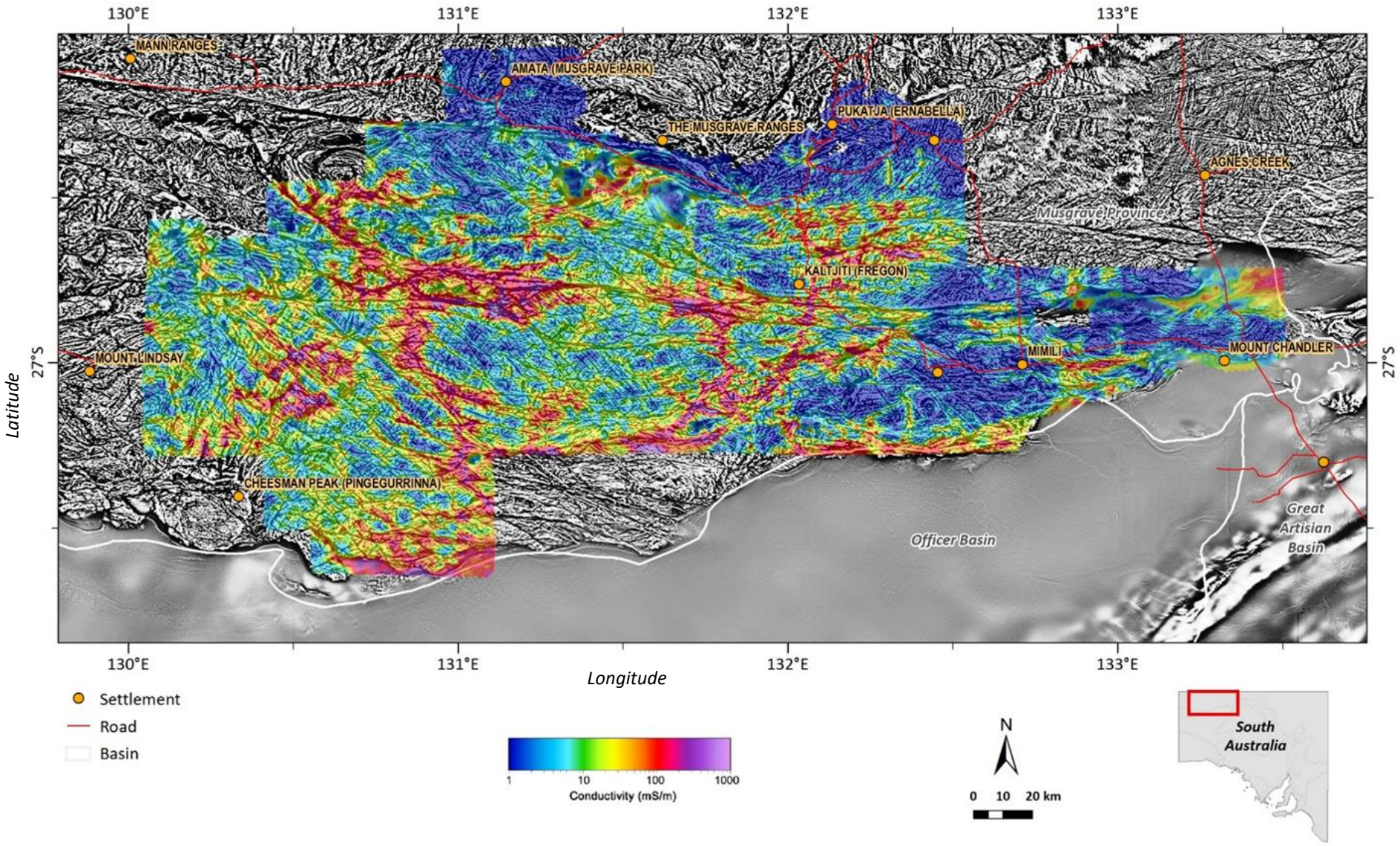

Figure 3-7. Pseudocoloured conductivity depth interval (50–60 m below ground surface) overlain on panchromatic 1st vertical derivative (1VD) airborne magnetics image.

Conductivity-depth sections have also been generated for each flight line through both regional surveys and for the infill areas. These have the depth of investigation (DOI) appended to assist interpretation. An example of the nature of these sections is presented in Figure 3-8. In this example, the section depicts the conductivity structure from an inversion of an E-W flight SkyTEM line in the central part of the study area, just south of Kaltjiti/Fregon.

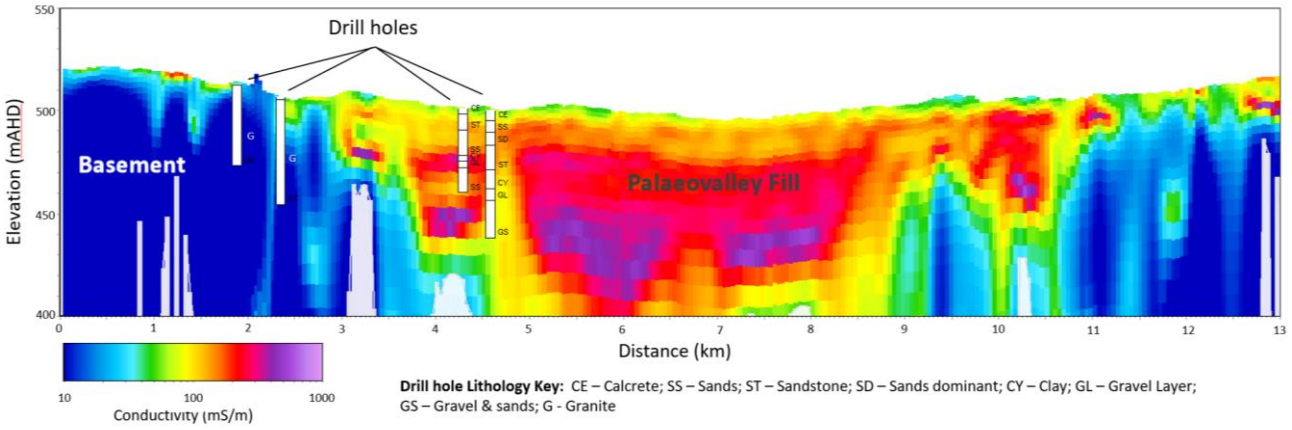

Figure 3-8. Conductivity-depth section from a smooth model Laterally constrained inversion (LCI) for a north-south SkyTEM flightline west of Kaltjiti/Fregon. The flight line transects a palaeovalley, which is represented as a conductive zone in the central part of the section.

3.3 Description of palaeovalley mapping and depth to basement

A key part of this study was an improved understanding of the geometry and extent of the palaeovalley fill systems across the study area, primarily because, as mentioned earlier, these sequences were likely to host the most significant groundwater resource in the region.

Two methods were investigated for defining the cover distribution and thickness across the areas surveyed by the two AEM systems. These included a geostatistical, or machine learning method, known as the Smart Interpretation method, and an approach involving the automated definition of a layer boundary using a resistivity or conductivity "cut-off". Both approaches assumed that the cover sequences (comprising regolith and sedimentary cover) in the study area were more conductive/less resistive than the underlying unweathered basement. The conductivity-depth section depicted above (Figure 3-8) supported that assertion. Their application also assumed that a change in a threshold conductivity value, whether determined by a manual means in the Smart Interpretation approach, or by other approaches could be equated to a change in lithology type, that is, a change from an overlying regolith or sediment to a crystalline basement.

3.3.1 BASEMENT SURFACE GENERATION USING A RESISTIVITY "CUT-OFF" VALUE

Given that the cover in the Musgrave Province was generally determined to be more conductive that the underlying basement, the option of defining a regolith or cover thickness product using a resistivity cut-off value presented itself. We employed the "general layer search" procedure in the Aarhus Workbench software (Auken et al., 2015) package for this purpose. The procedure allows for the definition of layer boundaries using certain criteria including particular conductivity or resistivity values (termed a "cut off" resistivity). More specifically it involves searching every model, derived from an inversion, for a layer that matched the user-defined criteria. When a matching layer is encountered, the search moves to next model and so on. The selection criteria employed for defining the base of the cover are defined in Table 3-1, and the assumption is that there are two layers in the model, a conductive upper layer and a resistive lower layer, with the upper layer having a minimum thickness of 0 m, but a maximum thickness of 175 m.

The settings defined in Table 3-1 were used to find the layer above the basement with a resistivity of less than 50 Ωm (20 mS/m). The actual resistivity value chosen was deemed an appropriate value to encompass largely unweathered basement rock types. Information on the petrophysical properties for regolith and unweathered rock collated by Munday (2008) indicates that the cut off figure of 50 Ωm is close to the average value for "wet saprock" (Table 3-2), and therefore may represent an appropriate starting point for defining the unweathered bedrock-regolith interface.

Table 3-1: Selection criteria employed in defining a "cut-off resistivity" boundary.

CRITERIA	VALUE
Property to extract	Depth of layer 1
Resistivity cutoff	50 Ωm
Layer thickness	0 m
Layer maximum thickness	175 m
Resistivity of basement	>50 Ωm
Depth to top of Layer 1	0 m
Depth to bottom of Layer 1	200 m
Search for layer boundary from top	True

Table 3-2: Representative petrophysical properties of the regolith and basement. Source: Munday (2008).

REGOLITH MATERIAL (FROM SURFACE TO BEDROCK)	RESISTIVITY [MEAN (STANDARD DEVIATION)]a (ΩM) (1 kHz)	DRY BULK DENSITY [MEAN (STANDARD DEVIATION)] (g/cm^3)	MAGNETIC SUSCEPTIBILITY [MEAN (STANDARD DEVIATION)] (K (SI X 10^{-5}))	APPARENT POROSITY [MEAN (STANDARD DEVIATION)] (%)	P-WAVE VELOCITY (m/s) [MEAN (STANDARD DEVIATION)] (500 kHz)	LITHOLOGY/MINERALOGY
ALLUVIUM, COLLUVIUM commonly hardpanised	1000 (dry) 10 (wet)	2.23 (0.31)	3603	23 (5)	2148 (507)	Clay/Fe saprolite-kaolinitic lithic clasts, with ferruginous clasts, sandy clay and clay horizons. Crypto-crystalline silica cement in hardpan, maghemite in finer grain fraction
FERRUGINOUS SAPROLITE	65	2.26 (0.23)	94 (71)	24 (10)		Hematite, goethite, kaolinitic clay; ~50 per cent iron oxides diffused through day-rich saprolite
SAPROLITE	7 (5)	1.78 (0.28)	112	35 (10)	2030 (519)	Smectite and kaolinite clays, some zones of reprecipitated silica; various original rock silicate minerals in progressive stages of breakdown
SAPROCK	131 (68)	2.66 (0.22)	743	8 (6)	935)	As for bedrock, but with minor alteration of quartz, feldspar, amphibole, pyroxene, mica, talc, chlorite, carbonate ± magnetite &/or pyrrhotite/pyrite
FRESH ROCK	> 5000+	2.96 (0.16)	96 (59)	1.6 (1.6)	5955 (540)	As for saprock but no alteration

The result of this process, where the elevation of the 50 Ωm surface for the area covered by both the regional TEMPEST and SkyTEM AEM surveys is displayed in a perspective view under the elevation of contemporary topography (Figure 3-9).

A regolith thickness product is then defined by subtracting the two elevation models (Figure 3-10). This relatively simplistic approach works remarkably well in a landscape where conductive transported materials sit on top of an unweathered (resistive) basement. The regolith thickness map and the basement geometry defined with the approach accord with available drilling and with the model defined in G-Flows Stage-1 that suggested the thicker valley fill sequences were coincident with contemporary lows or valleys in the more subdued relief of the plains that abut the Musgrave ranges in the South.

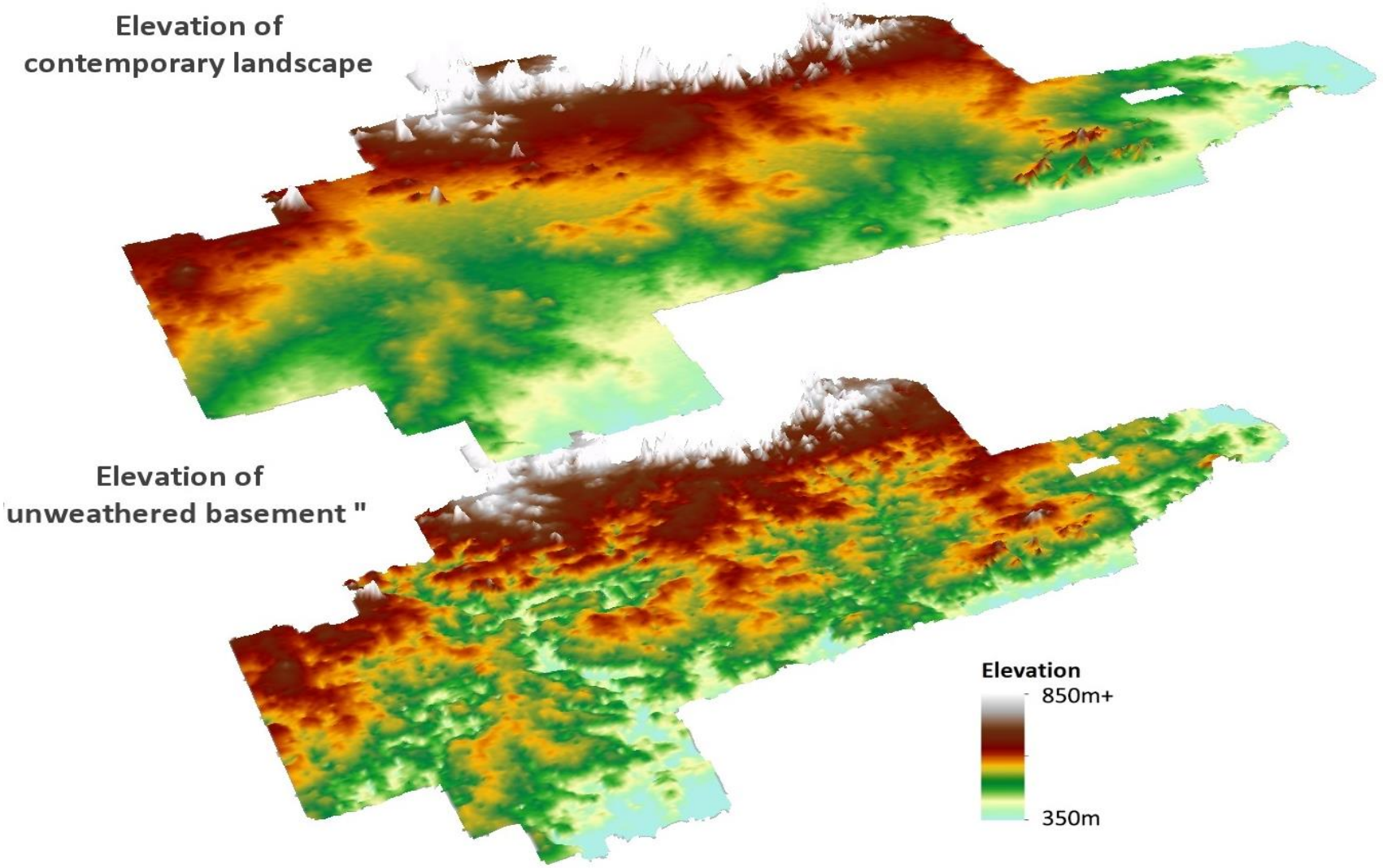

Figure 3-9. Elevation of the 50 Ωm surface for the area covered by both the regional TEMPEST and SkyTEM airborne electromagnetic surveys is displayed in a perspective view under the elevation of contemporary topography. Perspective view is to NNE from the SSW.

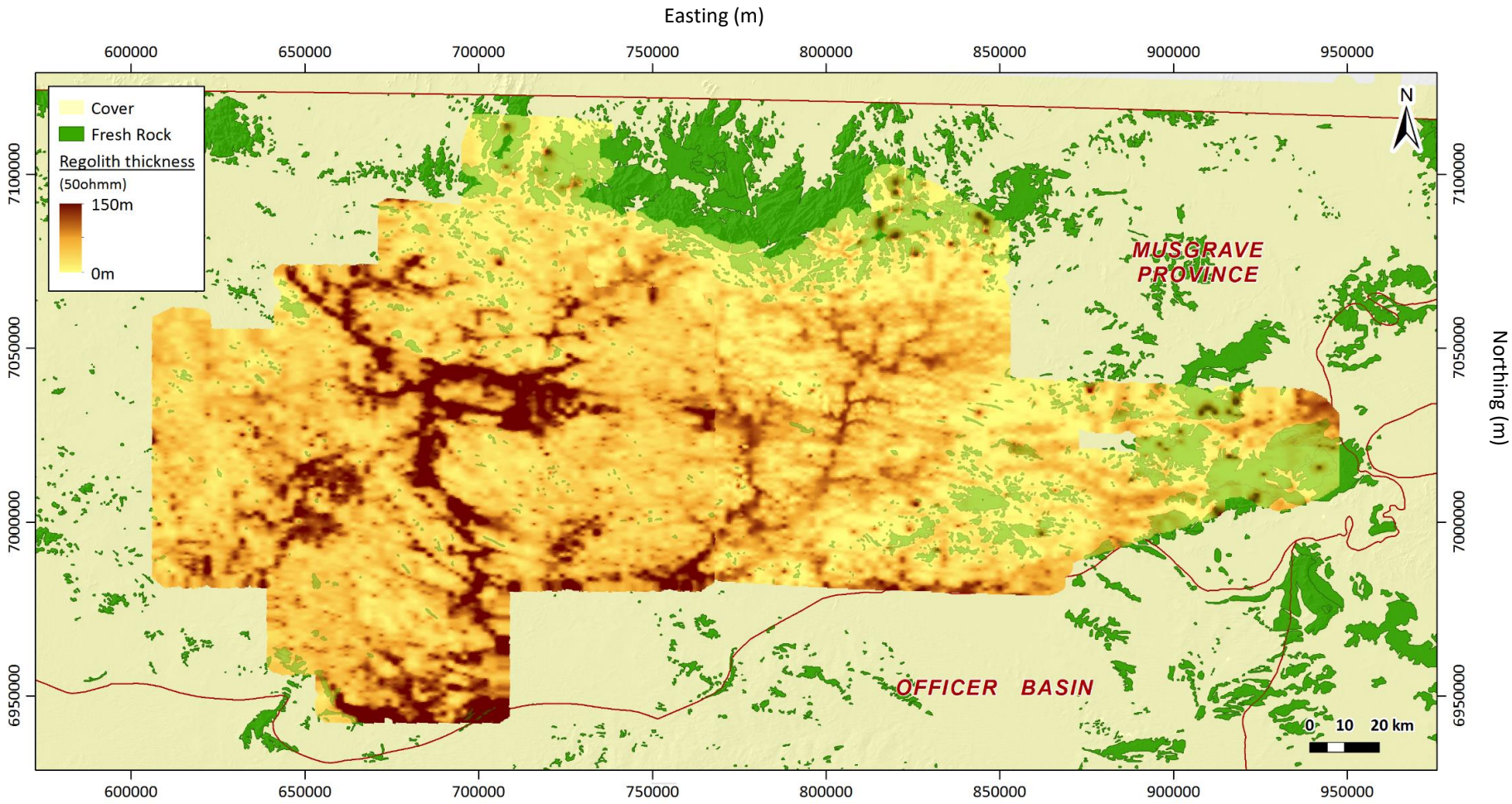

Figure 3-10. Interpreted regolith thickness product for the area covered by both the regional TEMPEST and SkyTEM airborne electromagnetic (AEM) surveys.

3.3.2 SMART INTERPRETATION

The Smart Interpretation method employed here is a machine learning approach described by Gulbrandsen et al. (2017). It is based on a linear regression technique developed for geological layer modelling and is summarised in Figure 3-11. The method uses a two-step approach with the first requiring a geologist or geophysicist ("the expert") to define a physical interface such as the boundary between two lithological units (d), or in this study the interface between an un-weathered basement and regolith cover. This definition is initially done by manually "picking" this surface or interface on a conductivity-depth section of inverted AEM data (M). While the expert is doing this manual picking, the algorithm tries to learn the relationship between the manually interpreted points and multiple available attributes associated with those points or picks (these are shown in Figure 3-13). These can include the conductivity around the point, and/or the elevation of the point.

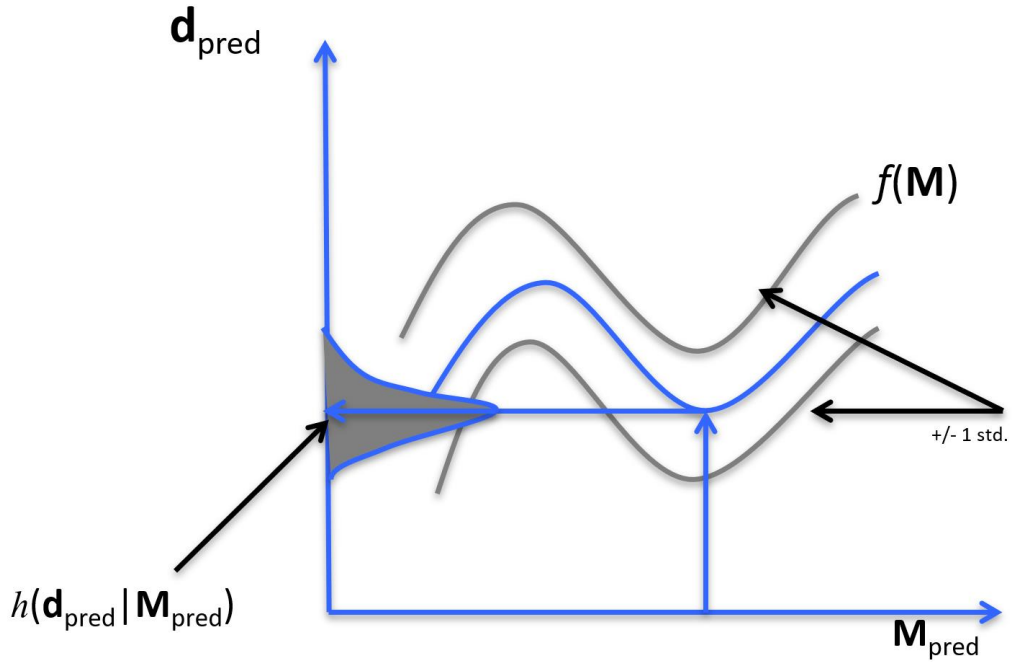

Figure 3-11. Overview of the Smart Interpretation method. The methodology infers a statistical model *h(d|M)* that describes the relation between a geological interpretation *d* and the information available to the geologist making the interpretation *M*. The focus is geological layer/boundary modelling, and by interpretation and interpretation points we refer to the interpretations of the depth to geological layer boundaries.

Specifically, the relationship is defined by the coefficients of a polynomial that are determined through linear regression, and attributes include any quantifiable piece of information such as the conductivity values, geographic coordinates, and elevation. After a few picks, when the algorithm has learnt the interpretation points attribute relation, it then, as a second step, proceeds to predict what the expert would interpret throughout the rest of the survey. This is simply done by applying the relationship learnt in the first step, to the rest of the inverted survey lines.

Workflow

The approach or workflow employed for the SkyTEM Musgrave AEM data set is illustrated in the following figures (Figure 3-12 to FFigure 3-16), and follows these steps:

1. Select conductivity depth section, and with reference to available information (e.g. borehole logs) define an interface; in this case between the resistive un-weathered basement and the overlying conductive cover materials (Figure 3-12).
2. Pick points within the section that define what the expert interprets is the boundary of interest (see Figure 3-13). In this example, the picked points are the red dots. The Smart Interpretation algorithm, having learnt the attributes of the experts points and their attribute relationship, then predicts a suite of other points that the 'expert" might have interpreted. These are shown in blue and are evenly distributed through the section. The process can be iterative and the interpreter can iterate the selection of picks, adjust them and visualise the predicted results.
3. With the relationship defined for the first line of data or section, the algorithm can then predict a set of "picks" for other lines in the survey area (see Figure 3-14).
4. Once the picks have been defined for all survey lines, a surface can be created by gridding all the picks across the survey area. This surface approximates the elevation of the un-weathered basement (see Figure 3-15).
5. To define "Regolith" or "Cover" thickness, the elevation grid for the un-weathered basement is subtracted from the elevation of the contemporary topography, and a grid showing the spatial variations of regolith thickness is the result (see FFigure 3-16).

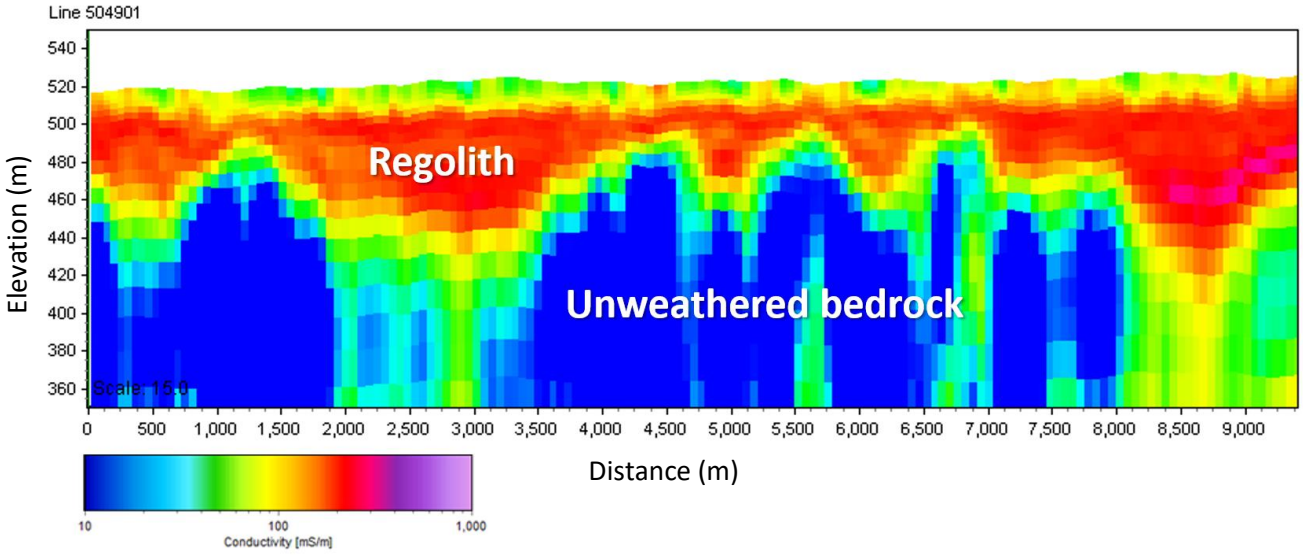

Figure 3-12. A conductivity-depth section from a line (504901) of SkyTEM data in the study area. The conductive parts of the section are interpreted to be the regolith cover, comprising a mix between transported sediments and *in-situ* saprolitic materials, and these overlie a resistive basement.

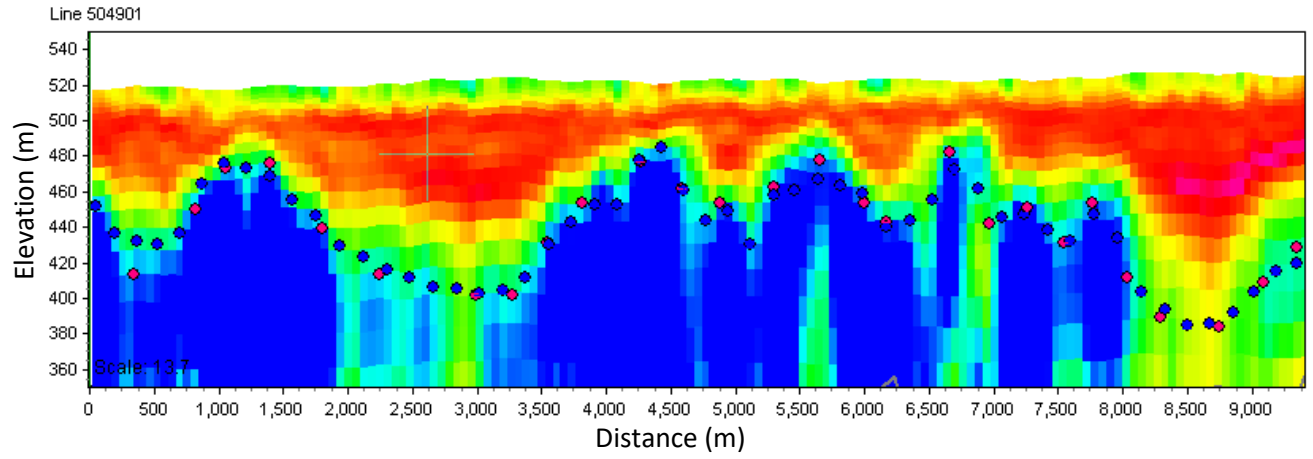

Figure 3-13. The expert picks, representing the interpreted interface between cover and the basement are identified in the red dots in the conductivity-depth section for line 504901. The algorithm then predicts what the expert would have picked and populates the section with a predicted set of "picks" (blue dots). (axis units are in metres).

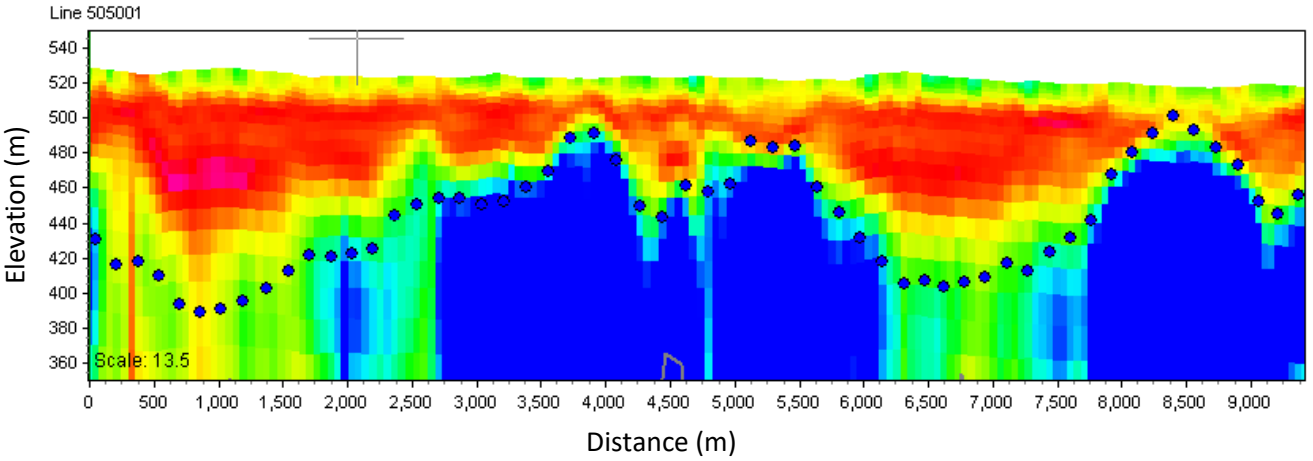

Figure 3-14. A conductivity-depth section from a line (505001) of SkyTEM data in the study area, with the predicted picks (blue dots) defined from the statistical relationship determined for the first line that was interpreted. (axis units are in metres).

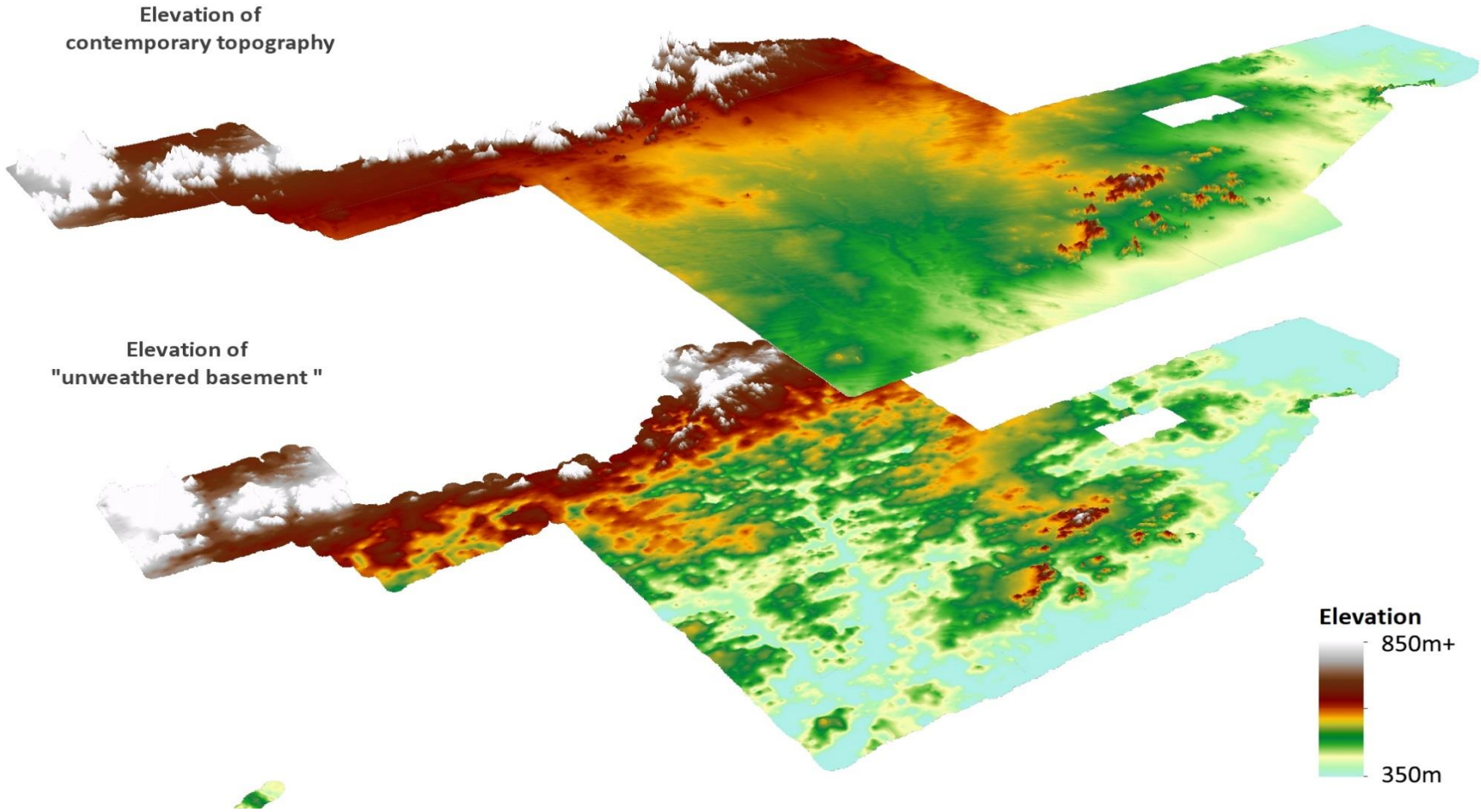

Figure 3-15. Perspective view of the SkyTEM survey area in the eastern Musgrave Province. The upper image shows a perspective view (looking NNE) of a pseudo-coloured image of the contemporary elevation, while the lower image shows a perspective view the elevation of the "top of unweathered basement" as defined from the Smart Interpretation workflow.

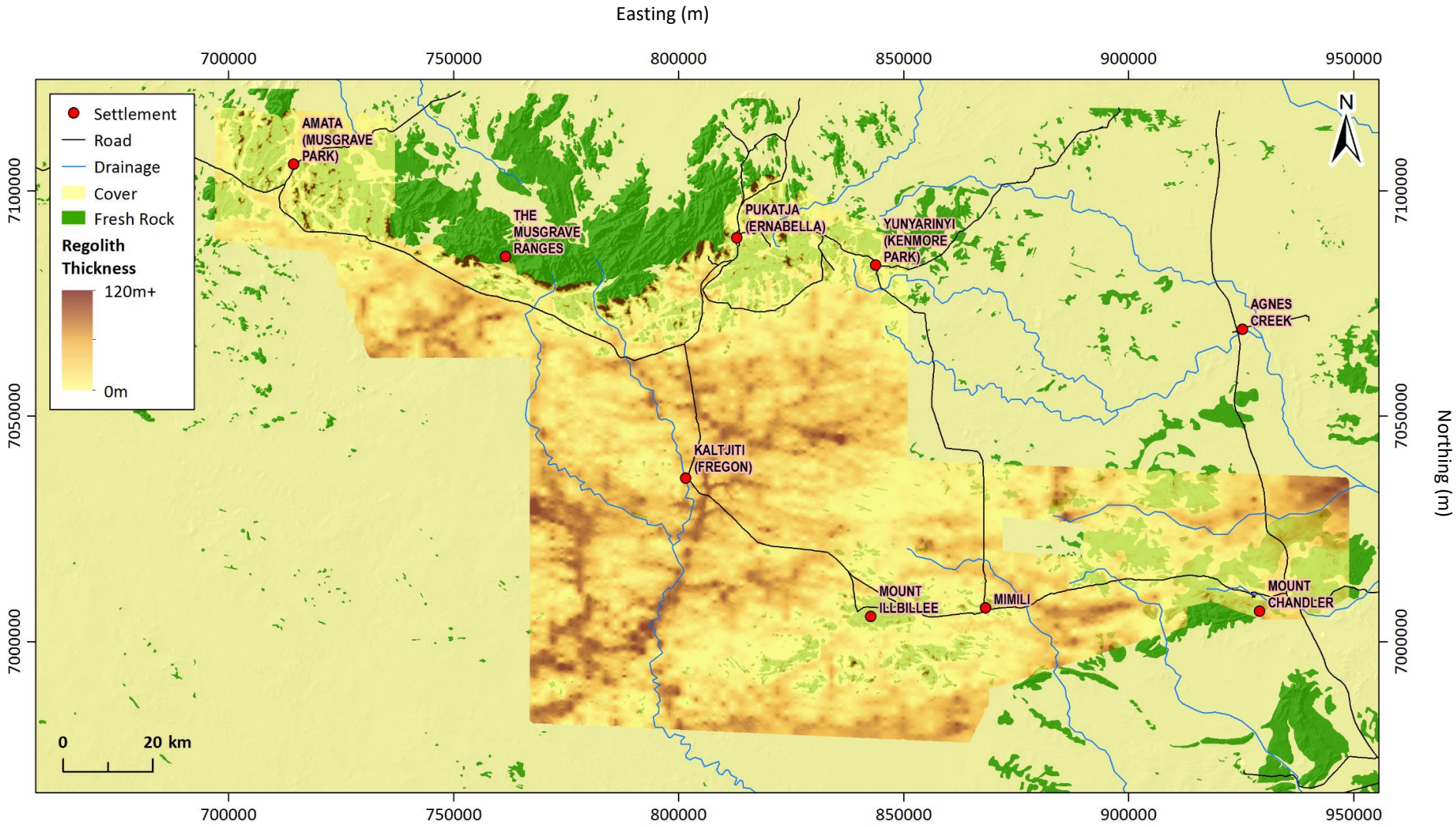

Figure 3-16. Map of regolith thickness derived from subtraction of the elevation derived for "unweathered basement" from the contemporary elevation. This map is for the eastern part of the Musgrave Province over an area covered by the regional SkyTEM survey. The cover thickness image is overlain on a map of cover versus outcrop.

3.3.3 ESTIMATING REGOLITH THICKNESS

In generating these estimates of regolith thickness from the regional AEM surveys over the Musgrave Province, we have assumed that the initial "expert" picks account for the variations in modelled conductivity representative of the base of weathering or sedimentary (transported cover) fill. Similarly the option of choosing a cut-off conductivity or resistivity value is an alternative approach that yields similar results in a geological setting such as encountered in the Musgrave Province. This outcome is primarily related to the conductivity structure encountered in the region; that is a conductive transported cover and in-situ regolith overlying a resistive unweathered crystalline basement.

It is important to note however, that the derived models of regolith thickness represent regional trends in cover. Finer scale variability is also present and can be similar in magnitude to the range observed in the derived products produced in this study. The definition of the finer scale differences relating to the geometry of the bedrock-regolith interface is best determined along the flight lines (see, for example, Figure 3-8). Between flight lines (where line spacing is of the order of kilometers), finer scale variations cannot be resolved and the interpolation of the conductivity structure best defines larger-scale trends.

3.4 Drilling program

G-Flows Stage-3 undertook a program of targeted drilling works at two locations in the APY Lands during late 2018. This program was designed to provide data to support the geophysics-based hydrogeological interpretation, and to help improve the conceptualisation of the hydrogeology in the Musgrave Province. The background, method and results from the drilling program are reported in Keppel et al. (2019).

Two primary objectives of the drilling program included:

1) Confirm the stratigraphy and depth of the Lindsay East Palaeovalley and to help support the AEM geophysical data and geophysical model presented in Soerensen et al. (2018) including the identification of water bearing zones within the palaeovalley; and
2) Develop further understanding of the groundwater characteristics in the shallow groundwater system.

Two drilling sites were chosen for drilling and well installation works:

1. Lindsay East Palaeovalley was targeted, just to the south-east of Kaltjiti/Fregon (Figure 3-17) to help in understanding the hydrogeological and geophysical characteristics of the deeper palaeovalleys in the region. Drilling near the centre of the Lindsay East Palaeovalley (DH1) suggested there are at least three, connected, groundwater bearing sequences (or aquifers); the shallow phreatic water-table of calcareous mixed sand plain deposits, an interlayered coarse-grained sandstone and clay horizon and a very fine to coarse grained residual sand; a saprolite/fractured rock aquifer which underlies these palaeovalley sedimentary sequences (Keppel et al., 2019). The coarse-grained sandstones (which overly a lacustrine claystone and mudstone) shows promise as a productive aquifer, with development yields varying between 5 and 20 L/sec and salinities <1000 mg/L TDS (Keppel et al., 2019).
2. The S22 drill transect (Figure 3-17) was selected to examine the shallow, or phreatic, groundwater system outside the main palaeovalley systems, although this site S22 (S22i) also incorporated a small-scale tributary to the Lindsay East Palaeovalley.

In total, 11 groundwater wells were constructed from 12 drill-holes and two continuous drill core samples were collected (DH1a and S22i). Their detailed interpretation is discussed further in Krapf et al. (2019). The shallow phreatic water-table was targeted, and development yields were generally low (<1 L/sec), with groundwater salinity varying between 1000 and 1500 mg/L TDS.

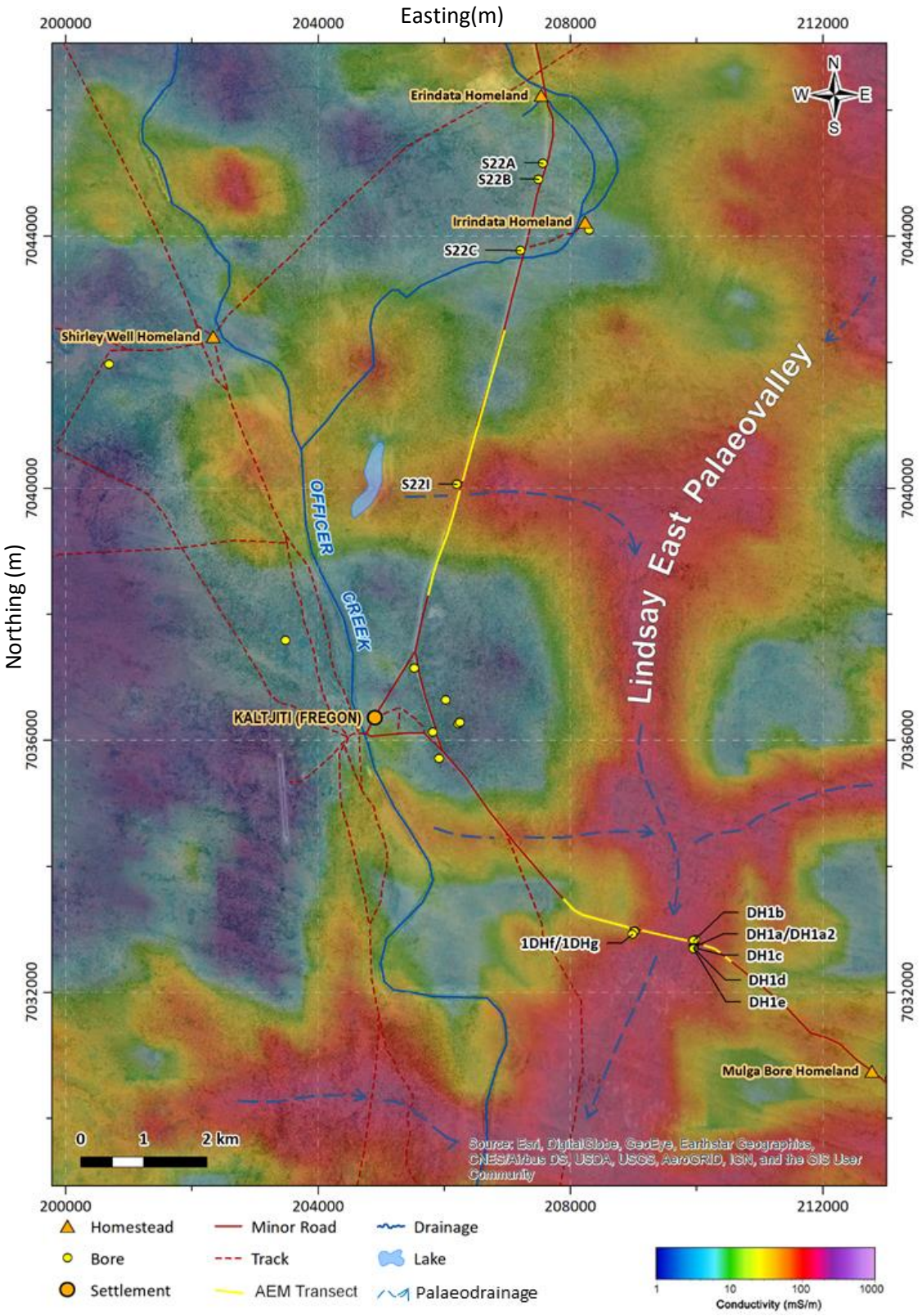

Figure 3-17. G-Flows Stage-3 drilling program locality map. Labelled bores were drilled for this project. The map shows a pseudocoloured conductivity depth interval of 50-60 m below the ground surface from the inverted SkyTEM airborne electromagnetic data set. The image is overlain on a satellite image, and the more conductive zones (reds and purples) representing the location of deeper conductive palaeovalley-fill. Drillholes around DH1, SE of Fregon targeted the Lindsay East palaeovalley, whist those on Transect S22, north of Kaltjiti/Fregon, targeted a variable subsurface, including what was interpreted as an E-W trending tributary of the main channel. The location of the AEM conductivity-depth section that transects the Lindsay East Palaeovalley (see Figure 3-18) and the inferred tributary at S22i are also shown.

3.4.1 VALIDATION OF AEM CONDUCTIVITY STRUCTURE FROM DRILLING AND BOREHOLE GEOPHYSICS

The AEM inverted products discussed in Section 3.2.2, were examined against available drill hole lithology data and borehole inductive conductivity data to assess their validity. The assessment of the inversion approach taken in this study; that is results from the smooth model one-dimensional (1D) constrained layered earth inversion was considered against drilling data in several locations, including the Lindsay East Palaeovalley (Figure 3-17). Although a smooth regularisation was employed for the regional data sets two other inversion methods were examined. These included a few layered, and a multilayered, sharp regularisation.

The inversion was undertaken using AarhusInv (Auken et al., 2015). Commonly used inversion options include an Occam-style regularisation using smoothly varying 1D models with fixed vertical discretisation. These produce smooth models where layer boundaries are sometimes hard to recognise. Discrete or few layer models with a fixed number of layers, where the layer boundaries are allowed to change in the inversion, are also employed where the conductivity structure might be relatively simple and laterally extensive. The smooth layered model have shortcomings in terms of defining layer boundaries, the few layer model on the other hand it can be difficult to pick a number of a layers that will be valid throughout a whole survey, and as a consequence artefacts can be introduced in areas of unexpectedly complex geology. The sharp inversion methodology outlined in Vignoli et al. (2017) is a focussed regularisation technique which allows for an accurate reconstruction of resistivity distributions while maintaining the capability to reproduce horizontal boundaries. The methodology promotes solutions that are compatible with the observed data and at the same time features a minimum number of spatial (vertical and lateral) model variations.

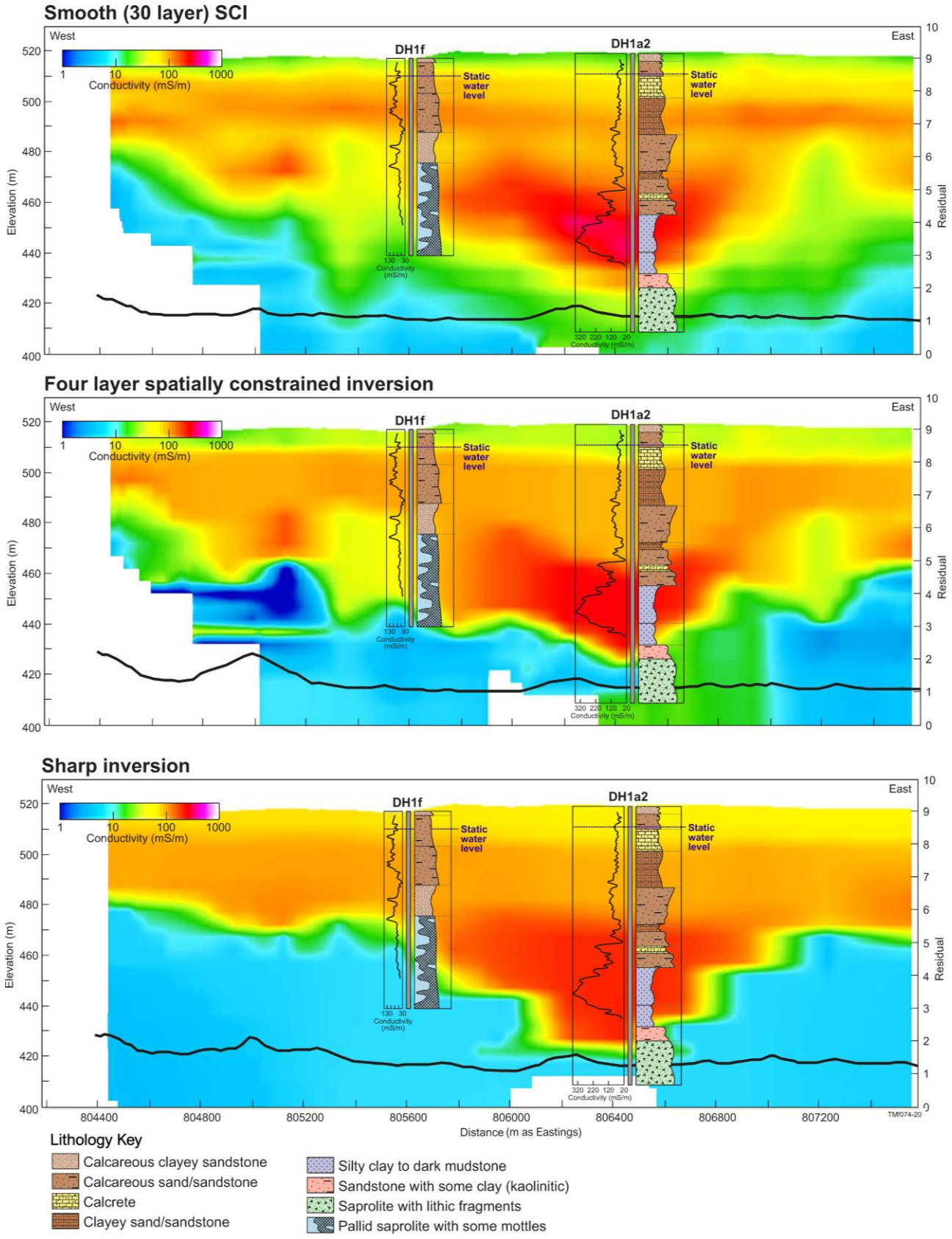

Figure 3-18. Conductivity-depth sections for the Lindsay East Palaeovalley transect. Top panel shows results for a smooth 30-layer inversion; the middle panel results for a four-layer blocky model; the lower panel, results for a smooth model sharp inversion. Drill hole lithology adapted from Keppel et al. (2019) and inductive conductivity logs are overlain on the AEM sections.

Results from the different approaches are presented in Figure 3-18. All methods have a low residual error indicating that the different inversions fit the data well (Figure 3-18). In all cases, the AEM inversions transition to a more resistive basement where the drilling identifies saprolite being present. The overlying transported palaeovalley-fill materials are more conductive relative to the saprolite and underlying basement. The amplitude of the modelled conductivity in the AEM sections accords with that observed in the borehole inductive conductivity logs. The borehole and AEM data indicate that the deepest part of the sediment fill is also the most conductive. We attribute these elevated conductivities to be primarily related to the solute content of the water contained in the sediment (TDS values ranging between 1000-1500 mg/L in the upper 30 m, decreasing to ~ 900 mg/L below that, but above the confining unit of clays and muds) (Costar et al., 2019). We note that elevated conductivities in both the AEM and inductive conductivity trace also coincide with presence of fluvio-lacustrine-marine silty clays (60–85 m – see Krapf et al., 2019). Groundwater salinities in the lower sedimentary sequences beneath the silty clays is ~1200 mg/L (Costar et al., 2019). Saprolitic materials at the base of the sequence also host groundwater with salinity of ~100 mg/L. See Section 4.1 for further discussion on groundwater salinity through the region.

The observed conductivity structure in the smooth model constrained inversion (top panel Figure 3-18) and its correspondence with the conductivity structure in logs for both bores DH1a2 and DH1f, provide confidence that this inversion model adequately represents that required for this study and provides relevant insight into the groundwater quality and aquifer systems present in the study area. Interpretation of the smooth model inverted section, incorporating available drillhole lithology logs yields a section shown in Figure 3-19. For the N-S AEM conductivity-depth transect that intersects drillhole S22i (targeting an E-W oriented tributary of the Lindsay East Palaeovalley, see Figure 3-17), the palaeovalley sediment also presents as a conductive unit overlying resistive basement (Figure 3-20). The conductivity-depth section indicates that the tributary is less incised than the Lindsay East Palaeovalley, and this was supported by the drilling log for S22i. From surface to ~46.3 m the drill hole intersected transported cover. Mottled *in situ* saprolite associated with weathered Pitjantjatjara Supersuite granite was intersected between 46.3 m and the end of the hole at 54.34 m. In contrast to drillhole DH1a2 (Figure 3-18), S22i intersected only sands and sandstones above the weathered basement (Krapf et al., 2019).

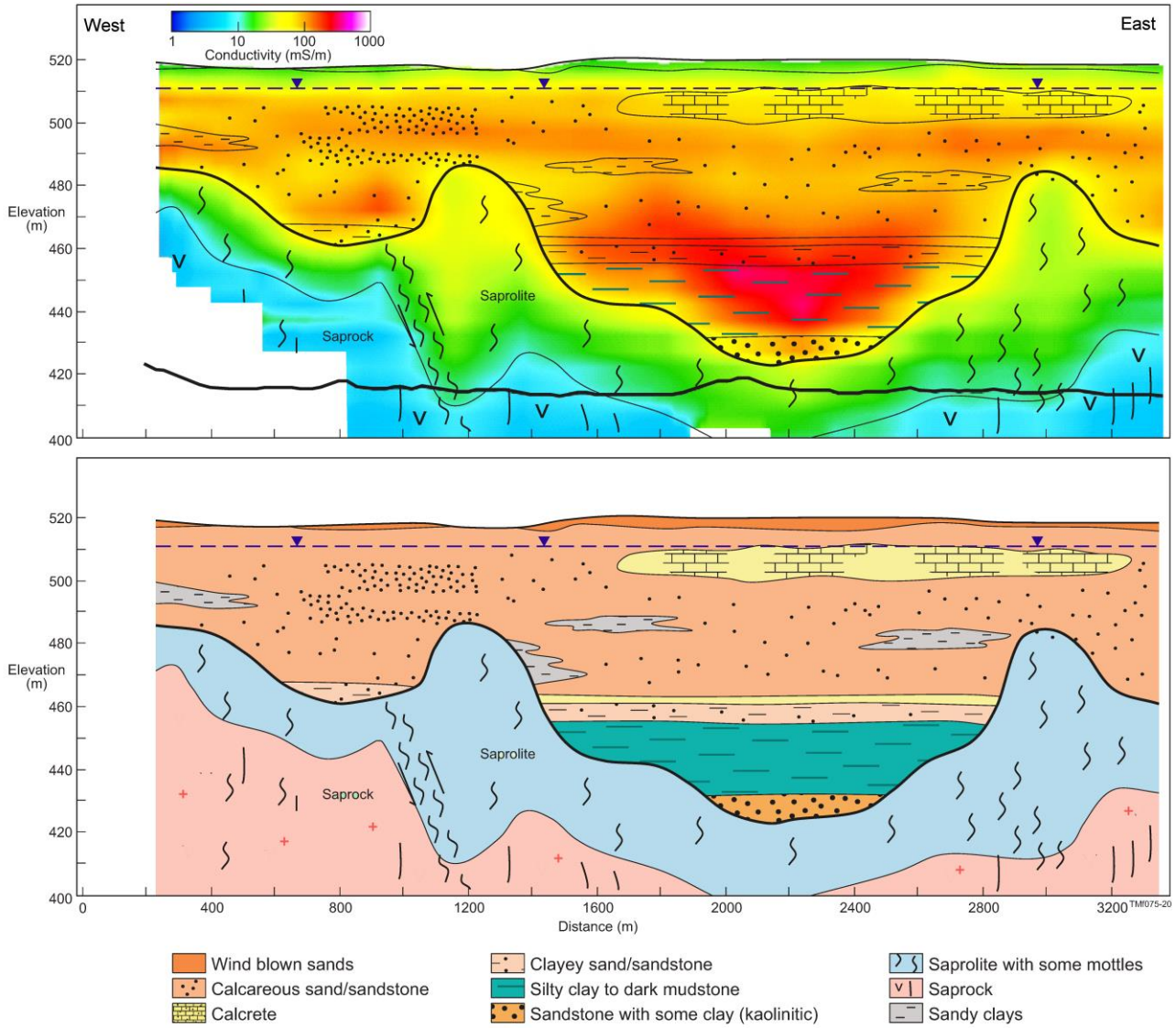

Figure 3-19. Smooth model conductivity depth section with interpreted geology overlain (upper panel). Interpreted geological section (lower panel) for the Lindsay East Palaeovalley transect.

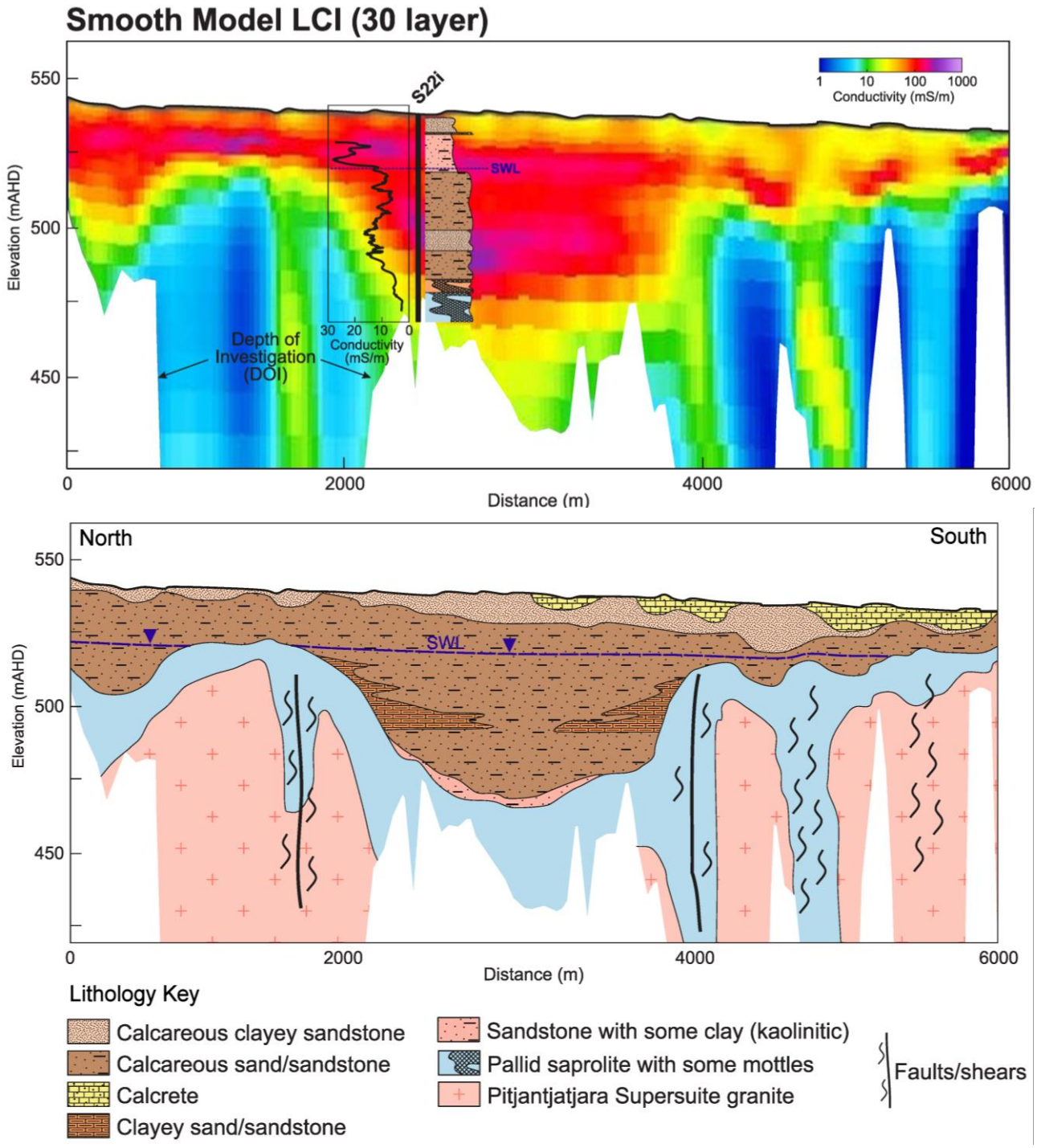

Figure 3-20. Smooth model conductivity-depth section (top panel) for N-S transect that intersects bore S22i (Figure 3-17). The interpreted geology for the section is depicted in the lower panel. The depth of investigation defined in the inversion is also shown in the conductivity-depth section (top panel).

The borehole conductivity log indicates that higher conductivities are found in the unsaturated zone above the standing water level (Figure 3-20). This may be the result of evaporative concentration of salts just above the water table. The modelled AEM section also suggests this part of the profile is more conductive. Groundwater salinities were of the order ~1000 mg/L.

Further to the south of Fregon, an E-W oriented SkyTEM flight line was also acquired over existing bores (Figure 3-21). This flight line crossed an interpreted palaeovalley which lay to the west of the Lindsay East system. Two bores (99A and 99B – see inset map in Figure 3-21) which were drilled in support of groundwater resource determination for the settlement of Walalkara intersected significant thicknesses of palaeovalley fill. Interpretation of a conductivity-depth section for the SkyTEM line indicated that these bores were located on the western side of a large palaeovalley system extending further to the east (Figure 3-22).

Recognition of thick (~20 m) of distinctive brown-black organic-sulfidic- and clay-rich basal muds overlain by thick massive gypsum layer and olive-green muds higher up in the succession between 65 to 85 m below the ground surface from core at DH1a2 (See Krapf et al., 2019; and Figure 3-17and Figure 3-18), and subsequent The palynological analysis indicated that the mud-rich succession was mainly deposited in a fluvial to lacustrine depositional subaqueous environment. Samples also contained taxa that were indicative of marine influence and record two intermittent marginal-marine to estuarine environmental conditions within the palaeovalley (Krapf et al., 2019). The interpretation of marginal marine-estuarine conditions was extrapolated across the study area by defining the elevation of the uppermost mud-rich sediment package and then "flooding" the derived basement topography (Figure 3-9) to determine the potential extent of associated sedimentary units across Musgrave Province (Figure 3-23). The palynological analyses and dating of the core samples from DH1a indicates a Late Miocene – Early Pliocene age (10–5 Ma) for the sampled interval (Krapf et al., 2019).

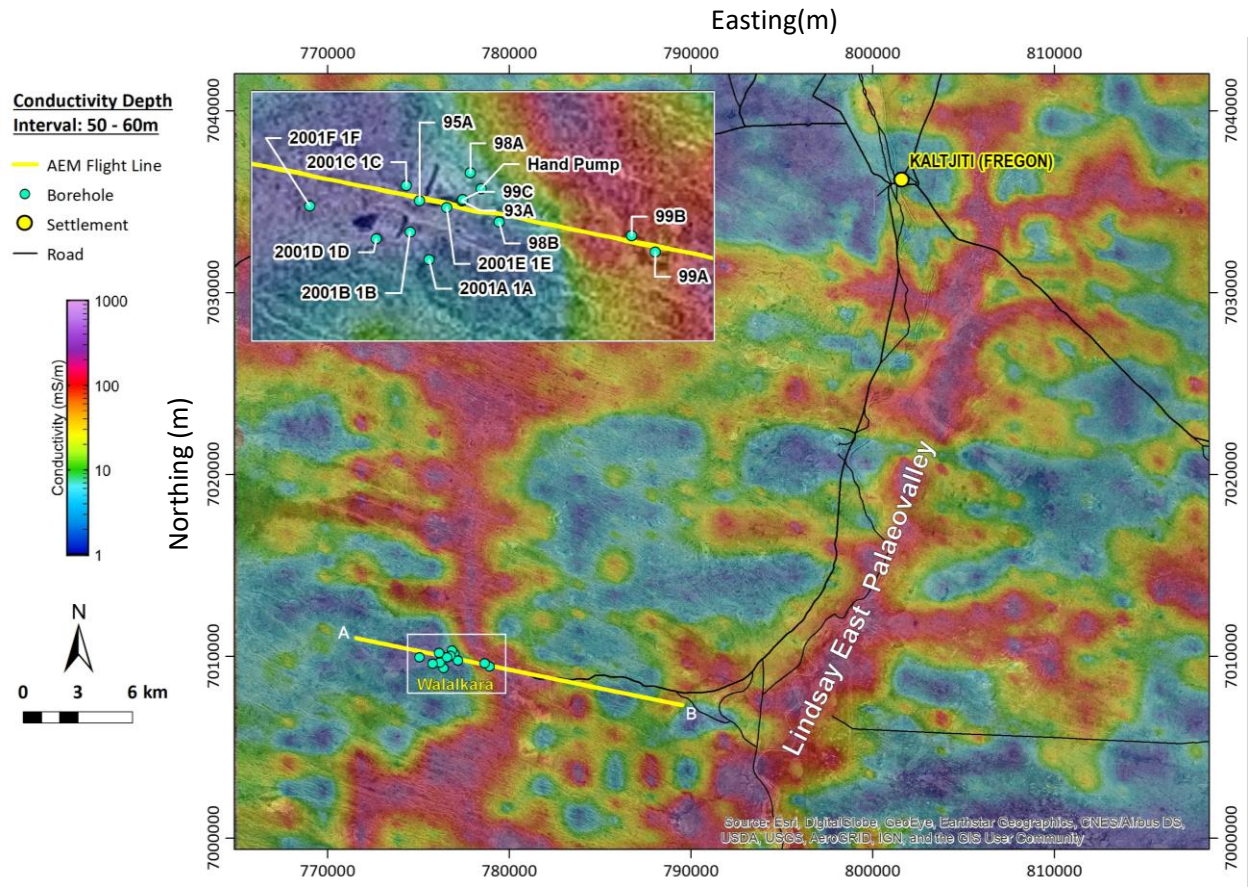

Figure 3-21. Pseudocoloured conductivity-depth interval for 50-60 m below ground surface, for an area south of Kaltjiti/Fregon. The location of a single east-west orientated flight line is shown (Line A-B) with bores clustered around the settlement of Walalkara indicated in blue. An inset map of the bore cluster around Walalkara is also shown in the top left of the image.

Assuming that mud-rich succession was mainly deposited in a marginal marine to fluvial to lacustrine depositional subaqueous environment, and that similar conditions prevailed in the lower parts of the palaeovalleys present across the Province, it is reasonable to assume this succession would be present in the interpreted palaeovalley that lies just east of Walalkara. In determining a geological section for this valley (Figure 3-22) we have assumed that materials similar to those recognised in DH1a are also present in this location. Coincidently the highest conductivities resolved in the conductivity-depth section are associated with the interpreted marginal marine sequence of silty clays and dark mudstones (top panel of Figure 3-22).

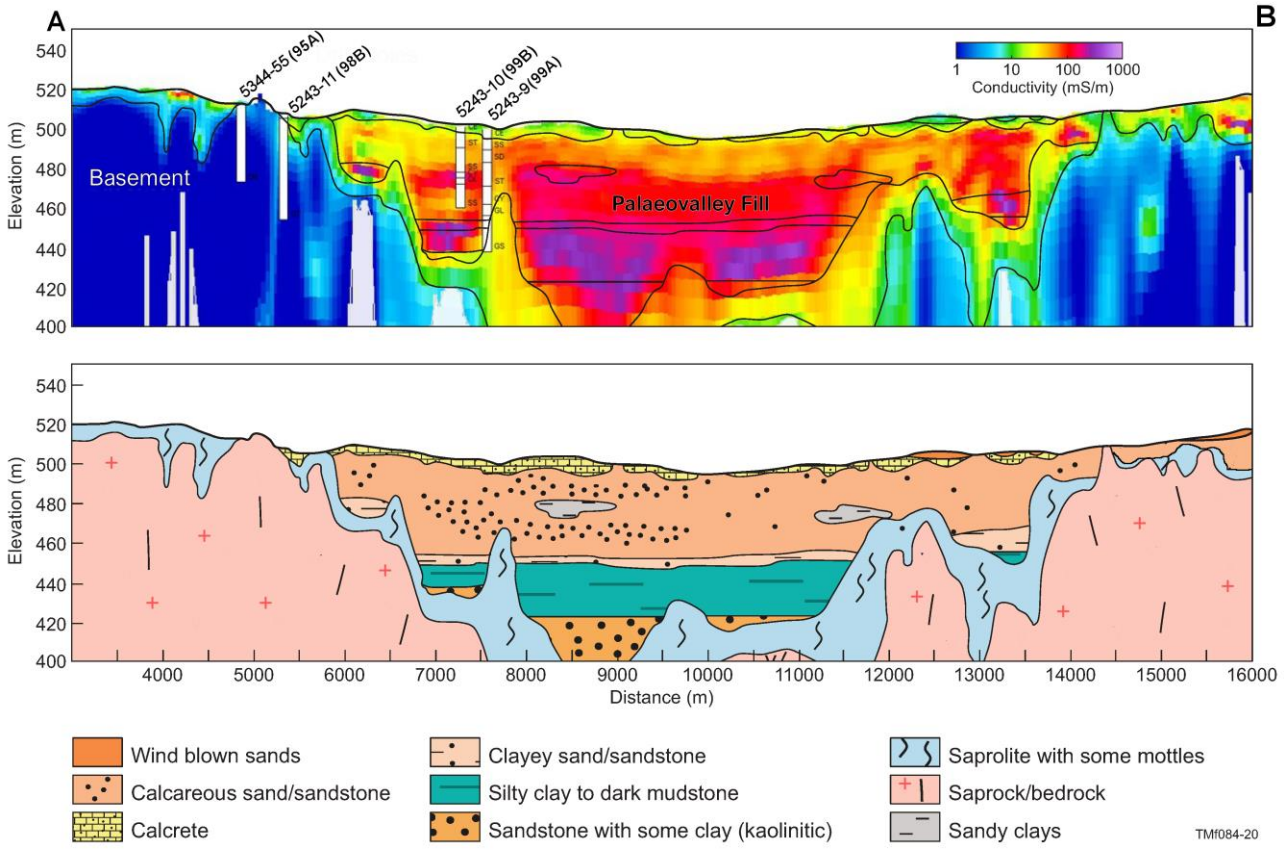

Figure 3-22. Interpreted geological cross section and associated conductivity-depth section for the airborne electromagnetic flight line A – B depicted in Figure 3-21. Several of the drillholes located on the eastern side of the palaeovalley are plotted on the conductivity-depth section (top panel).

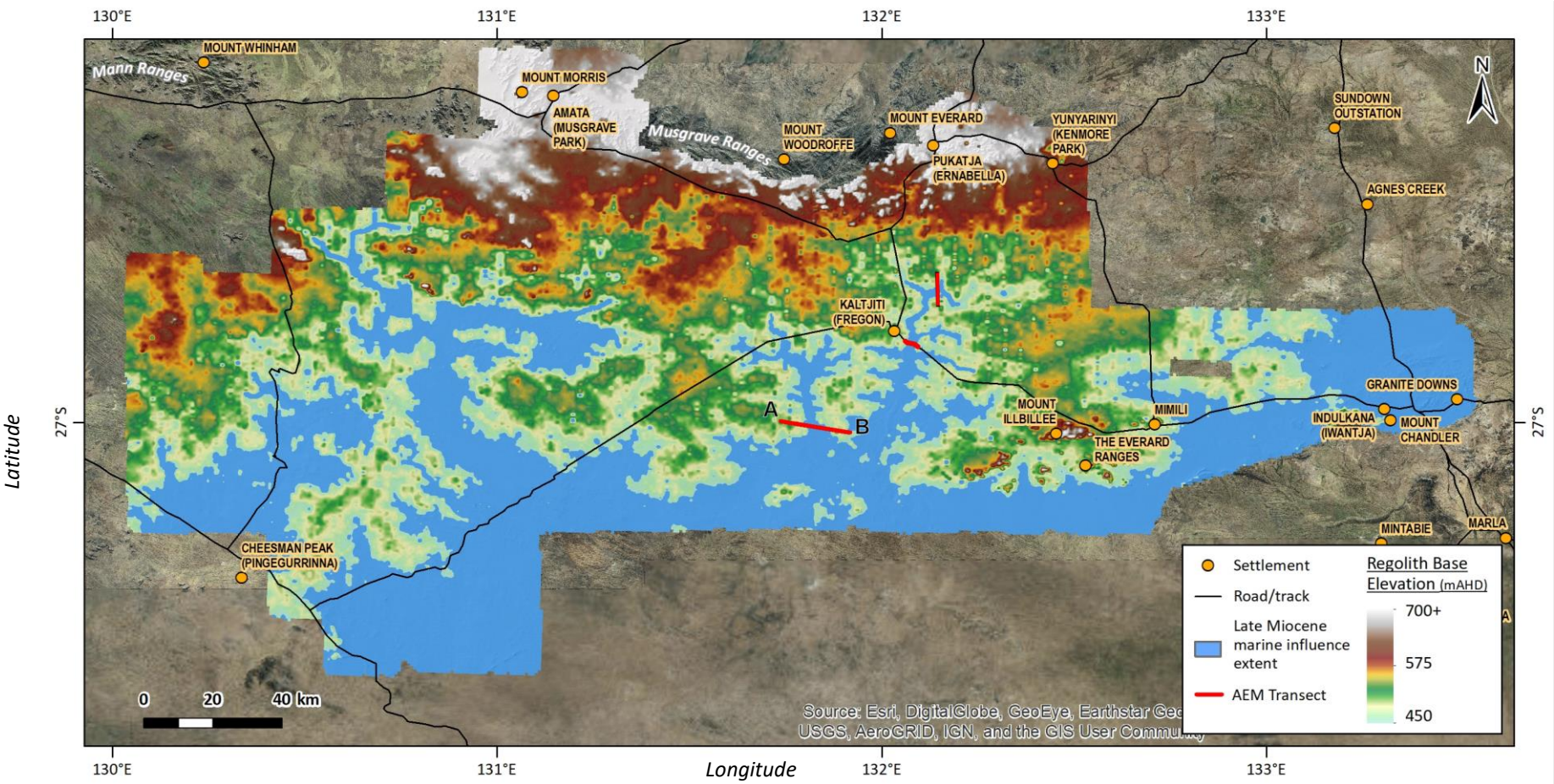

Figure 3-23. Modelled extent of an interpreted Late Miocene – Early Pliocene (10-5 Ma) marine influence across the Musgrave Province. The potential for marginal marine-estuarine facies present in the base of the palaeovalleys extends to the foothills of the contemporary Musgrave Ranges. The location of flight line A-B is indicated to the SSW of Kaltjiti/Fregon.

3.5 Groundwater recharge and flow

3.5.1 ENVIRONMENTAL TRACERS

Environmental tracers in groundwater are useful tools when coupled with traditional hydrogeological data (i.e. water level, chemistry, aquifer geometry, hydraulic properties) for developing a hydrogeological conceptual model (Cook and Böhlke, 2000), particularly in data-sparse regions. A wide range of tracers exist to characterise infiltration conditions, water–rock interactions, mixing of different groundwater sources and a large range in mean residence times (MRT) in aquifers (i.e. a few years to a million years). Mean residence times where multiple tracers are used or residence times (RT) for groundwater flow using a single tracer has been adopted as the preferred terminology in this report. The application of environmental tracers has proved invaluable in previous hydrogeological investigations in arid zones of central Australia (Calf et al. 1991; Cresswell et al. 1999; Cresswell et al. 2002; Harrington et al. 1999; Jacobson, 1989). In this report, environmental tracers and chemistry in groundwater previously published in Dodds et al. (2001), Craven (2012), Custance (2012), Leaney et al. (2013) and Kretschmer and Wohling (2014) have been collated, reviewed and where possible re-interpreted to either better conceptualise groundwater flow processes, estimate MRT in aquifers and or estimate groundwater recharge. In this report, the environmental tracers collated, reviewed and in some cases reinterpreted include, general chemistry (pH, electrical conductivity and alkalinity) as well as major and minor ions and tracers including stable hydrogen (^{2}H) and oxygen (^{18}O) isotopes, chlorofluorocarbons (CFCs, CFC-11 and CFC-12), carbon-13 (^{13}C), carbon-14 (^{14}C) and noble gases helium (He), neon (Ne), argon (Ar), krypton (Kr) and xenon (Xe).

3.5.2 RECHARGE ESTIMATION

Recharge estimates were derived where appropriate (i.e. either existing data as published in the previous studies including adequate bore construction, groundwater level information and field chemistry data, or by obtaining additional data from WaterConnect (DEW,2018)) using environmental tracers.

Chloride

The chloride mass balance (CMB) method is the most widely used approach for estimating recharge globally (Scanlon et al., 2006), and in Australia (Crosbie et al., 2010). It is popular because it is robust over many climate zones and is cost effective, requiring only analyses of chloride in groundwater and rainfall. It has previously been used across the Musgrave Province (Craven, 2012; Custance, 2012; Leaney et al., 2013; Kretschmer and Wohling, 2014) and the application here is an improvement from previous work by providing additional constraints that adhere more stringently to the assumptions of using CMB compared to previous estimates.

Wood (1999) listed the important assumptions behind estimating recharge using the CMB method as: (i) chloride in groundwater originates from rainfall falling on the land surface over an unconfined aquifer and not from flow from underlying or overlying aquifers; (ii) chloride is conservative in the system; (iii) steady-state conditions are assumed in that the fluxes of chloride and water have not changed over time; and (iv) there is no recycling of chloride within the aquifer.

The CMB is possible because chloride is excluded from evapotranspired water during evaporation and transpiration and so concentrates in the root zone. This concentrated water then leaches downwards to the watertable to become recharge. At its simplest, recharge is calculated as:

$$R = \frac{100 \times D}{Cl_{gw}} \quad (1)$$

where *R* is mean annual recharge (mm/year), *D* is mean annual chloride deposition (kg/ha/year) (Davies and Crosbie, 2014; Davies and Crosbie, 2017), Cl_{gw} is chloride concentration of the groundwater (mg/L) available from bores in the Musgrave Province (DEW, 2018).

The CMB method was employed here for estimating point recharge at individual bores only where groundwater chloride was measured for bores screened <10 m below the water table using equation (1). All other bores were excluded as chloride in groundwater at depths >10 m below the water table are likely to have evolved from lateral flow upgradient of the bore. Recharge was therefore estimated only where groundwater had been sampled from unconfined portions of the aquifers (at a depth of <10 m below the groundwater table) in order to meet the assumptions of the method in that all chloride comes from rainfall, is conservative and is in steady state.

3.5.3 GEOCHEMICAL MODELLING

Geochemical modelling using field measurements of groundwater pH and temperature, as well as major ion chemistry was performed using the PHREEQC model (Parkhurst and Appelo, 2013). The purpose of the modelling was to: (i) determine the saturation indices (SI) for groundwater with respect to calcite and gypsum, and (ii) ascertain the chemical speciation of aqueous CO_2 and HCO_3 in relation to the total dissolved inorganic carbon (TDIC) in groundwater. The latter was necessary to correct initial ^{14}C values in groundwater for the potential addition of dead carbon from either mixing with atmospheric CO_2 during recharge or isotopic exchange during flow through the aquifer, and to derive ^{14}C corrected RTs.

Accounting for dead carbon to total dissolved inorganic carbon (TDIC)

Dead carbon – that is, carbon devoid of ^{14}C due to extensive radioactive decay – can be added to the TDIC pool through production of CO_2 by oxidation of old organic matter, and weathering of carbonate in either the soil, unsaturated zone or saturated zone of the aquifer. There are a number of existing 'correction schemes' or models for estimating the initial activity (Ao) of ^{14}C when dilution by water-rock interactions (i.e. carbonate weathering) is considered to be important (Fontes and Garnier, 1979; Ingerson and Pearson, 1964; Mook, 1980; Tamers, 1967). In this assessment, four of these existing models (Tamers, Pearson, Fontes Garnier and Mook), which use a combination of chemical (field pH, field alkalinity, major ions) and isotopic data (^{13}C and ^{14}C), were adopted to provide and evaluate range of MRTs that account for addition of dead carbon. Aqueous CO_2 and HCO_3 speciation results from PHREEQC were used along with the following assumed values for soil gas and carbonate minerals ^{14}C activity and $\delta^{13}C$ ratio, as well as stable isotope enrichment between CO_2 and HCO_3 (Egb), or HCO_3 and carbonate minerals (Ecb) (Table 3-3). The basis for these assumptions is that soil gas is derived from predominantly C3-type vegetation in the arid zone, and carbonate minerals are primarily from pedogenic calcrete present in numerous lithological logs from drilling. The values adopted are similar to those used by both Kretschmer and Wohling (2014) for their study in the Musgrave Province.

Table 3-3: Assumed values for various end members used in ^{14}C corrections.

END MEMBER	VALUE	UNIT
Soil gas ^{14}C	104	pmC
Soil gas $\delta^{13}C$	–14	‰
Carbonate ^{14}C	0	pmC
Carbonate $\delta^{13}C$	0	‰
E_{gb} (CO_2 to HCO_3)	5	‰
E_{cb} (HCO_3 to carbonate)	0	‰

Chlorofluorocarbons and carbon-14

Unconfined aquifer – piston flow model

All of the groundwater samples previously published come from unconfined portions of aquifers. In this case, long-term mean annual recharge rates were estimated based on an assumption of only vertical flow (piston flow model – PFM), which is acceptable provided the depth of sample is small relative to the thickness of the aquifer (in this case only for samples collected >10 m below the groundwater table). Accordingly, recharge rate *R* (mm/year) is given by:

$$R = \frac{z\varepsilon}{t} \tag{2}$$

where *z* is depth of sample below watertable, taken as the mid-point of the screen [m], ε is aquifer porosity and *t* is the RT (years). For samples where the residence time was able to be determined from ^{14}C (<104 pmC), and was greater than zero, these values were used in equation (2). Otherwise where 'modern' ^{14}C residence times (i.e. zero years) were derived, the residence times derived from CFC-12 data were used as input to equation (2). Residence times derived from CFCs assumed the atmospheric CFC history is similar to that recorded at Cape Grim. For ^{14}C, RT was calculated using equation (3):

$$t = (1/\lambda).\ln(C_o/C) \tag{3}$$

where (C_o) is the initial concentration of ^{14}C for each sample, (λ) is ln2/($t_{1/2}$) using a ^{14}C half-life of 5730 years and (C) is the measured ^{14}C concentrations in groundwater.

Unconfined aquifer – exponential mixing model

Whilst all of the groundwater samples were collected from unconfined portions of the aquifer, many different samples were collected from aquifers in different hydrogeological units where the depth below the watertable (DBWT) was >10 m and therefore the assumption of only vertical flow may not be valid, particularly with increasing depth below the watertable. In this case, the exponential mixing model (EMM) was considered to estimate long-term mean recharge rates where groundwater flow is initially vertical, but as the depth below the watertable increases, it eventually is horizontal. That is, the conceptual model is that the MRT exponentially increases with depth below the watertable (Vogel, 1967). Using this conceptual model and its assumptions, a recharge rate can be estimated using a MRT that is derived from either CFC or ^{14}C concentrations in the aquifer:

$$t = \frac{H\varepsilon}{R}\, ln\left(\frac{H}{H-z}\right) \tag{4}$$

where *H* is the aquifer thickness (m) and all other parameters are as previously defined.

4 Results

4.1 Groundwater salinity

Groundwater salinity data represented as total dissolved solids (TDS) were collated from WaterConnect (DEW, 2018). These data have been superimposed over the Multi-resolution Valley Bottom Flatness (MrVBF) topographic index (Gallant and Dowling, 2003) to evaluate the spatial trends in groundwater salinity in relation to erosional outcropping bedrock versus extensive depositional areas including alluvium, colluvium and buried palaeovalleys (Figure 4-1). Overall, salinity ranges from 105 to 38,710 mg/L (n=440) with a mean and median salinity of 2159 and 988 mg/L respectively. At opposing ends of the salinity data distribution, salinity values for the 25th percentile of all samples (n=110) is 680 mg/L and for the 75th percentile (n=330) is 1,633 mg/L. Spatially, salinity in bedrock aquifers of the Birksgate Complex, Giles Complex and Pitjantjatjara Supersuite around the Musgrave, Mann and Tomkinson ranges is generally fresh (i.e. <1000 mg/L). Moving away from the ranges, salinity increases from fresh to brackish (i.e. 1000 to 3000 mg/L) with increasing distance from the ranges. The highest salinity occurs in the south-east geological boundary of the Musgrave Province where alluvium/colluvium is prominent and groundwater recharge is low.

4.2 Groundwater chemistry

Chemistry data from a total of eighty-two bores in five different aquifers (alluvial/colluvial, bedrock, calcrete, sandstone and siltstone aquifers) were collated and reviewed. The interpretation of hydrochemical data has focussed only on those samples whose chemical analyses from various analytical laboratories returned a charge balance error (CBE) within ±20 %. While ±20 % is considered a 'reasonable' error, the CBE calculations highlighted that many samples have a CBE higher than 10 %, likely reflecting the differences in both the nature of field sampling techniques as well as the analytical facilities at different laboratories used in the previous studies. The chemistry analyses from a total of 25 groundwater bores have been excluded from the interpretation of results as they returned a CBE >20 %.

The ion composition of groundwater samples collected from both the alluvial/colluvial (n=13) and bedrock aquifers (n=26) generally displays a hydrochemical evolution from magnesium-bicarbonate to sodium-chloride type waters (Figure 4-2). Those samples with a calcium-magnesium-bicarbonate composition are generally from groundwater bores in the northern more elevated parts of the province in areas of either outcropping bedrock or adjacent outcropping bedrock where alluvium and colluvium have accumulated over shallow bedrock. Those samples with a sodium-chloride composition were collected from groundwater bores further south in the province out on the plains where bedrock outcrops are less prominent, and alluvium and colluvium are thicker and more extensive. Only a handful of samples were collected from the sandstone (n=3) and calcrete (n=3) aquifers given their limited and patchy existence across the province. In both cases, all samples are of a sodium-chloride composition (Figure 4-2).

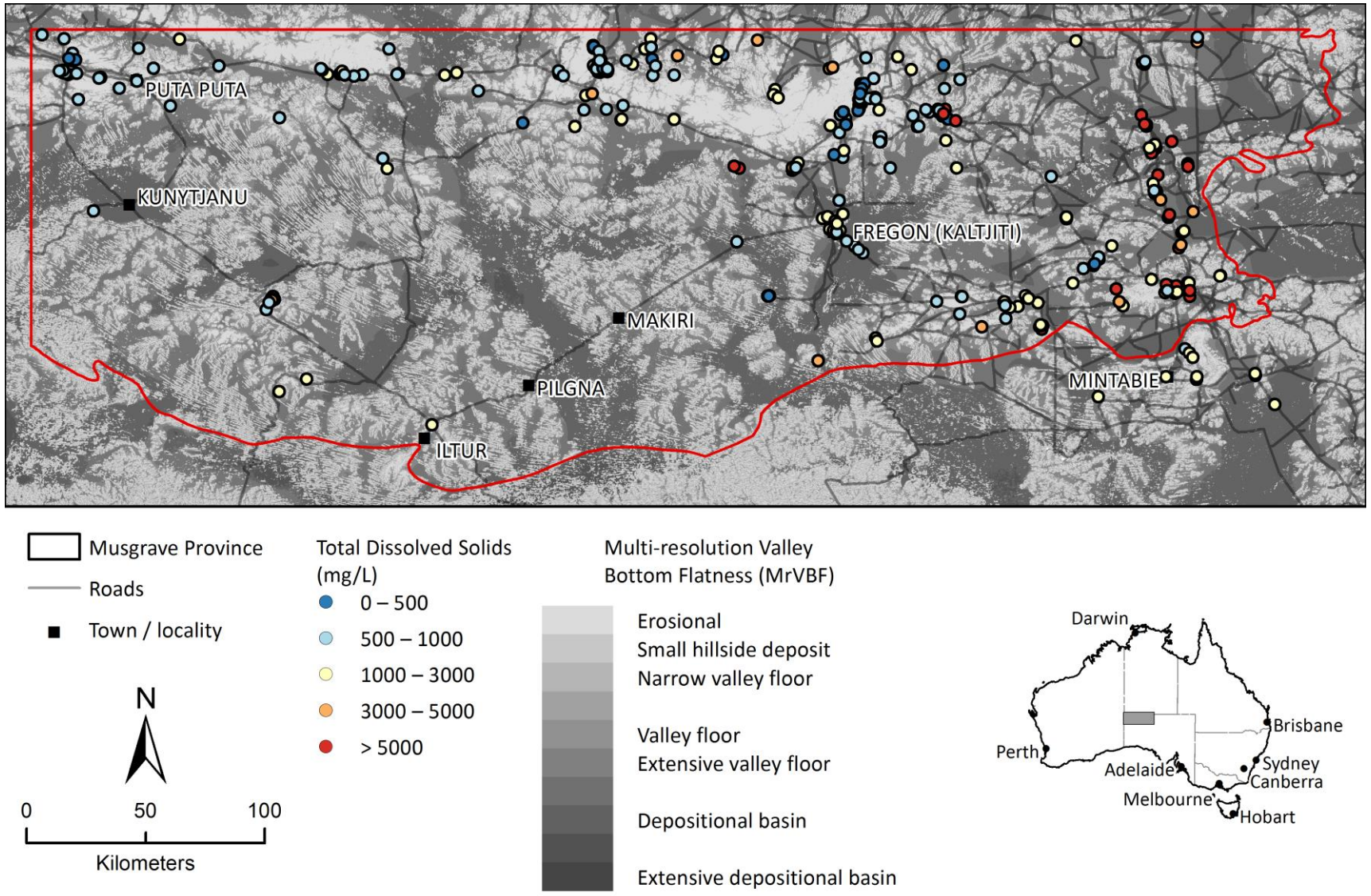

Figure 4-1. Groundwater salinity for groundwater bores across the Musgrave Province. Spatial data collated from WaterConnect (DEW, 2018).

Groundwater samples from most aquifers are enriched in sodium (Na), calcium (Ca), bicarbonate (HCO_3) and magnesium (Mg) relative to rainfall of marine origin, the exception being a few samples from the sandstone and calcrete aquifers lacking enrichment in Na (Figure 4-3a to d). Chloride (Cl) to bromide (Br) ratios relative to Cl (Figure 4-3e) do not indicate halite dissolution indicating that Cl is conservative in the system and its only source is from rainfall. Sodium to HCO_3 ratios are significantly lower than that of rainfall of marine origin (Figure 4-3f) suggesting an additional source of HCO_3. An analysis of lithology logs from groundwater bores indicates several pedogenic calcrete horizons occur in patches across the central part of the province. The source of some calcium and most HCO_3 is likely from the mineral weathering of these calcrete units. Geochemical modelling results using PHREEQC indicate that most groundwater samples have significant portions of their TDIC as aqueous HCO_3 compared to CO_2 (Table 4-1). All samples were below saturation (saturation index <0) with respect to gypsum, but half of the samples were saturated with respect to calcite again reflecting a source of additional carbonate to groundwater.

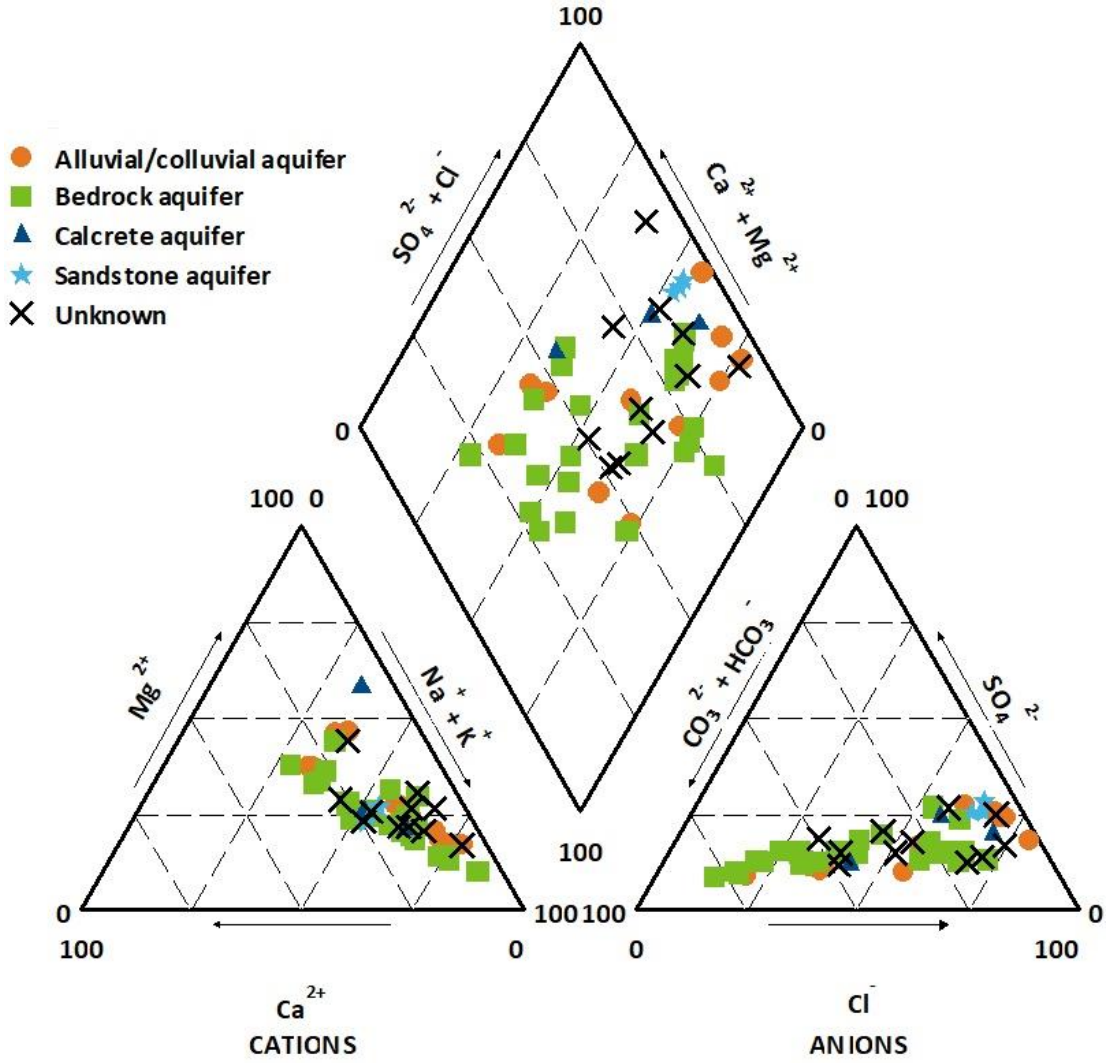

Figure 4-2. Piper diagram of the major ion composition of groundwater from aquifers in four different hydrogeological units across the Musgrave Province. Data collated from Dodds et al. (2001); Craven (2012); Custance (2012); Leaney et al. (2013) and Kretschmer and Wohling (2014).

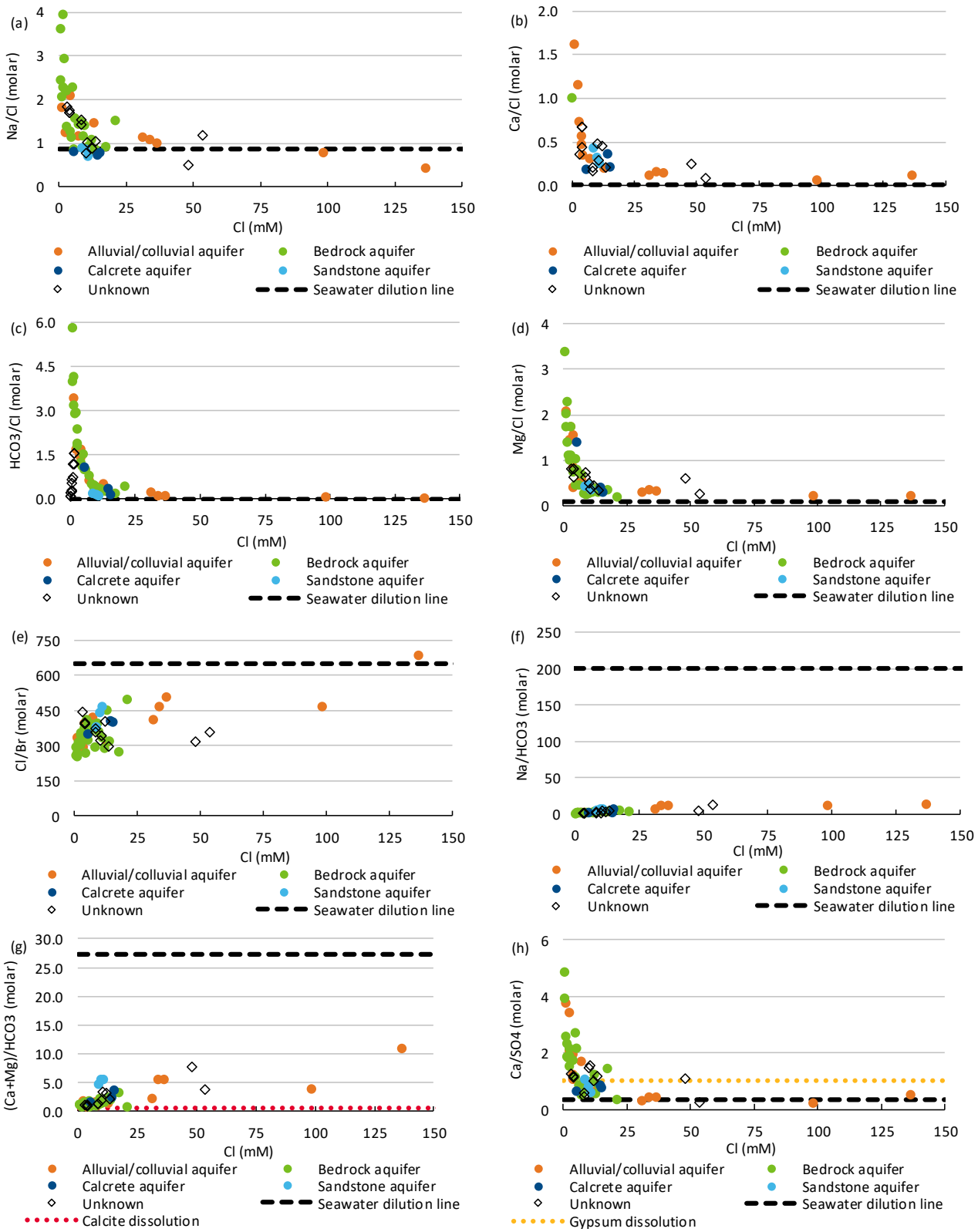

Figure 4-3. Major ion ratios relative to chloride for groundwater from aquifers in four different hydrogeological units. Data collated from Dodds et al. (2001); Craven (2012); Custance (2012); Leaney et al. (2013) and Kretschmer and Wohling (2014).

Table 4-1: Speciation results from geochemical modelling.

UNIT NUMBER	AQUIFER	AQUEOUS CO_2 (mM)	AQUEOUS HCO_3 (mM)	SATURATION INDEX (SI) CALCITE	SATURATION INDEX (SI) GYPSUM
534400018	Alluvial/colluvial aquifer	0.90	5.67	-0.41	-2.22
534500021	Alluvial/colluvial aquifer	0.32	6.39	0.20	-2.11
524400018	Bedrock aquifer	0.42	5.42	-0.15	-1.94
534400035	Bedrock aquifer	0.26	3.29	-0.09	-1.49
544300028	Bedrock aquifer	0.15	3.83	0.08	-1.94
544300025	Bedrock aquifer	0.32	4.09	-0.19	-1.97
544300028	Bedrock aquifer	0.15	3.83	0.08	-1.93
544400015	Bedrock aquifer	0.58	7.41	0.10	-2.06
554500051	Bedrock aquifer	0.35	5.10	1.15	-1.39
534300002	Unknown aquifer	0.13	2.11	-0.14	-1.81
534400008	Unknown aquifer	0.23	4.53	0.07	-2.10
534400050	Unknown aquifer	0.50	3.29	-0.11	-2.19
534400071	Unknown aquifer	0.32	6.47	-0.08	-6.92

4.3 Groundwater yield

Bore yield data were collated from WaterConnect (DEW, 2018). These data have been superimposed over the Multi-resolution Valley Bottom Flatness (MrVBF) topographic index (Gallant and Dowling, 2003) to evaluate the spatial trends in bore yield in relation to erosional outcropping bedrock versus extensive depositional areas including alluvium, colluvium and buried palaeovalleys (Figure 4-4). Overall, bore yields range from 1 to 10 L/s (n=198), with a mean and median of 2 and 1 L/s respectively. At opposing ends of the bore yield data distribution, bore yield values for the 25th percentile of all samples (n=106) is 1 L/s and for the 75th percentile (n=157) is 2 L/s. Spatially, bore yields in bedrock aquifers of the Birksgate Complex, Giles Complex and Pitjantjatjara Supersuite around the Musgrave, Mann and Tomkinson ranges are generally low (i.e. $\leq$ 1 L/s). Moving away from the ranges, bore yields increase slightly in depositional areas of alluvium, colluvium and buried palaeovalleys. The highest bore yields (i.e. >5 L/s) occur sporadically around the ranges in the northern part of the Musgrave Province where colluvium is prominent at the foot of the ranges in valleys. It is important to note that these bore yields are only indicative of 'potential' groundwater abstraction rates. These data almost entirely come from short duration (i.e. 1 to 3 hour) bore yield tests by air lifting or submersible pumps at the time of drilling. Evaluation of this bore yield data is limited because of the lack of the duration of tests, the capacity of the air compressor or submersible pumps used and the nature of the bore construction. Long-term pump tests (i.e. 24 to 48 hours) and adequate bore construction are required to better evaluate bore and aquifer yield rates.

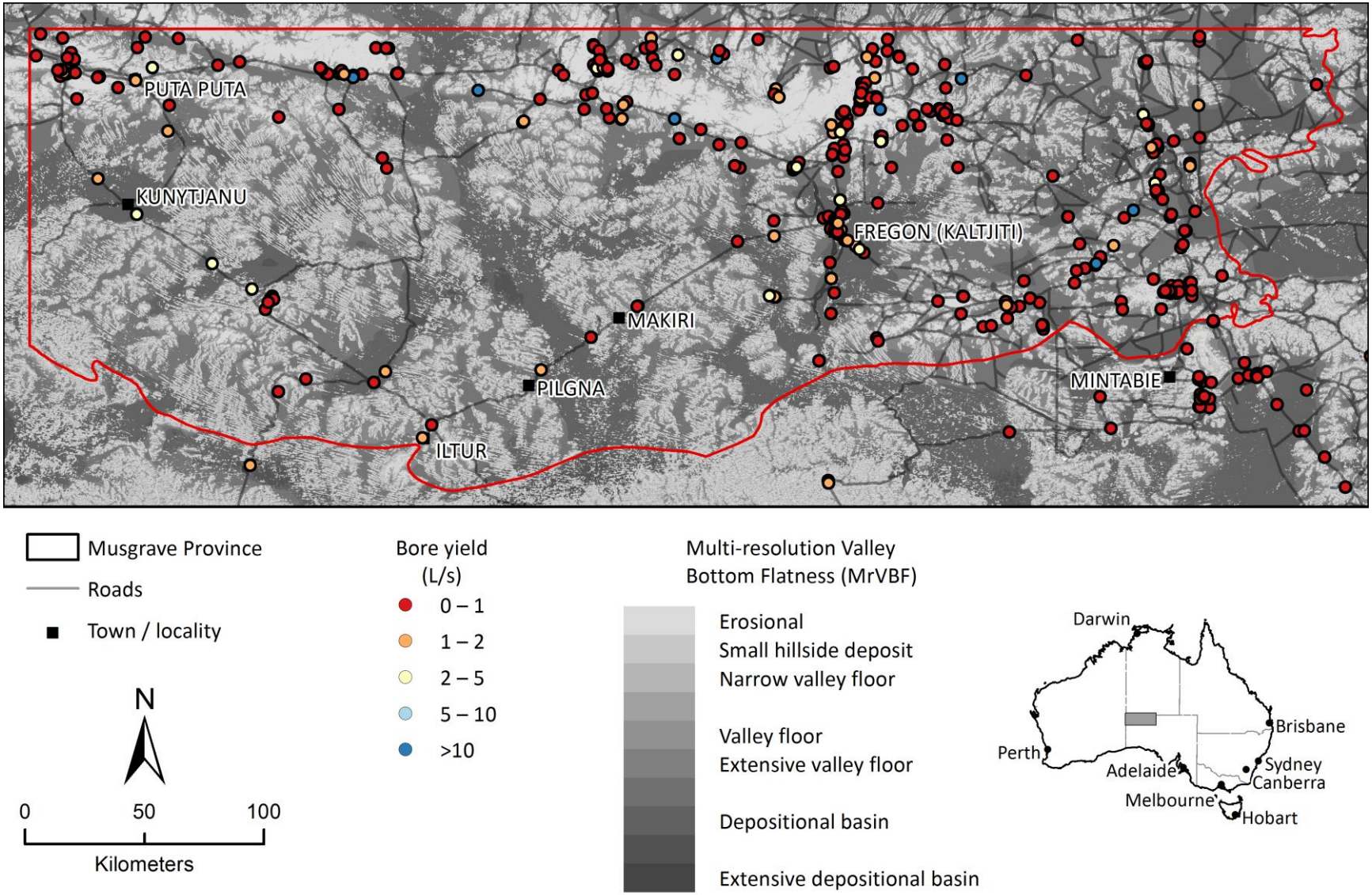

Figure 4-4. Bore yield for groundwater bores across the Musgrave Province. Spatial Data collated from WaterConnect (DEW, 2018).

4.4 Hydrogeological framework

4.4.1 THREE-DIMENSIONAL VISUALISATION OF REGIONAL AIRBORNE ELECTROMAGNETIC DATA

3D visualisation of spatial patterns of ground conductivity at varying depth intervals below the ground surface. Each image shows the entire AEM depth section draped onto the 3D (Figures 4-5 – 4-11).

4.4.2 3D GEOLOGICAL MODEL OF PALAEOVALLEY SYSTEMS

The 3D geological model of the Musgrave Province has been developed using AEM conductivity-depth slices from the inversion models presented in previous sections and SRTM digital elevation data using SKUA-GOCAD® 3D geological modelling software (Figure 4-12). The conductivity-depth slices of the 10 m intervals were imported into the 3D geological modelling software framework, to assess the spatial patterns of subsurface conductivity at varying depth intervals below the ground surface.

As described by Munday et al. (2013), the AEM data permit the definition of the extent of the palaeovalley systems and their spatial relationships to the geological basement (i.e. characterising the interface between the palaeovalley depositional system (representing alluvial aquifer systems) and the basement which is comprised of fractured rocks). In the current version of the 3D geological model developed for the Musgrave Province, only two categories were differentiated (palaeovalley sediments versus undifferentiated basement).

Colluvial sediments are likely to be restricted to a small area in the northern part of the Musgrave Province near the Musgrave Ranges, where steep topographic gradients exist. Krapf et al. (2019), based on lithological logs of the new drill-hole DH1a in the Lindsay East palaeovalley system, suggested that the interface between surficial sandplain deposits (Holocene Aeolian sediments) and palaeovalley systems is intersected at a depth of approximately 30 m. Krapf et al. (2019) therefore assumed a conductivity depth slice of 26.2-–31.8 m as the top of the palaeovalley system network for mapping of the extent of the palaeovalley system network in the APY lands. This is similar to the patterns shown in the AEM depth slices (Section 4.5.1).

At the 0-10 and 10-20 m AEM depth intervals, applying a threshold of 45 or 50 Ohm, much of the Musgrave Province except for outcropping basement highs is characterised by conductive sediments above the threshold and the definition of the palaeovalley systems remains relatively poor. This may suggest that sandplain sediments form a relatively continuous cover over much of the Musgrave Province at these depths apart from topographically elevated basement highs. Starting from approximately the 30–40 m AEM depth interval, the definition of the palaeovalley systems becomes significantly clearer with a well-defined network of major alluvial channels and tributary systems.

For the current version of the 3D geological model, colluvial sediments at the foothills of the Musgrave Range, sandplain (aeolian) sediments and palaeovalley (alluvial) sediments were not yet differentiated, as there is an insufficient spatial coverage of drill hole data throughout the area to distinguish these units at the regional scale, with most existing bores located within the eastern part of the model domain north of Kaltjiti/Fregon and only few bores drilled in the western part. However, based on the observation from the AEM data and if we assume that the thickness of the surficial sandplain deposits overlying the palaeovalley sediments is similar throughout the APY Lands, it is possible to use the information from DH1a and from the regional AEM to derive an additional model realisation where the upper approximately 30 m are considered as sandplain deposits.

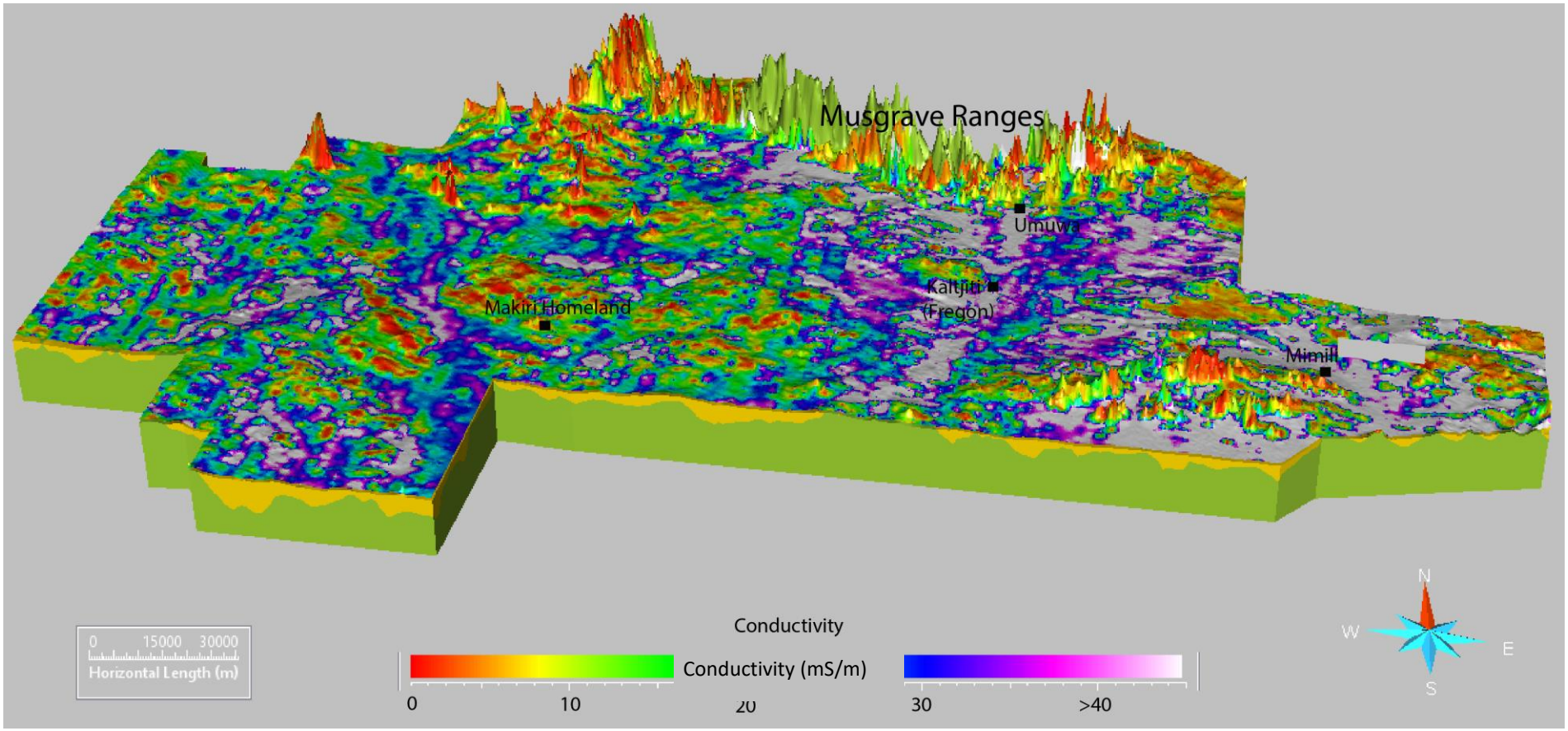

Figure 4-5. Three-dimensional representation of airborne electromagnetic data at 0-10 m depth.

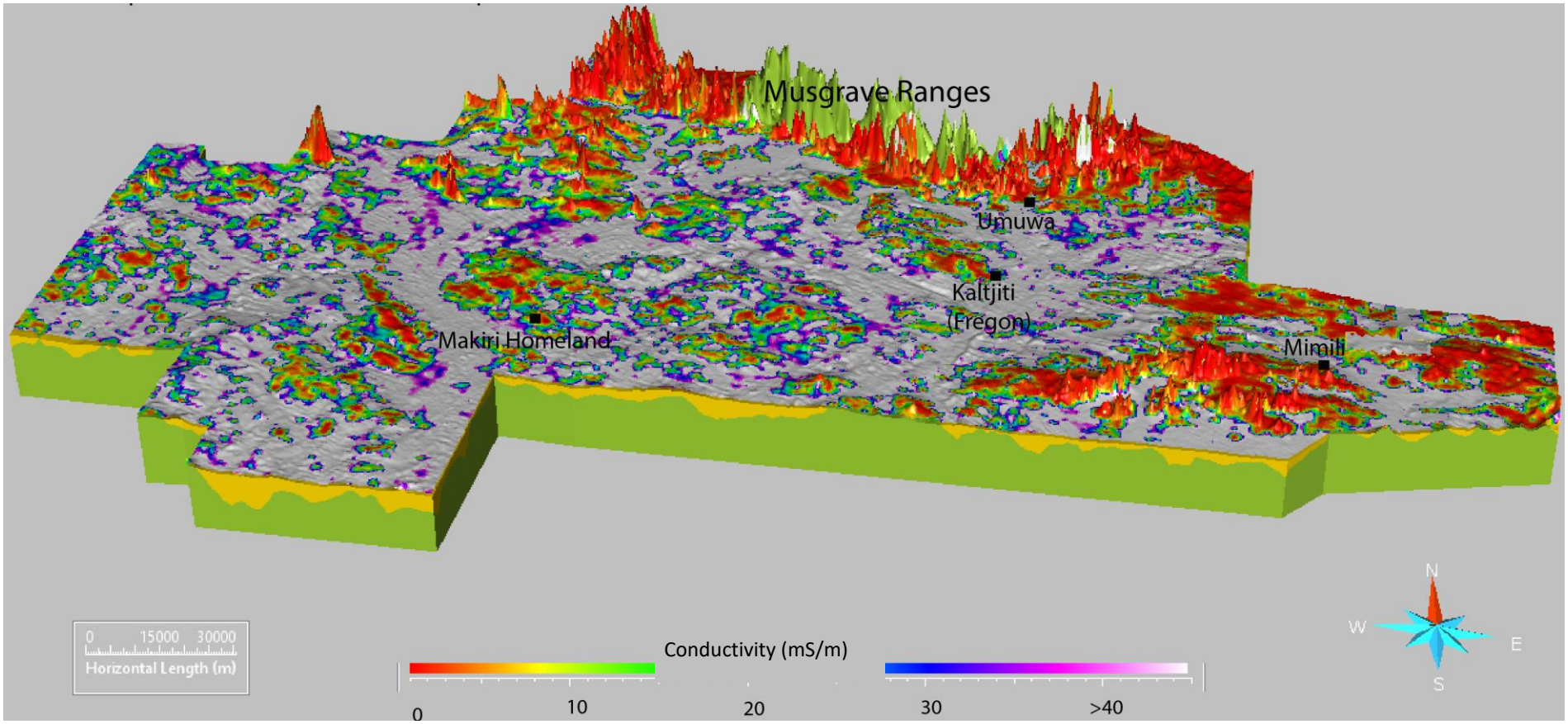

Figure 4-6. Three-dimensional representation of airborne electromagnetic data superimposed on 3D geological model at 10-20 m depth.

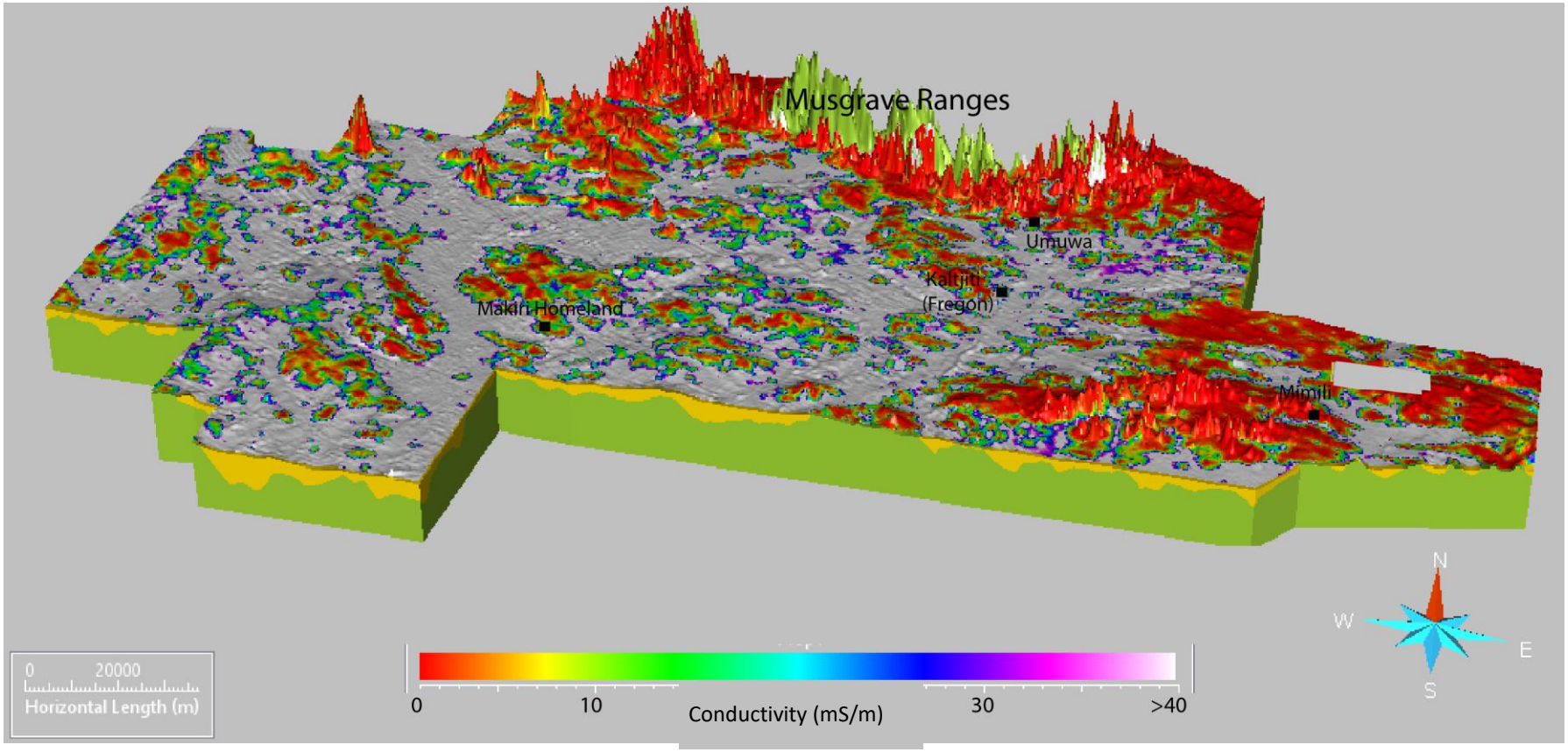

Figure 4-7. Three-dimensional representation of airborne electromagnetic data superimposed on 3D geological model at 20-30 m depth.

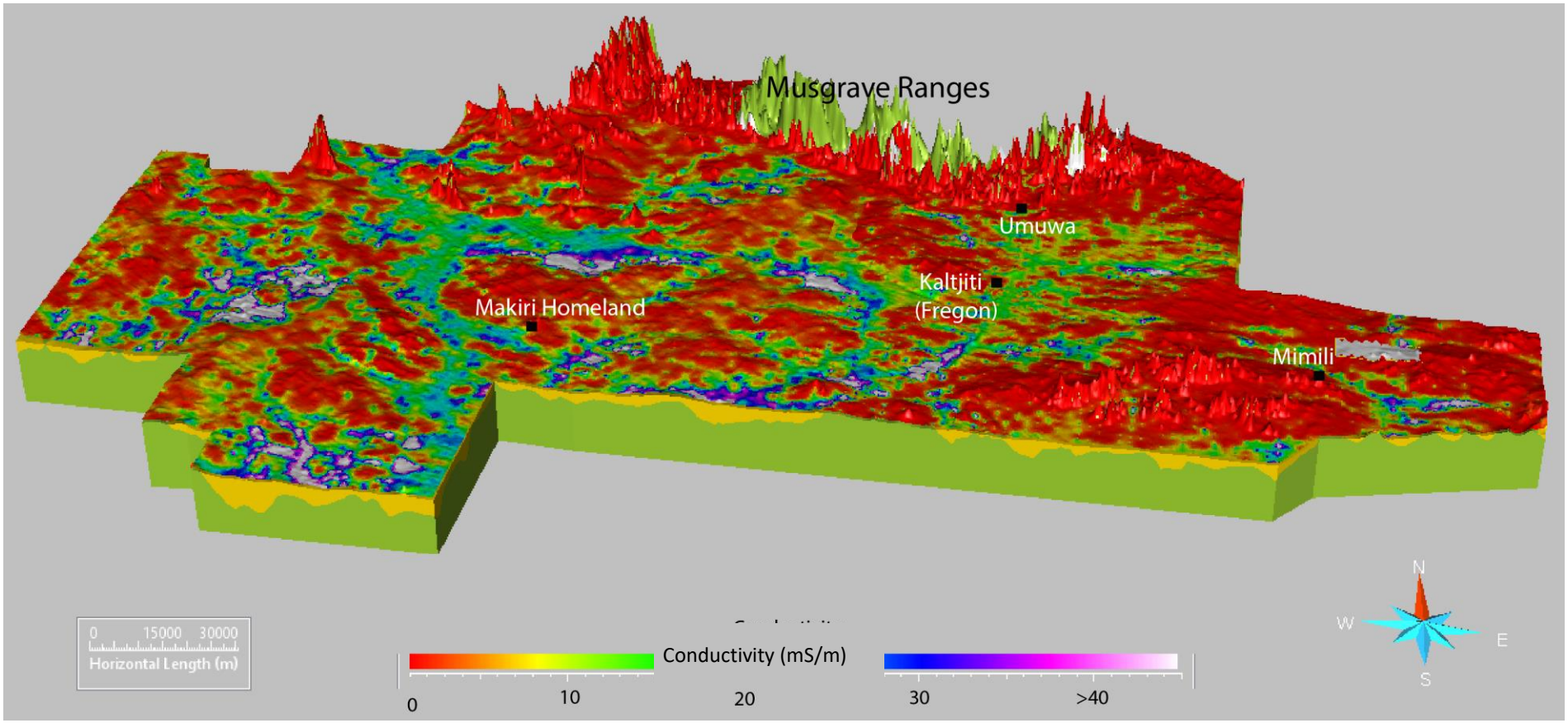

Figure 4-8. Three-dimensional representation of airborne electromagnetic data superimposed on 3D geological model at 30-40 m depth.

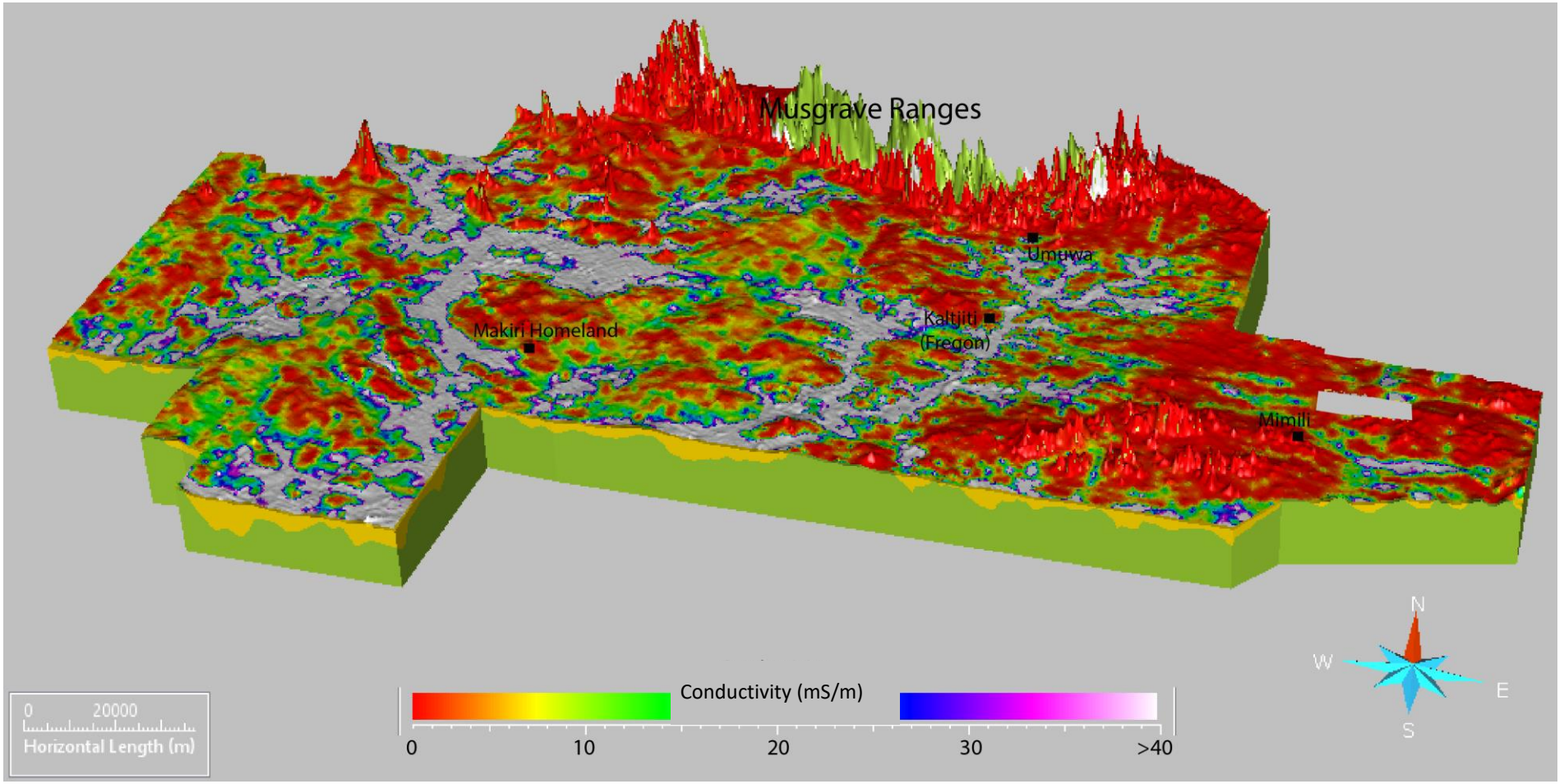

Figure 4-9. Three-dimensional representation of airborne electromagnetic data superimposed on 3D geological model at 60-70 m depth.

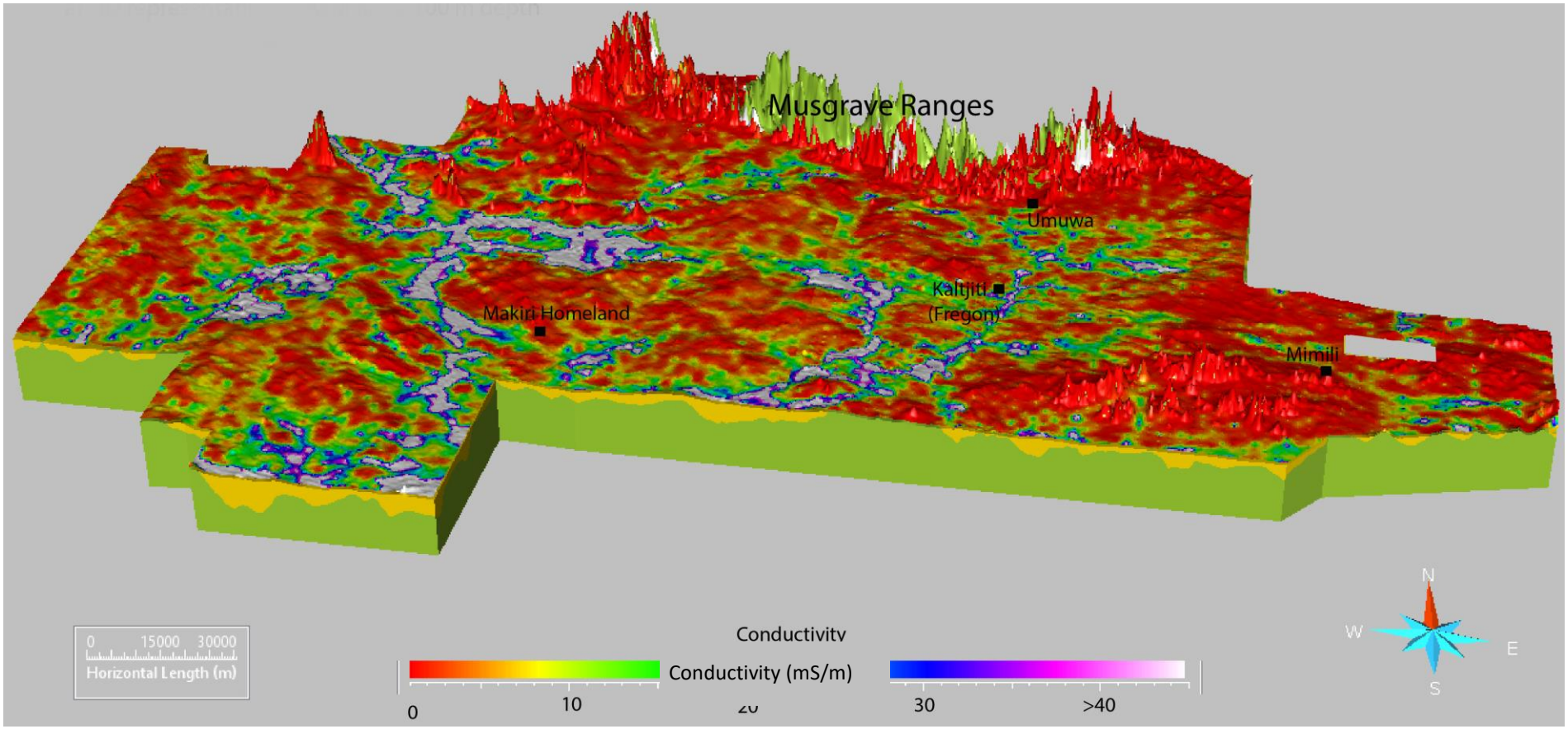

Figure 4-10. Three-dimensional representation of airborne electromagnetic data superimposed on 3D geological model at 90-100 m depth.

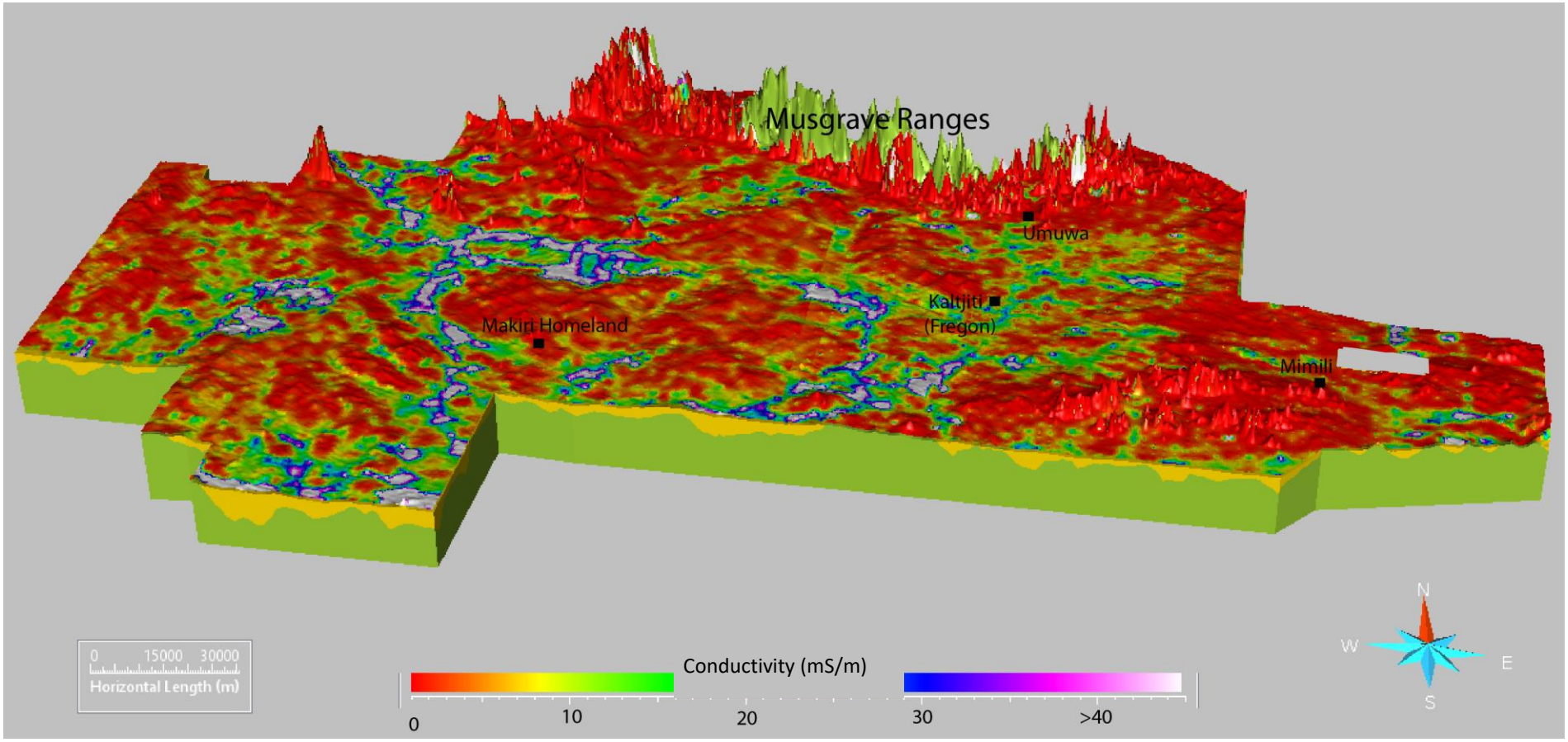

Figure 4-11. Three-dimensional representation of airborne electromagnetic data superimposed on 3D geological model at 130-140 m depth.

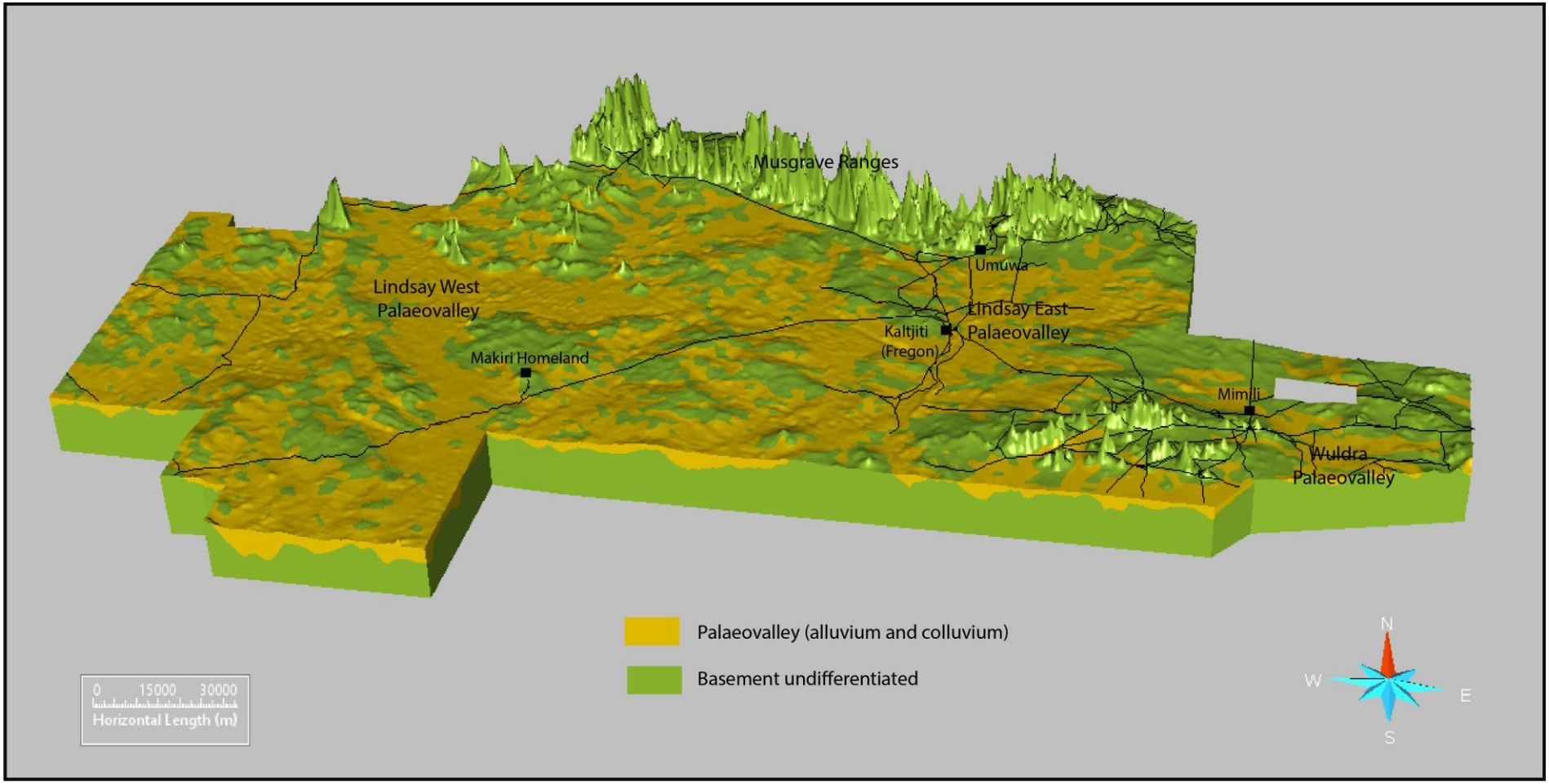

Figure 4-12. Three-dimensional geological model of the Lindsay West and Lindsay East palaeovalley systems with regional road network and communities.

In the 3D geological model (Figure 4-12), several major palaeovalley systems can be differentiated. The geometry of the palaeovalley systems at depth is shown in Figure 4-13 a to c. These figures highlight that two major palaeovalley systems, the Lindsay East and Lindsay West palaeovalley systems, exist within the model domain. The relationship between the course of the palaeovalleys and outcropping bedrock is shown in Figure 4 13 c. Regionally, the orientation of the main channels of the Lindsay East and Lindsay West palaeovalley systems is from north to south. However, in some areas such as north of the Makiri Homeland, the courses of the palaeovalley systems are significantly diverted. In this location, for instance, the Lindsay West palaeovalley system is diverted to the west flowing around a prominent basement high (Figure 4-13 c) and then changes course to the south. Smaller basement highs also exist within some channels of the palaeovalley systems, resulting in local diversions of the course of the streams which deposited the alluvial sediments.

Palaeovalley system thicknesses are presented in Figure 4-14. The thicknesses shown here include the sandplain sediments (approximately 20-30 m), and the actual thicknesses of the palaeovalley (alluvial) deposits are consequently lower by about 20-30 m. Actual maximum thicknesses of the palaeovalley systems are likely to be approximately 90-100 m. The thickness of palaeovalley sediments in the Lindsay West Palaeovalley system appears to be higher than in the Lindsay East Palaeovalley system, and the width of the Lindsay West Palaeovalley system also appears to be larger than that of the Lindsay East Palaeovalley system.

4.4.3 THE INFLUENCE OF GEOLOGICAL STRUCTURE ON PALAEOVALLEY DEVELOPMENT, DISTRIBUTION AND GEOMETRY

Faulting is widespread throughout the Musgrave Province, the extent of which is alluded to in the regional airborne magnetic images (Figure 3-2, Figure 4-15, and Figure 4-16) which are characterised by a series of laterally continuous, approximately east–west-striking, magnetically low, lineaments. Several of these have been interpreted as major structures (Major and Conor 1993; Rankin and Newton 2002). The steeper strike-slip structures (Aitken et al. 2009; Korsch and Kositcin 2010 and Pawley et al. 2014), located in the core of the province, include the Mann, Echo and Wintiginna faults (see Figure 4-16).

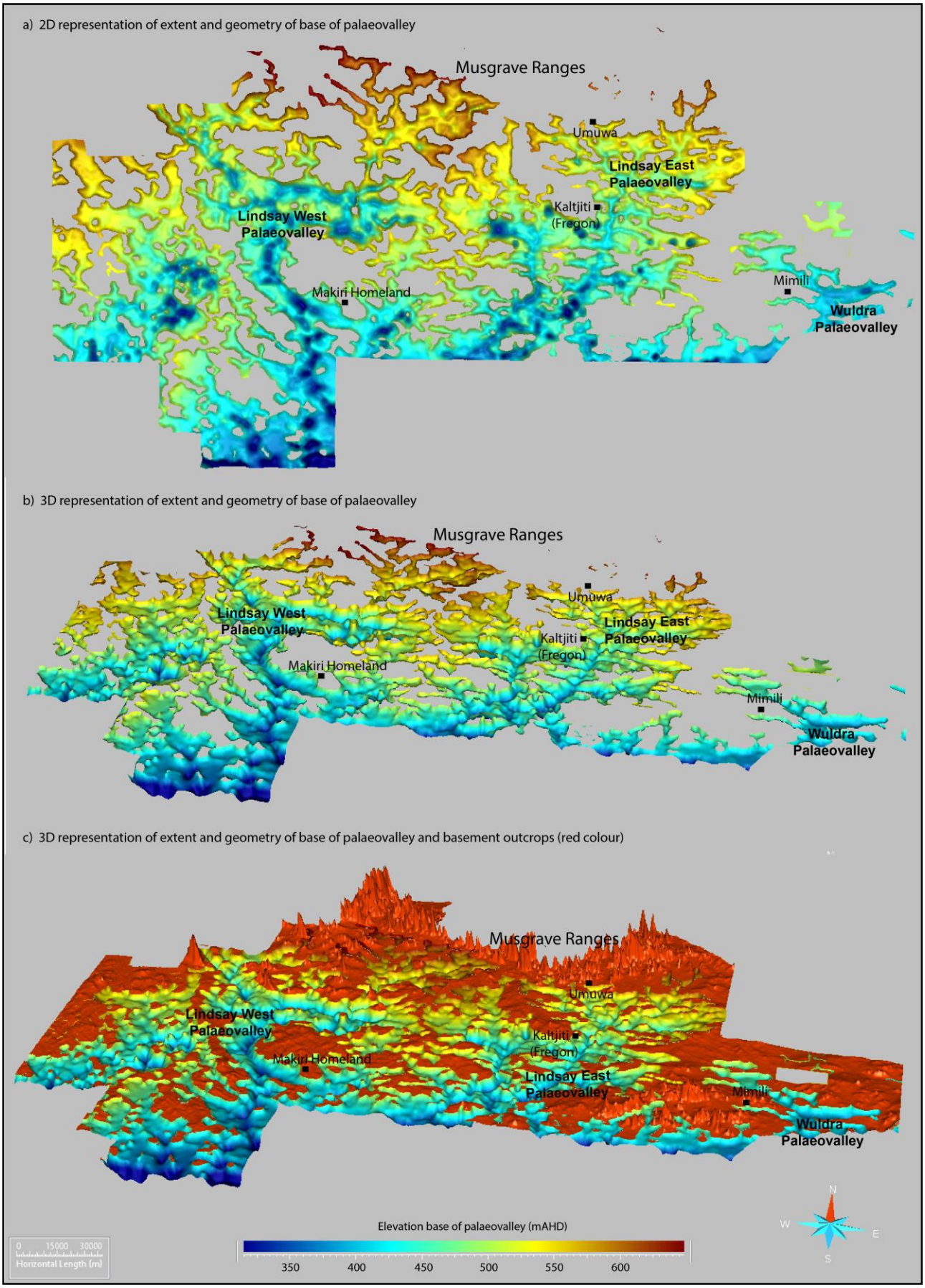

Figure 4-13. Representation of extent and geometry of base of palaeovalley in a) two-dimensional view b) three-dimensional view and c) three-dimensional view with outcropping basement (represented by the red colour).

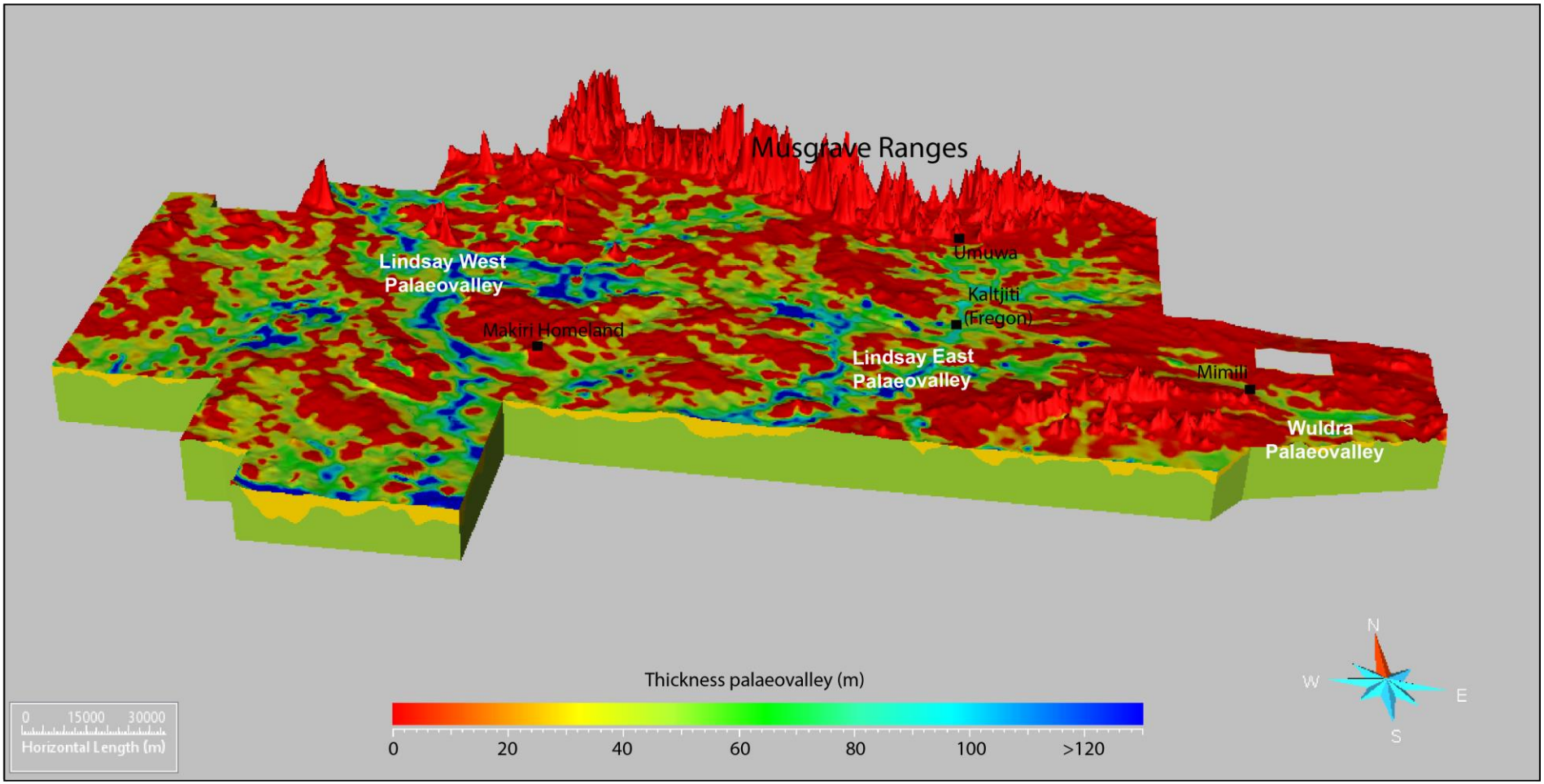

Figure 4-14. Thickness of palaeovalley fill.

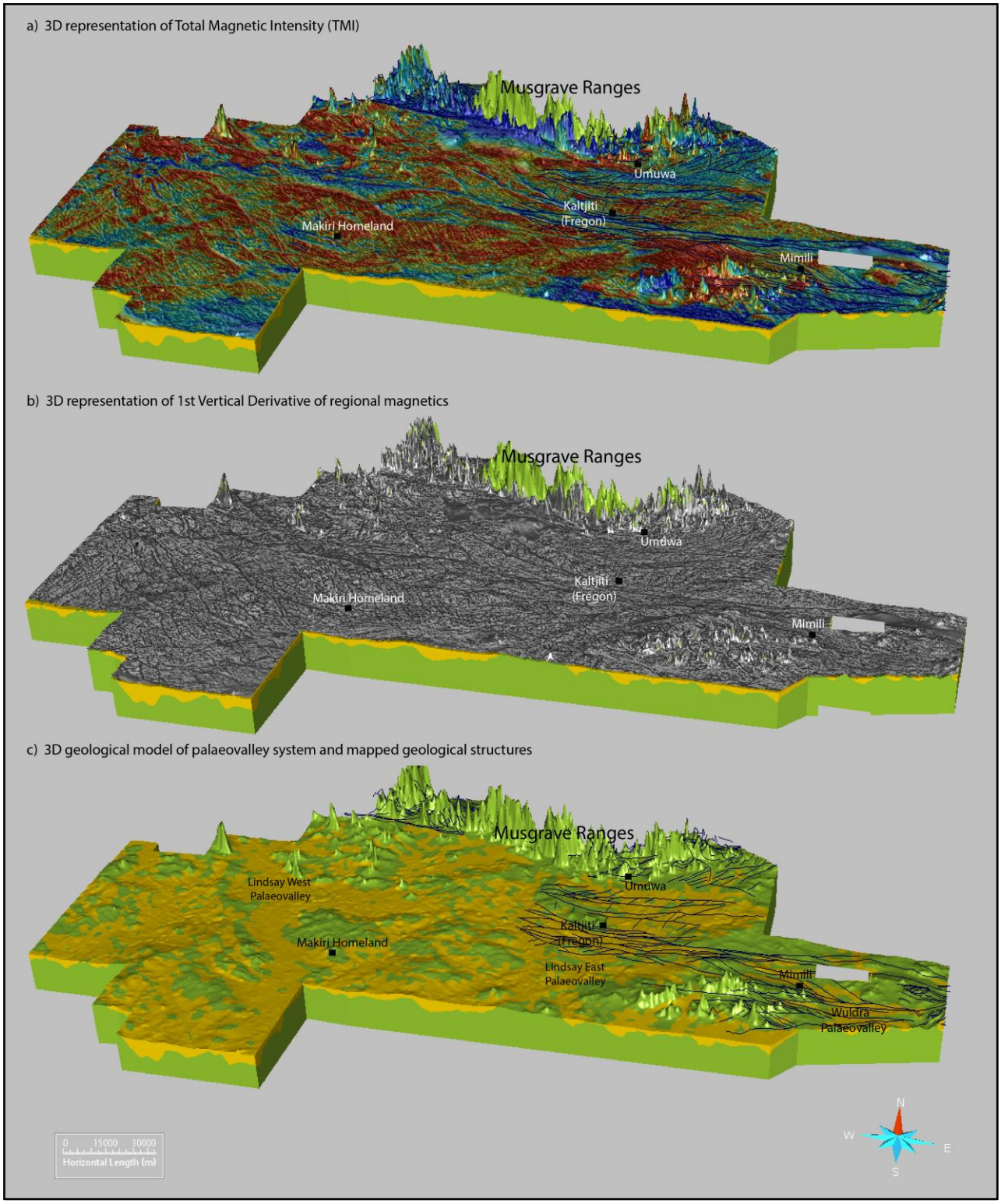

Figure 4-15. Three-dimensional representation of: a) Total Magnetic Intensity (TMI); b) 1st Vertical Derivative of TMI and; c) geological model of palaeovalley system with mapped geological structures on the eastern part of the Musgrave Province superimposed.

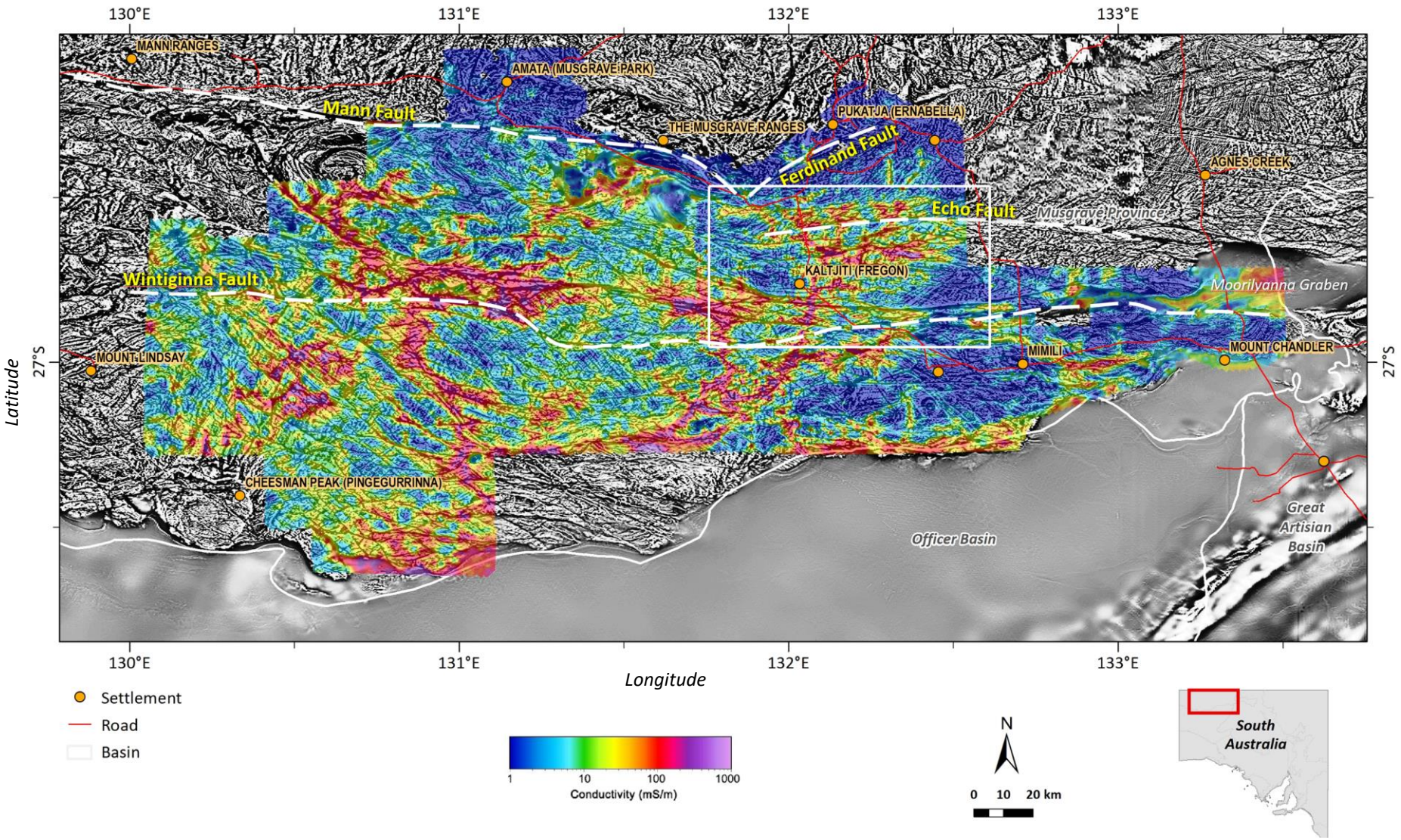

Figure 4-16. Pseudocoloured airborne electromagnetic interval conductivity (50-60 m) overlain on grey scale 1st vertical derivative of the regional magnetics. Major faults are indicated but magnetic data indicate numerous (assumed to be fault/shear related) lineaments present across the study area, with the observed conductivity structure aligned with these features in many instances. The white rectangle is a sub-set of the data which is shown in Figures 4-17 – 4-19.

The relationship between the orientation of palaeovalleys and structures was originally identified as part of exploration work by RTZ, Pepinnini Minerals and Musgrave Minerals between 2010 and 2015 in the western Musgrave Province. Subsequently, as part of G-Flows Stage-1, Munday et al. (2013) built on those observations and determined through the analysis of exploration airborne electromagnetic data, that the Province was likely characterised by a very complex palaeodrainage system that eroded pre-existing structures and then filled many of the resulting palaeovalleys. This sedimentary fill was relatively more conductive than the underlying basement, and their study illustrated the potential for a regional airborne electromagnetic survey to further elucidate the nature and variability of regolith cover across the Province, including the definition of palaeovalley geometry and variability. Parsekian et al. (2014) extended this work in a ground-based geophysical investigation of what Rankin and Newton (2002) described as dextral wrench graben structures to the north-north east of Kaltjiti/Fregon in the vicinity of Morrisons Bore (Figure 4-17). They undertook a series of TDEM and surface NMR soundings across an interpreted (from the airborne magnetics) wrench-graben resulting from the reactivation of steep Petermann-aged faulting (Pawley et al. 2014), which accommodated dextral strike-slip movement and led to the development of pull-apart basins at varying scales. The ground geophysical investigation confirmed the presence of alluvial fill in a graben-like structure and reinforced the significance of structure in controlling the orientation and thickness of fill sequences.

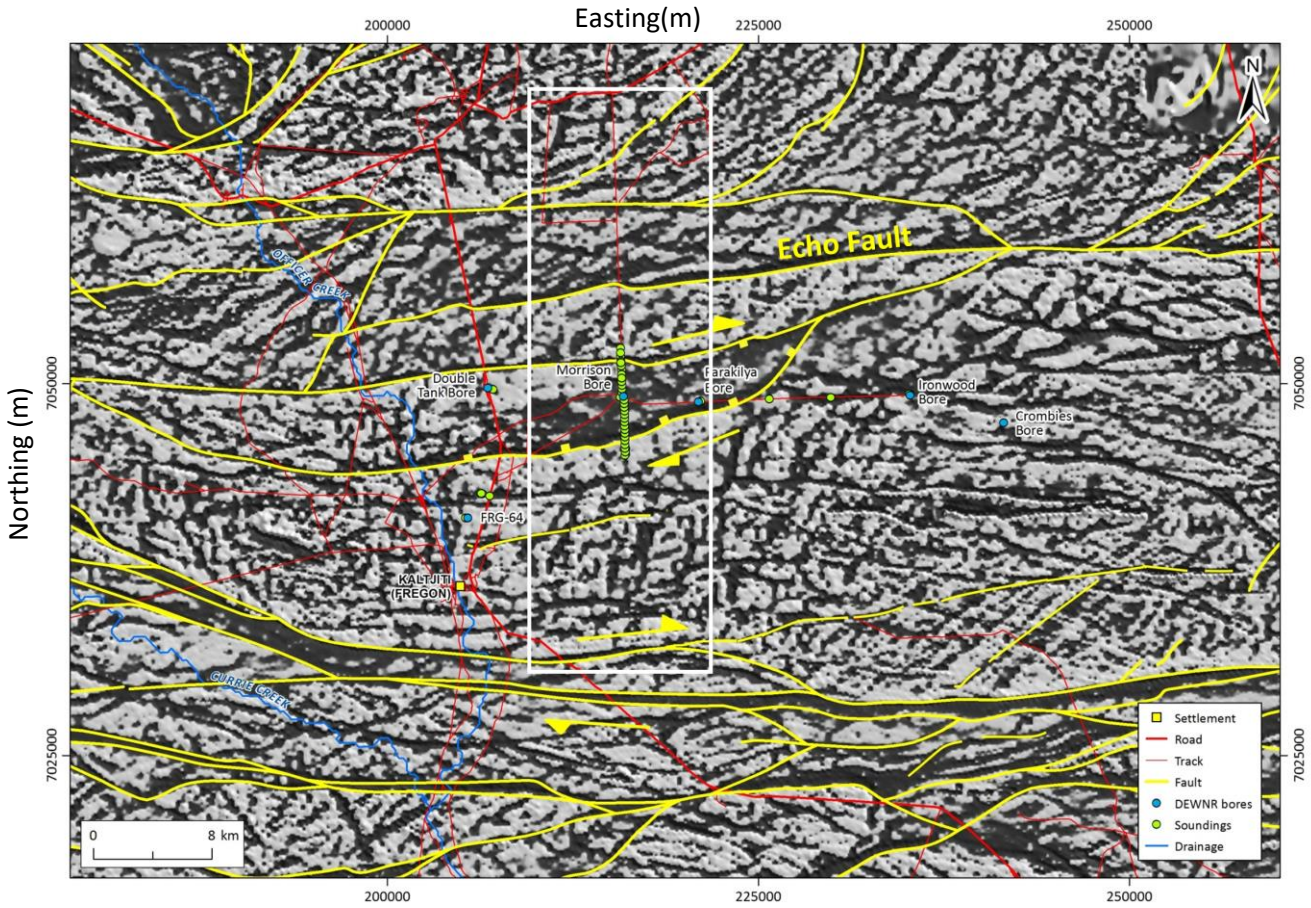

Figure 4-17. First vertical derivative airborne magnetics with major east-west orientated faults indicated in yellow. The Morrisons Bore time domain electromagnetic / surface nuclear magnetic resonance transect is identified as a green line in the centre of the image. The area defined by the white polygon is shown in Figure 4-21.

The advent of the regional AEM survey across the central and eastern Musgrave Province (Soerensen et al. 2018), provided the opportunity to better define the location, orientation and geometry of palaeovalleys across the Province, and to examine their affiliation with structure. Munday et al. (2016) reported further on this association and flagged the likelihood of neotectonics in influencing the observed conductivity structure. Abrupt discontinuities in the modelled conductivity structure, aligned with faults interpreted in the regional magnetics was cited as evidence for this. The influence of neotectonism on the observed conductivity associated with palaeovalley fill sequences has been reported previously by Munday et al. (2001). More recently Lawrie et al. (2016) demonstrated that in several of Australia's low gradient floodplains, fault scarps and concealed fault systems, manifest as conductivity discontinuities in airborne electromagnetic data, may have large 'keystone' effects on surface water and groundwater systems.

Krapf et al. (2019) extended the discussion of the role of neotectonics on the distribution of palaeovalleys across the region. They noted the role of structure in influencing the east-west orientation of palaeovalley fill, but also that the main trunk of these palaeovalley systems was orientated perpendicular to that orientation (Figure 4-15c). Interpretation of the AEM interval conductivity data over the first vertical derivative (1VD) of the regional magnetics (Figure 4-18) suggest that some northeast-trending structures, interpreted as the structural grain of the Musgravian Orogeny (Aitken and Betts 2008; Wade et al. 2008), may have also been exploited during the initial phase of erosion and deposition to allow the N-S orientation of the main valleys to develop.

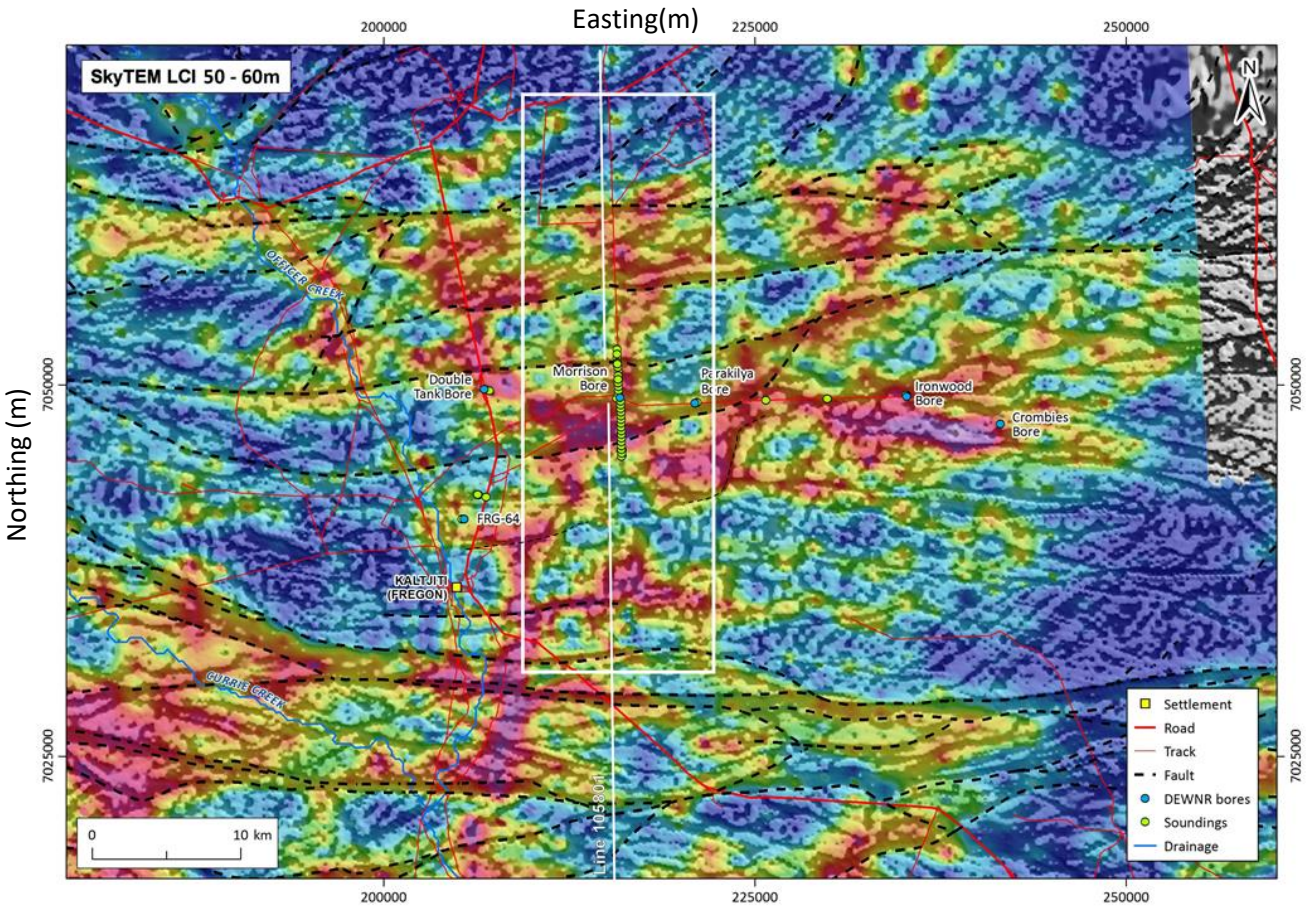

Figure 4-18. SkyTEM pseudocoloured interval conductivity (50-60 m below ground surface) over 1st vertical derivative of the airborne magnetics (intensity), with Morrison Bore transect in green in the centre of the image. Flight Line 105801 which runs parallel to the Morrison bore time domain electromagnetic / surface nuclear magnetic resonance transect is indicated. Area represented by white polygon is shown in Figure 4-21.

Consideration of the regolith thickness for the area shown in Figure 4-19, further illustrates the role of structure in compartmentalising the cover sequences, and its influence on the orientation of the palaeovalleys. The deeper (thicker) palaeovalley sequences appear strongly aligned with east-west oriented faults. It is interesting to note that the modelled thickness of the N-S orientated trunk valleys appears discontinuous across some faults. This supports the observation of Krapf et al. (2019) who noted that these basement structures may have been active during and after palaeovalley development and that recent seismic activity may suggest some are still active. Consequently, it is possible that some of these fault systems propagate through the cover materials and may create hydromorphic barriers, constraining lateral groundwater movement. Similar effects have been noted by other researchers (see, for example, Rutherford et al. 2001).

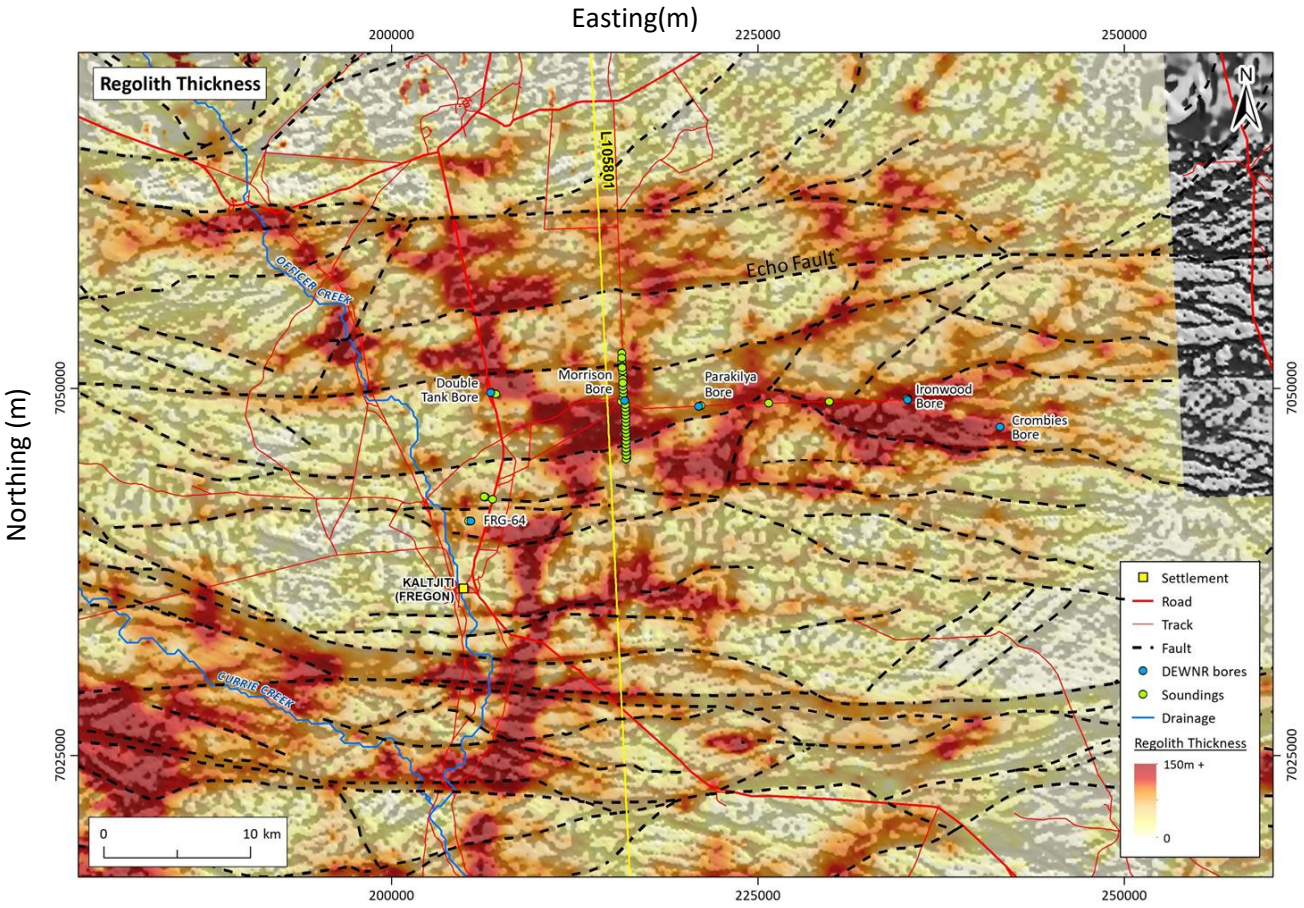

Figure 4-19. Regolith thickness map for area outlined in Figure 4-16, overlain on 1st vertical derivative of the airborne magnetics. Interpreted faults systems are also indicated as black dashed lines.

Detailed geological interpretation of the AEM flightlines allows for the better definition of how structure has controlled the development of the palaeovalley fill sequences. Figure 4-20 shows an interpretation of a subset of inverted SkyTEM data (Line 105810) near-coincident with the Morrison Bore transect (Figure 4-21). The conductivity-depth section shows a stepped conductivity structure which is interpreted as a stepped graben infilled with sediment. Incidentally, these AEM sections may permit a more detailed structural interpretation of the province than might be gained from the magnetic data alone.

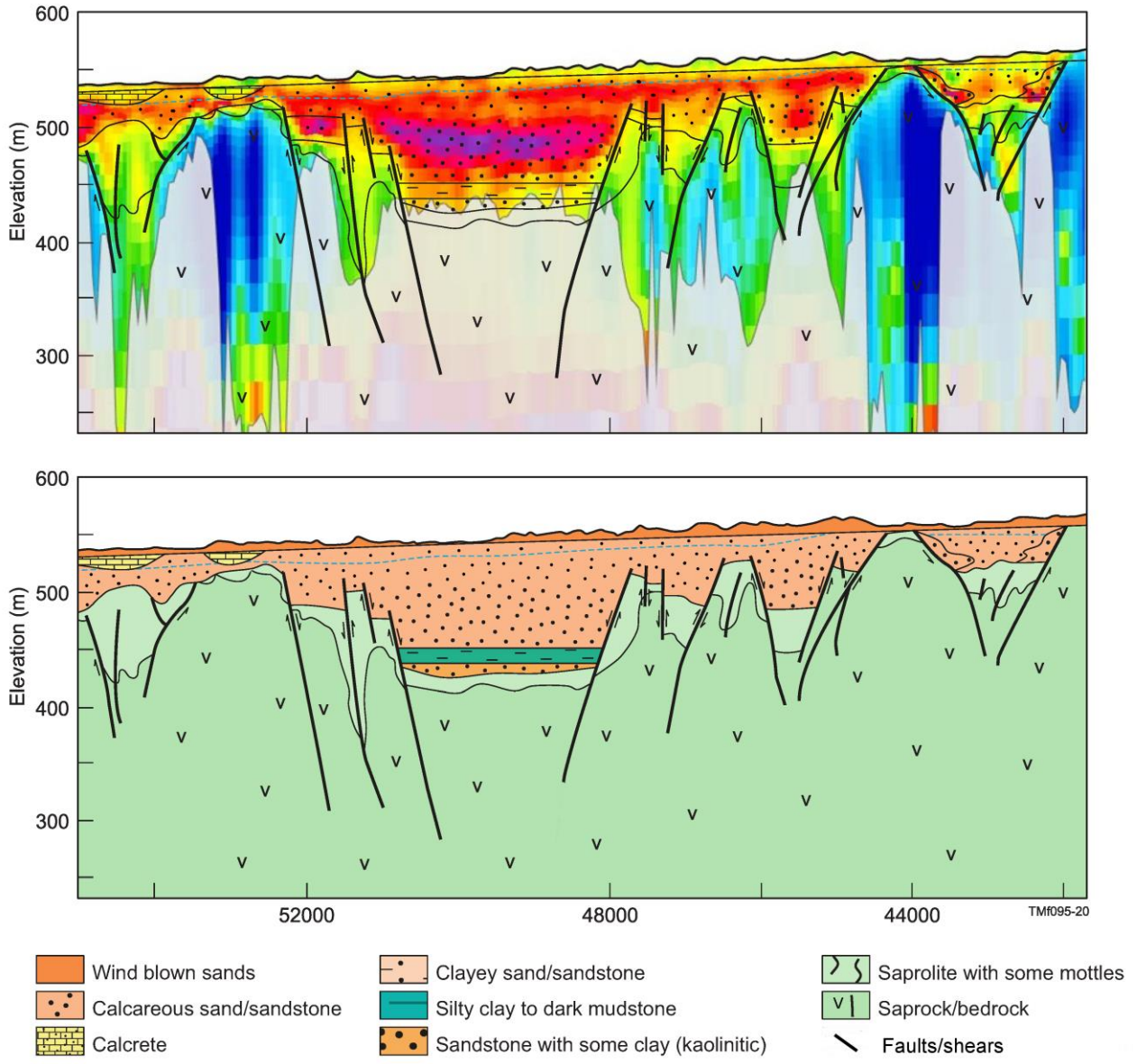

Figure 4-20. A conductivity-depth section for a subset of line 105801 with interpreted geology overlain. The conductive units are associated with transported fill that was deposited within an interpreted stepped dextral wrench-graben that may have developed as a subsidiary structure to larger east-west steeply-dipping regional strike slip faults (e.g. the Echo fault) that extend across the Musgrave Province (see Figure 4-16).

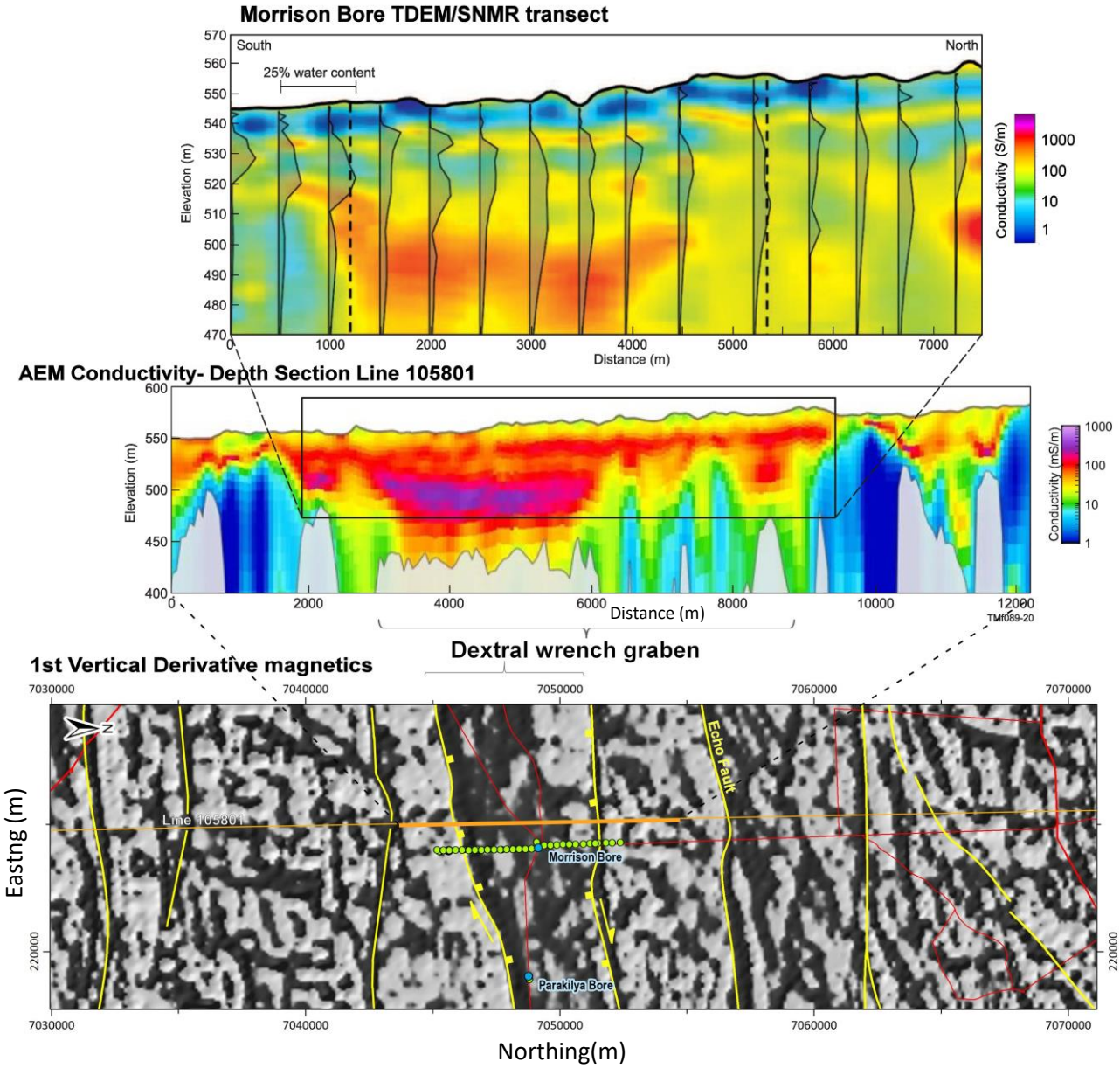

Figure 4-21. Morrison Bore transect, illustrating the influence of structure (in this case a stepped dextral wrench graben) on the development of a palaeovalley and its infilling as represented by the conductive material shown in the ground time domain electromagnetic (TDEM) soundings from Parsekian et al. (2014) (top panel), and a near coincident conductivity-depth section of SkyTEM airborne electromagnetic (AEM) line 105801 (middle panel). The lower panel is a subset image of the 1st vertical derivative of the magnetics shown in Figure 4-17. The geological interpretation of the airborne electromagnetic (AEM) section is shown in Figure 4-20.

The sediment infill as shown in the deeper part of the palaeovalley is derived from an extension of observations made by Krapf et al. (2019) around drill site DH1, and from the suggestion that an estuarine - marine influence noted at that site could have extended past the Morrison Bore transect, potentially providing for the deposition of muds and clay-rich units (see Figure 4-22).

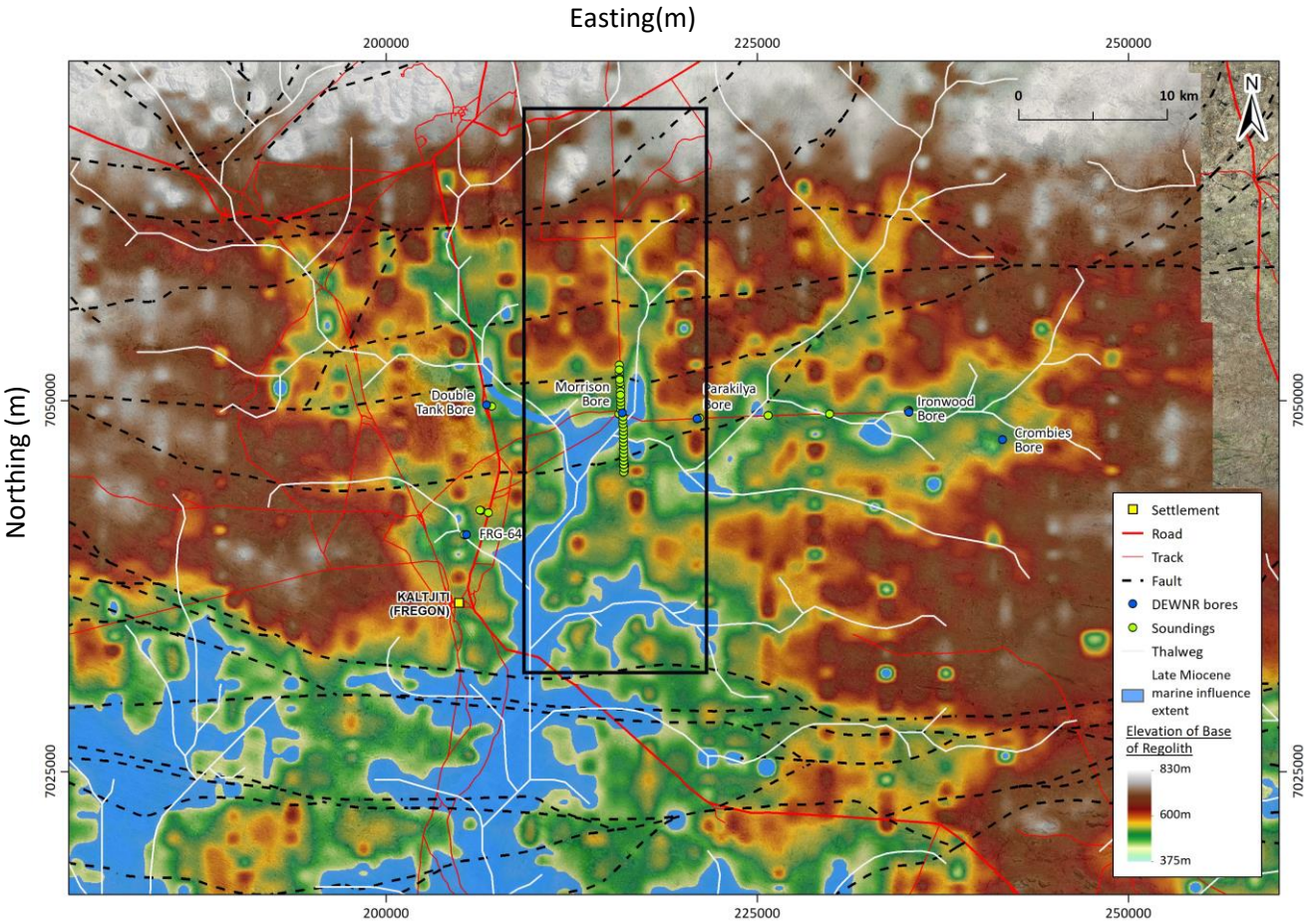

Figure 4-22: Suggested extent of Late Miocene marine influence in the vicinity of Morrison Bore site north of Kaltjiti/Fregon. Black rectangle is the area shown in Figure 4-21. The extent of this marine influence is determined from flooding the elevation of the basement surface derived from the regional airborne electromagnetic data set.

Conceptualisation of the evolution of the palaeovalley in the vicinity of Morrisons Bore is summarised in Figure 4-23. Similar processes are expected to have guided the regional development of the palaeovalley systems across the Musgrave Province and the stratigraphy they contain (see Krapf et al. 2019). Specifically the conceptualisation details the role of structure in constraining the initial location drainage, erosion and deposition, which accelerated with the onset of deep weathering in the Late Mesozoic (Figure 4-23A). Intermittent estuarine and marginal marine sedimentation was interpreted to occur in the Miocene-mid Eocene (Krapf et al. 2019), occupying the deeper reaches of the palaeovalley systems (Figure 4-23B), particularly in the southern parts of the Musgrave Province. Intermittent fluvial sedimentation occurred through the Late Miocene – Early Pliocene (Figure 4-23C) but increased through the Early-Late Pliocene resulting in the valleys filling up (Figure 4-23D). Increased aridity in the Late Pliocene through to Holocene resulted in sheetwash, fluvial and colluvial sediments being deposited across the landscape. Aeolian processes started to dominate in the Holocene with the development of extensive sand plains and sand sheets. Local induration occurred forming calcrete in subdued, shallow and laterally extensive valley floors (Figure 4-23E).

A: Onset of deep weathering
(Late Mesozoic to Early Palaeogene – ~65Ma), fluvial erosion and sedimentation of faulted crystalline Mesoproterozoic basement rocks. Erosion and sedimentation developed preferentially along structural discontinuities with fluvial deposition occurring through the Palaeocene and Eocene (~6—30Ma).

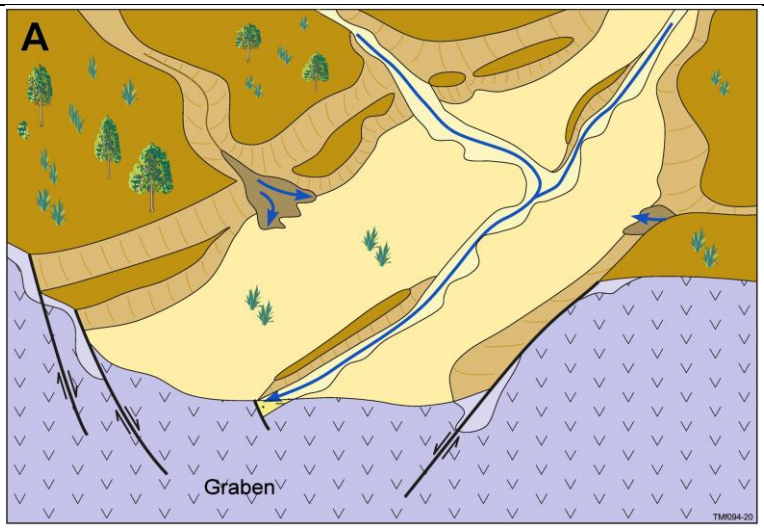

B. Freshwater and marine environmental reversals
(Palaeogene - Neogene), with intermittent marine incursion and sediment deposition into incised palaeovalley estuarine environment through the Miocene to mid-Eocene (~40 - 13Ma). The marine influence receded with brackish to freshwater lake systems occupying the valley floors. Deposition of organic rich fine-grained sediments occurred in parts.

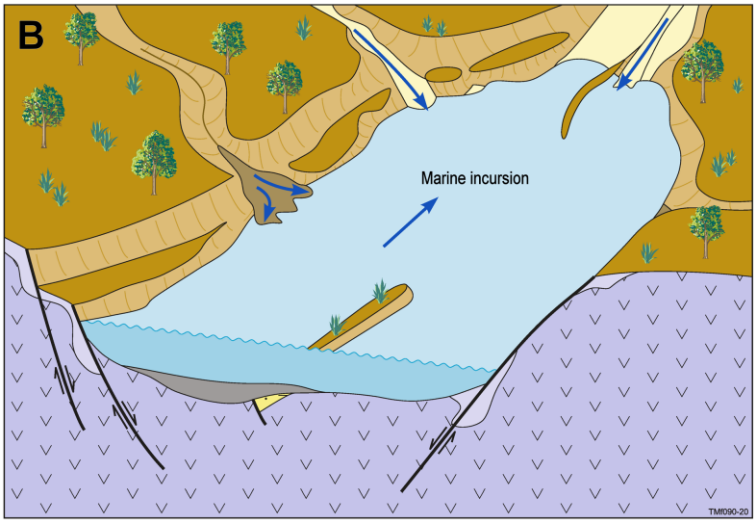

C. Drying out and evaporation starts to dominate
(mid Neogene) with the development of playa lakes accompanied by intermittent fluvial sedimentation through the Late Miocene to Early Pliocene (~10 – 3Ma).

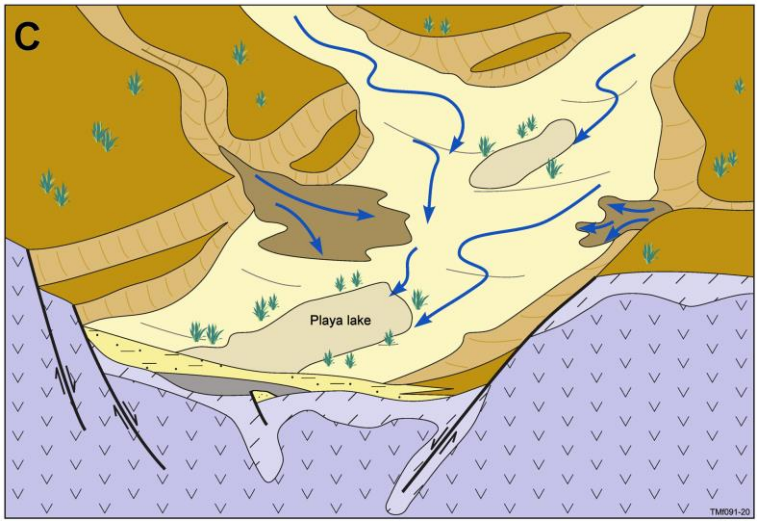

D. Wetter conditions through the early Neogene resulted in increased erosion of the ranges to the north, and an acceleration of sequential fluvial sedimentation infilling the palaeovalley systems (Early to Late Pliocene - ~ 2.5 – 5Ma).

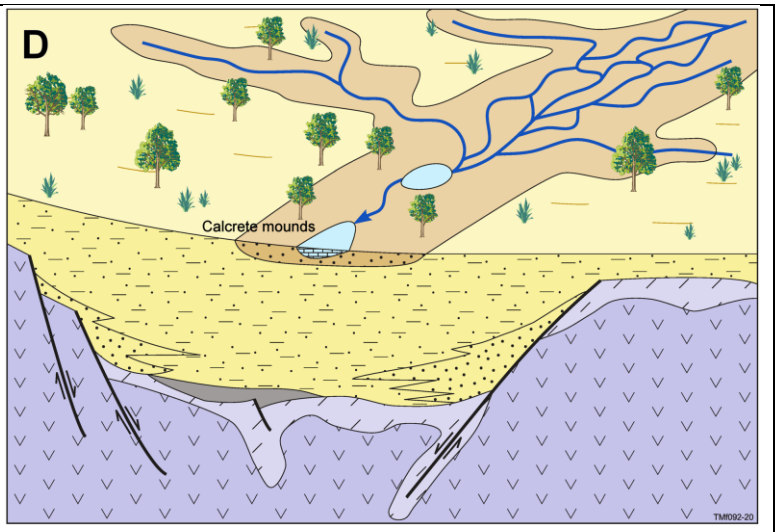

E. Sedimentation continued after the palaeovalley systems were infilled through the early Neogene into the Quaternary, with sheetwash, fluvial and colluvial sediments being deposited across the landscape with increased aridity. Aeolian processes started to dominate in the Holocene with the development of extensive sand plains and sand sheets. Local induration occurred forming calcrete in subdued, shallow and laterally extensive valley floors (Pliocene – Holocene ~4Ma to present).

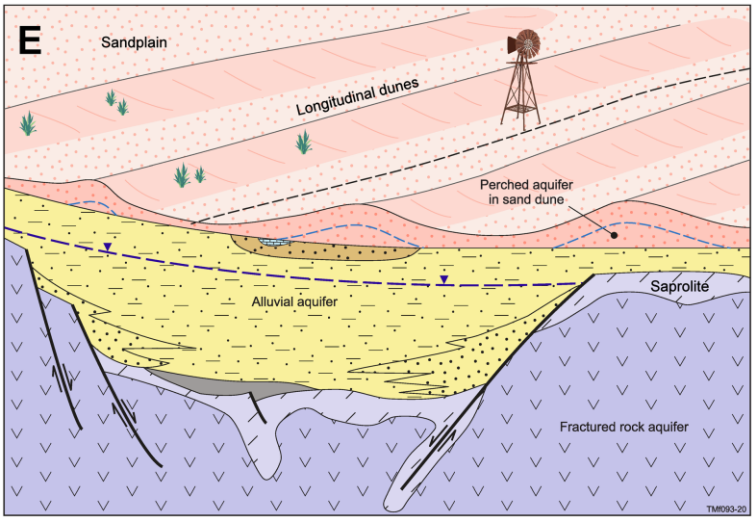

Figure 4-23. Conceptualised landscape development processes leading to location and orientation of palaeovalleys in the Musgrave Province (adapted from Munday et al. 2016 and Krapf et al. 2019). In this conceptualisation, the influencing role of strike slip pull apart structures, represented by that interpreted to be present at Morrisons Bore (A), in determining the location of the initial valleys and sedimentation, and subsequent estuarine – marginal marine deposition (B) is shown. Intermittent infilling, which continued through the Cenozoic (C) to the present day (D and E), illustrates the development of the alluvial- colluvial aquifer system that dominates much of the Musgrave Province.

Within the area of the Lindsay West Palaeovalley system (particularly in the south-western part), a north-west to south-east trend of lineaments can be observed in addition to the east-west trend. This northwest – southeast trend appears to coincide with the orientation of the southern part of the main channel of the Lindsay West palaeovalley system west of Makiri Homestead, whereas some of the tributary systems to the main channel coincide with the east-west trend (Figure 4-24).

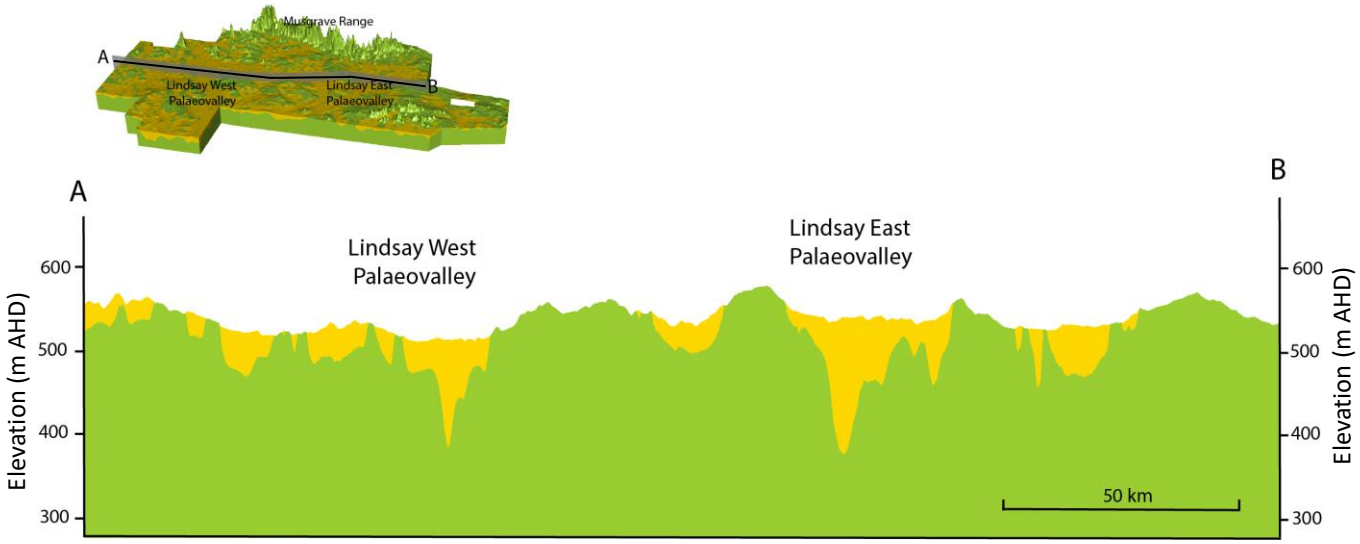

Figure 4-24. West-east geological cross-section through the Lindsay West and Lindsay East palaeovalley systems. The orientation of the cross-section is shown in the three-dimensional geological model above the section.

4.5 Groundwater flow

4.5.1 GROUNDWATER FLOW DIRECTIONS

Multiple versions of water table and potentiometric surfaces have been developed for the APY Lands. An interpreted watertable surface presented by Costar et al. (2019) shows that the general regional groundwater flow direction follows topography in an approximately southerly direction from the topographic highs in the north (Musgrave Ranges) towards the lower-lying southern parts of the APY Lands.

The same regional patterns are shown in a potentiometric surface (hydraulic heads from both ouctropping bedrock and alluvial/colluvial aquifers) map developed for unconfined aquifers across the Musgrave Province (Figure 4-25). This map also highlights that although there is a relatively good spatial coverage with groundwater level data within the extent of the Lindsay East palaeovalley system, very few or no groundwater level measurements exist further west in Lindsay West palaeovalley system, resulting in a higher uncertainty of the spatial interpolations.

Furthermore, a static water level/water table was generated using a Gaussian Process (GP) machine learning model. Unlike a regular interpolation that only relys on measured water table data, the GP model also learns the relationship between water table and digital elevation model and takes this into account for prediction. The predicted water table is shown in Figure 4-26. Figure 4-27 demonstrates the GP model performance by comparing the prediction with tens of records that are not used in the training dataset. The scatter plot shows a very good match with an r^2 of 0.985.

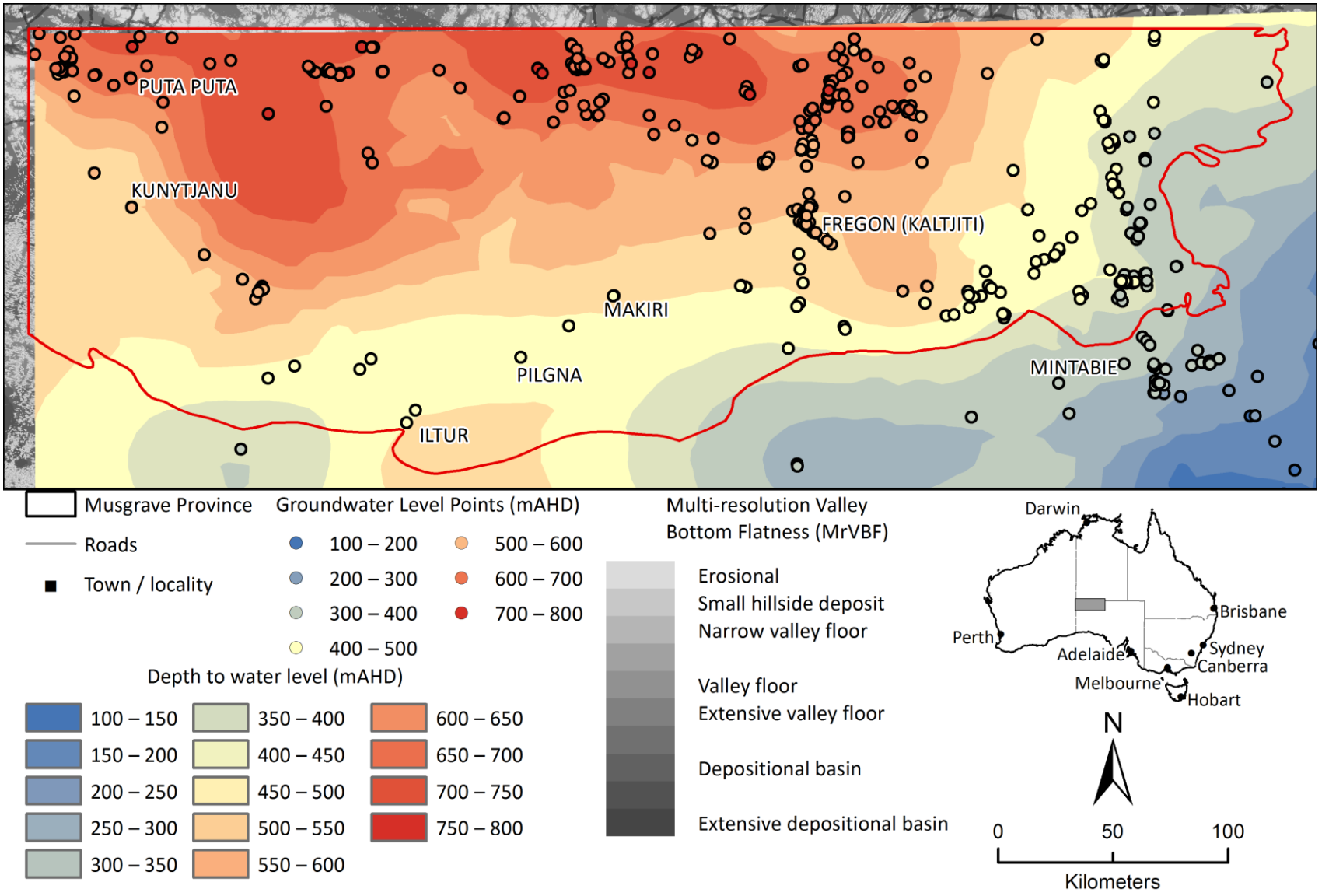

Figure 4-25. Interpolated potentiometric surface for unconfined aquifers across the Musgrave Province. Spatial groundwater level data used for the interpolation was collated from WaterConnect (DEW, 2018).

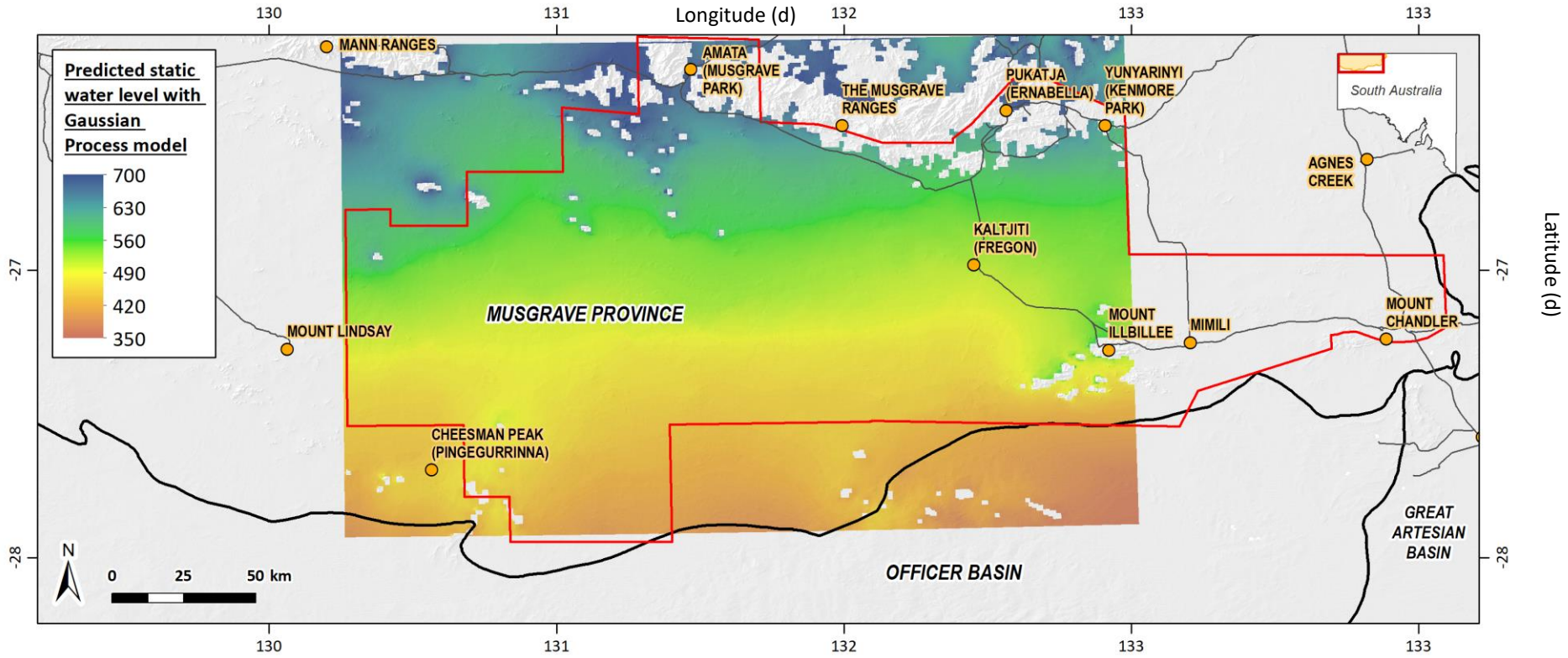

Figure 4-26. Predicted static water level (m AHD) with Gaussian Process model.

The uncertainty map (Figure 4-28) shows that the uncertainty increases towards areas with lower data density, and overall, the uncerainty does not change significanlty across the model domain (10.05 to 10.35). However, although the validation indicates a good prediction performance, attention still needs to be paid when interpreting results located far away from available groundwater monitoring sites. The distribution of data points in Figure 4-25 shows that there is a bias in the distribution of groundwater level records, as most groundwater level measurements were collected from the Lindsay East pallaeovalley area, and there is a possibility that most validation samples are close to the training data when all the measurements are clustered to a few locations.

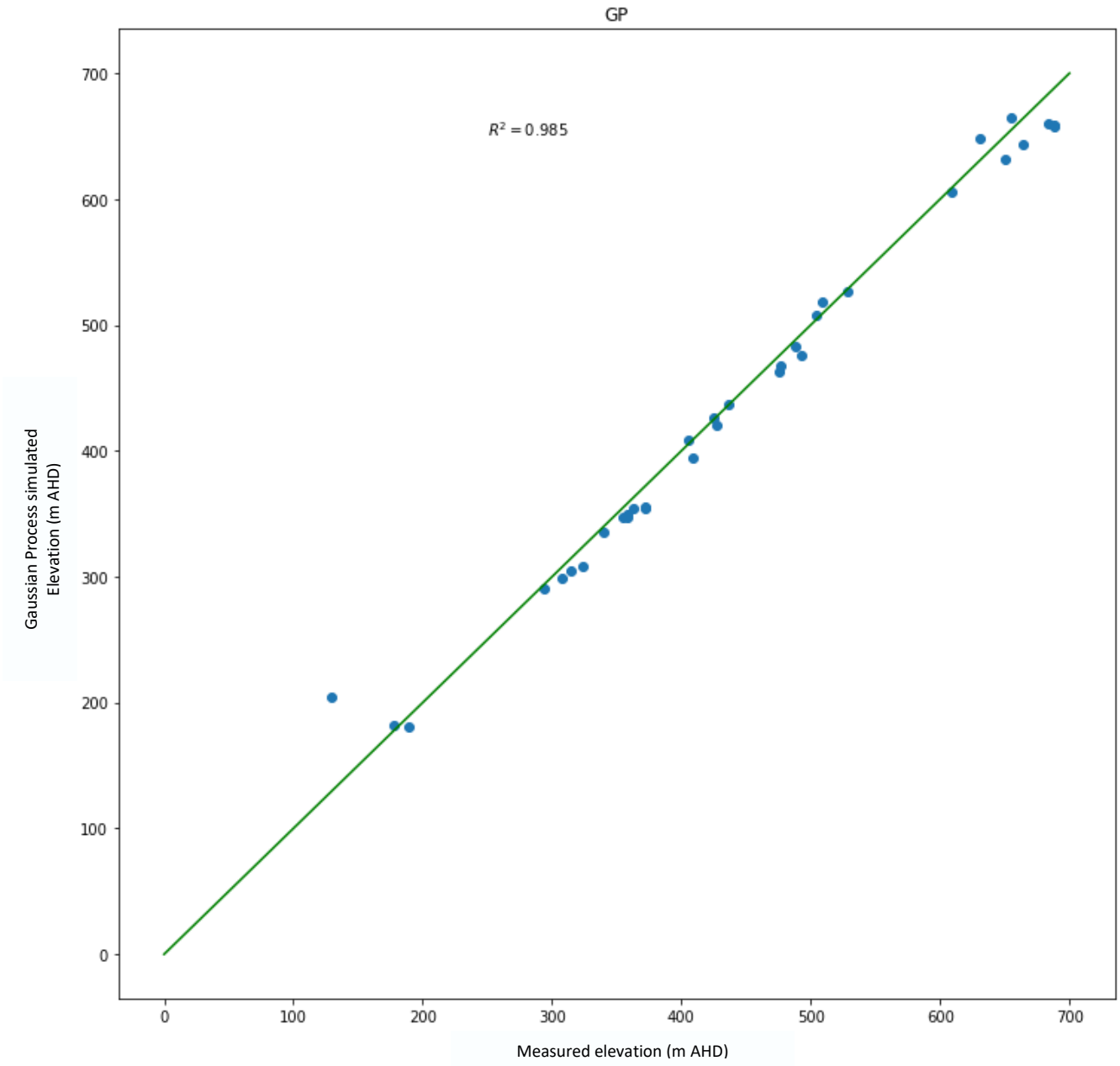

Figure 4-27. Validation results comparing measured with predicted groundwater table elevation, using records that are not included in the training dataset.

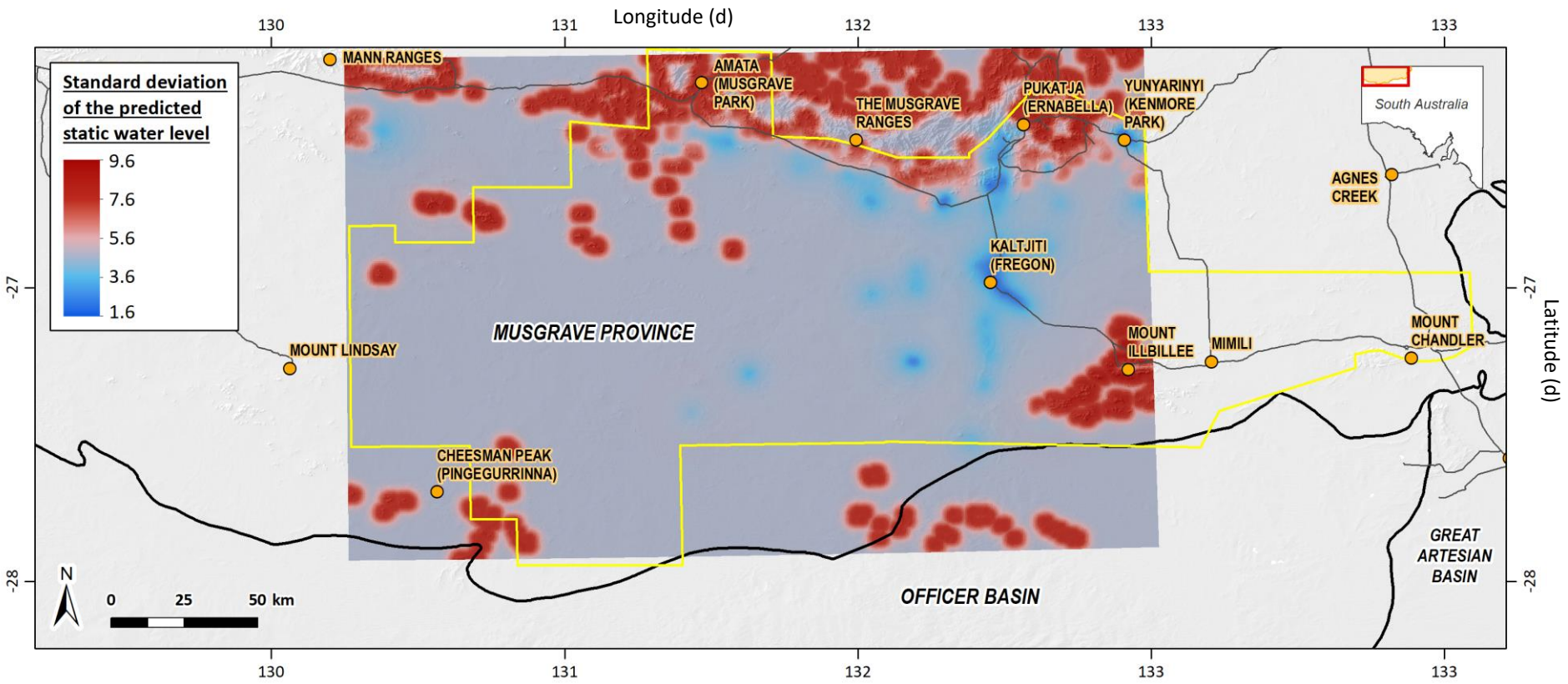

Figure 4-28. Standard deviation of the predicted static groundwater level.

4.5.2 UNCERTAINTIES AND LIMITATIONS

A likely limitation arising from the data distribution that should be taken into account when interpretation local-scale flow direction from these regional-scale maps is highlighted by the purple arrow in Figure 4-29 and blue arrow in a north-south oriented geological cross-section (Figure 4-31). In this area, all available potentiometric surface maps indicate a north-southerly flow direction. However, this would require that groundwater from the palaeovalley system needs to flow through a very prominent basement high, comprised primarily by Mesoproterozoic metasediments (gneiss and granulite), that extends over more than 20 km from north to south and which is topographically elevated compared to the palaeovalley systems up- and downgradient. Although there is evidence for significant faulting in this area as indicated by the Total Magnetic Intensity (TMI; Figure 4-15a), the orientation of structural lineaments is predominantly east-west in this area, and they are unlikely to form north-southerly conduits through this basement high. This means that in such cases, the projected regional groundwater flow direction is likely to be incorrect. Instead, rather than penetrating significant low-permeability basement highs, groundwater within the palaeovalley may more likely be either stagnant, discharges to the surface or follows the approximate direction of the thalweg around the basement highs.

This indicates that basement topography may be a more suitable or additional parameter for prediction of groundwater flow directions within the palaeovalley systems than surface topography.

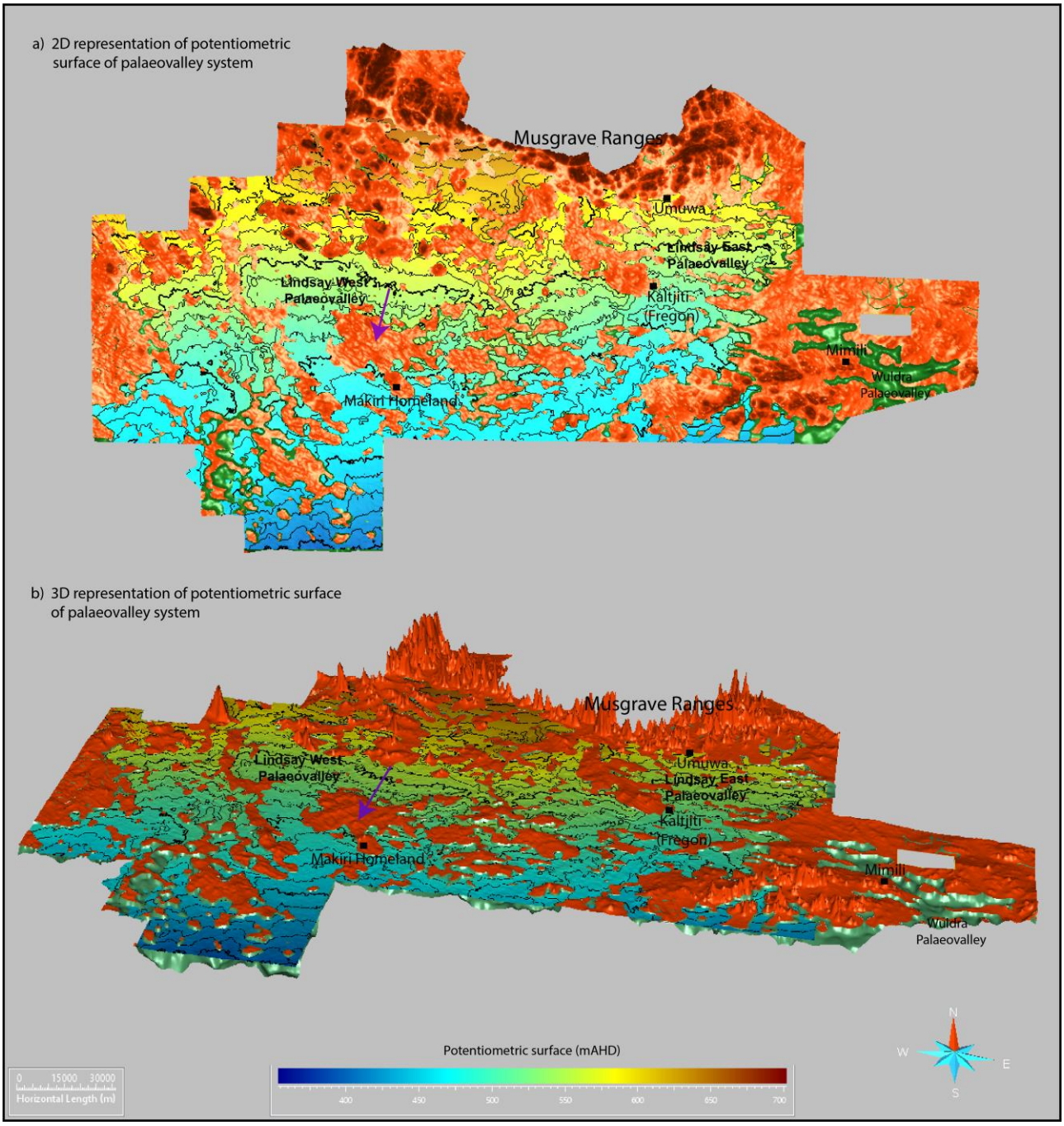

Figure 4-29. Two-dimensional (a) and three-dimensional (b) representation of potentiometric surface in palaeovalley system. The outcropping basement is shown in red. Purple arrow is highlighting an example of a very data sparse area where the actual potentiometric surface is likely to deviate significantly from the predicted regional potentiometric surface due to the presence of a basement high.

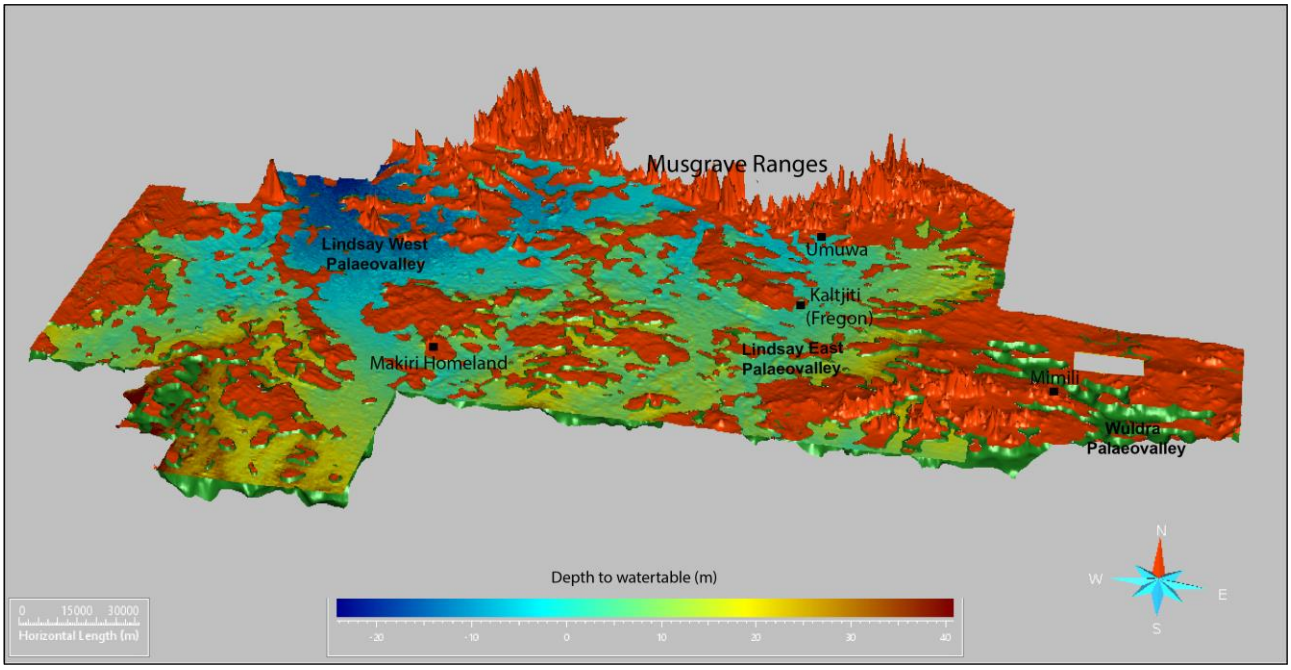

Figure 4-30. Three-dimensional representation of predicted depth to watertable in palaeovalley systems. The outcropping basement is shown in red.

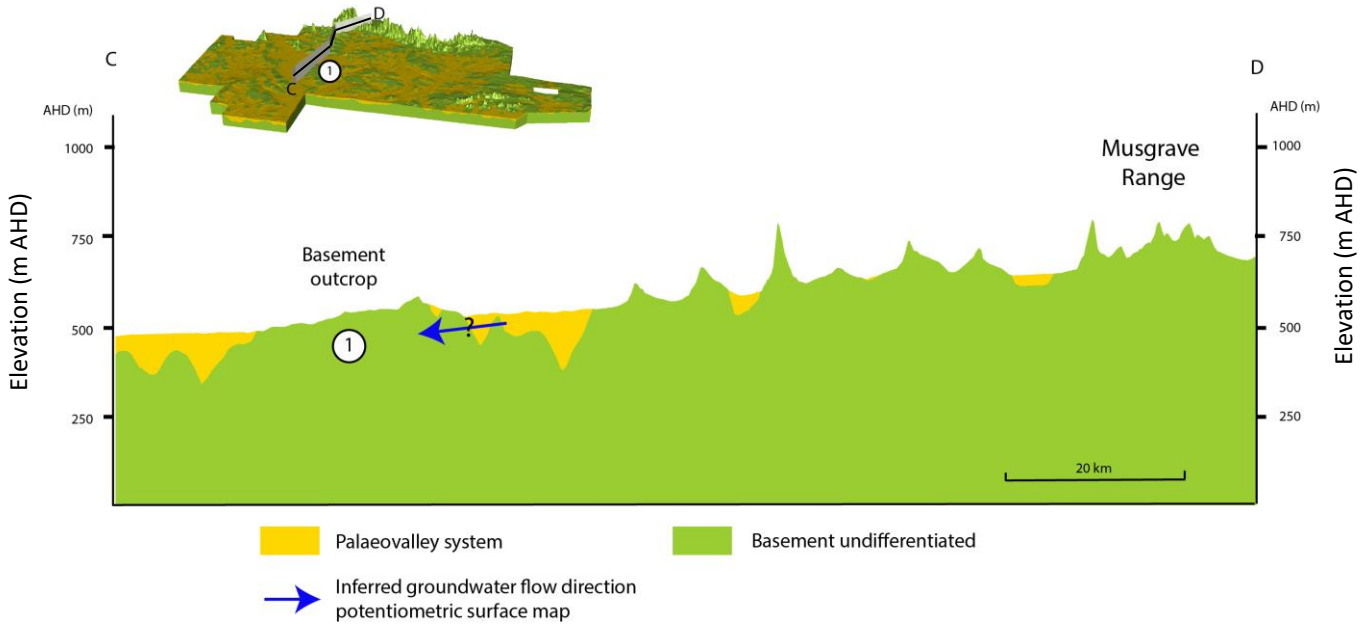

Figure 4-31. North-south geological cross-section through the Lindsay West Palaeovalley system. The orientation C-D of the cross-section is shown in the 3D geological model above the section.

4.6 Environmental tracers

4.6.1 RECHARGE PROCESSES

Figure 4-32 shows a comparison of the ^{2}H and ^{18}O composition of 175 groundwater samples from aquifers in five different hydrogeological units compared to that of the 'amount-weighted' composition of mean monthly rainfall thresholds for Alice Springs (IAEA/WMO, 2019). Most groundwater samples plot along a straight line parallel to the Alice Springs local meteoric water line (LMWL) with a $\delta^{2}H$ displacement ranging between zero and approximately 20‰. The exception is for the sandstone and siltstone aquifers. It is therefore not possible to have a line of best fit through all the groundwater data that eventually intersects the LMWL at depleted compositions. This suggests that while the LMWL for Alice Springs (the closet one available - Crosbie et al. 2012) may not be ideal for representing that of local precipitation. However, the $\delta^{2}H$ displacement is lower for the depleted $\delta^{2}H$ and $\delta^{18}O$ samples collected from the northern part of the province indicating less evaporation during localised recharge. Conversely, samples collected further south in the province have an enriched $\delta^{2}H$ and $\delta^{18}O$ composition and a larger $\delta^{2}H$ displacement indicating evaporation during diffuse recharge through the vadose zone. The amount-weighted composition of mean monthly rainfall thresholds indicate that at least 40 mm of rainfall in a single month is required to overcome soil moisture deficits and for groundwater recharge to some of the outcropping bedrock and isolated sand stone aquifers (Figure 4-32). However, more broadly across the Musgrave Province at least 60 mm of rainfall in a single month is required for recharge to occur to the majority of the bedrock and alluvial/colluvial aquifers.

The range for both $\delta^{2}H$ and $\delta^{18}O$ in most aquifers is significant ranging from –80.6 to –34.5‰ and from –11.1 to –4.3‰ for ^{2}H and ^{18}O respectively. The clear exception to this is for samples from the sandstone aquifer which exhibit a much narrower range for both $\delta^{2}H$ and $\delta^{18}O$ is from –49.4 to –43.1‰ and from –7.4 to –5.5‰ for ^{2}H and ^{18}O respectively. For the remaining aquifer types the range for both $\delta^{2}H$ and $\delta^{18}O$ for the alluvial/colluvial aquifer (n=47) is from –80.6 to –34.5‰ and from –11.1 to –4.3‰ for ^{2}H and ^{18}O respectively. For the bedrock aquifer (n=90) the range for both $\delta^{2}H$ and $\delta^{18}O$ is from –65.7 to –37.3‰ and from –9.3 to –4.8‰ for ^{2}H and ^{18}O respectively. For the calcrete aquifer (n=4) the range for both $\delta^{2}H$ and $\delta^{18}O$ is from –56.4 to –38.69‰ and from –8.0 to –4.9‰ for ^{2}H and ^{18}O respectively. For the siltstone aquifer the range for both $\delta^{2}H$ and $\delta^{18}O$ is from –44.5 to –44.2‰ and from –6.7 to –5.4‰ for ^{2}H and ^{18}O respectively. There were also 23 samples from groundwater bores without lithology logs and therefore could not be attributed to an aquifer.

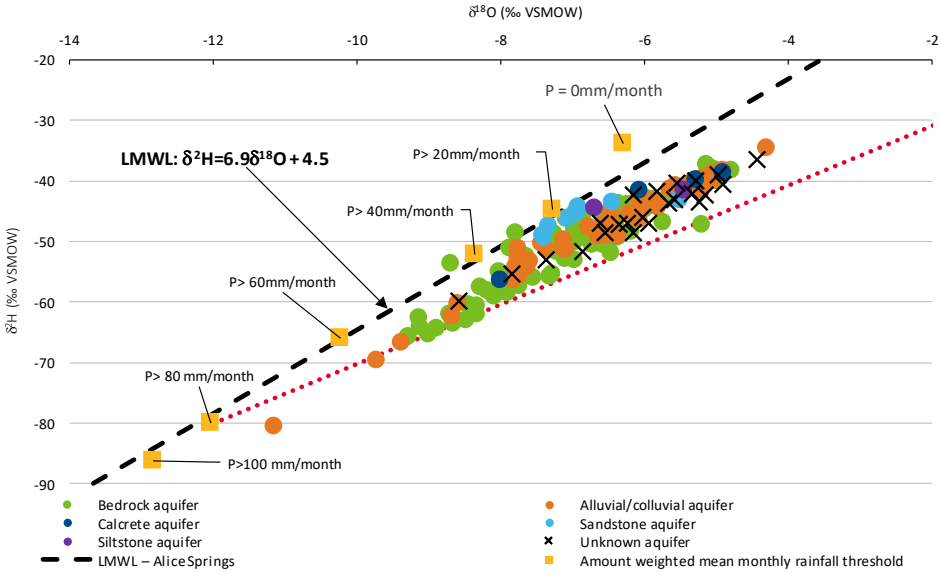

Figure 4-32. Stable hydrogen and oxygen isotopic composition for groundwater from aquifers within five different hydrogeological units. Data collated from Dodds et al. (2001); Craven (2012); Custance (2012); Leaney et al. (2013) and Kretschmer and Wohling (2014).

4.6.2 GROUNDWATER RECHARGE AND FLOW

Chlorofluorocarbons

Figure 4-33 displays the CFC-11 versus CFC-12 composition measured for 27 groundwater samples in aquifers from four different hydrogeological units. Of the 27 groundwater samples, 24 samples had measurable CFC concentrations above the detection limit (0.18 and 0.16 pmol/kg for CFC-11 and CFC-12 respectively). Most samples plot on or close to different modelled compositions of CFCs assuming a mean annual recharge temperature of 20°C (mean annual recharge temperature). Those samples which plot to the right of the different modelled lines indicate that CFC-11 has been degraded. By aquifer type, the CFC-11 and CFC-12 concentrations for the alluvial/colluvial aquifer (n=5) range from 0.24 to 0.98 pmol/kg and from 0.17 to 1.1 pmol/kg for CFC-11 and CFC-12 respectively. For the bedrock aquifer (n=8) concentrations range from 0.25 to 1.88 pmol/kg and from 0.17 to 1.36 pmol/kg for CFC-11 and CFC-12 respectively. The highest concentrations for CFC-11 and CFC-12 in both the alluvial/colluvial and bedrock aquifers come from groundwater bores installed either directly in outcropping bedrock or in alluvium and colluvium adjacent outcropping bedrock in the northern part of the province. Single samples were collected from both the calcrete and siltstone aquifers. For the calcrete aquifer, the CFC-11 and CFC-12 concentrations are 0.25 and 0.17 pmol/kg for CFC-11 and CFC-12 respectively. For the siltstone aquifer, the CFC-11 and CFC-12 concentrations are 1.49 and 1.07 pmol/kg for CFC-11 and CFC-12 respectively. There are 11 samples collected from groundwater bores that do not have lithology logs and therefore cannot be attributed to an aquifer.

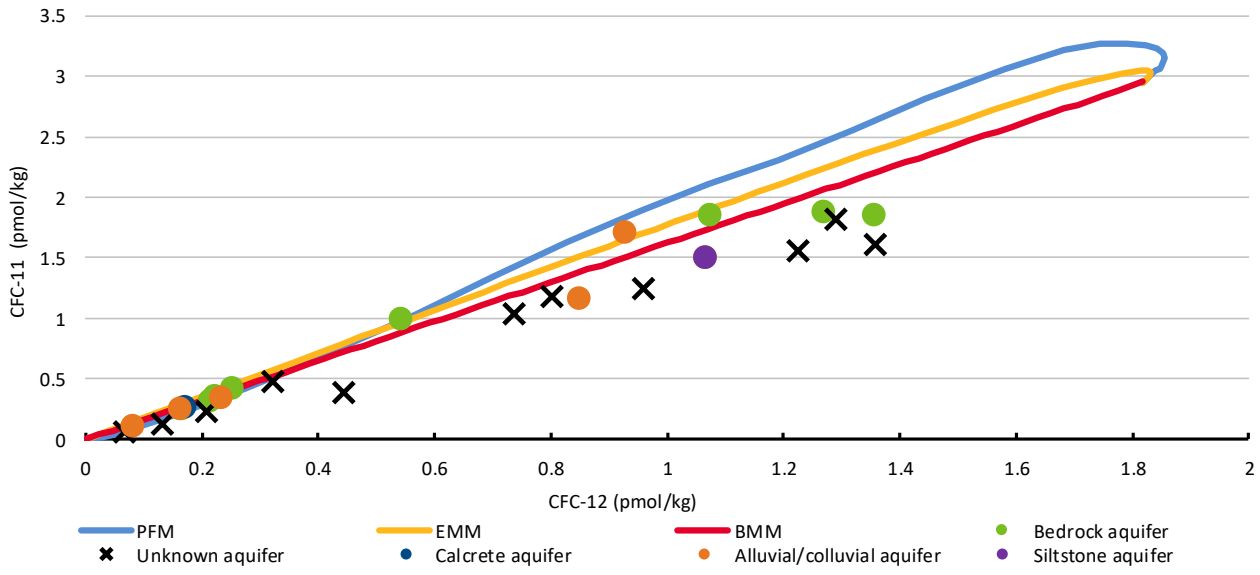

Figure 4-33. Relationship between CFC-11 and CFC-12 concentrations in groundwater from aquifers within four different hydrogeological units. Data collated from Dodds et al. (2001); Craven (2012); Custance (2012); Leaney et al. (2013) and Kretschmer and Wohling (2014). The solid lines represent different models of the expected compositions of CFCs in groundwater assuming a mean annual temperature of 20°C. The solid blue line represents the expected composition of groundwater recharged under a piston flow model (PFM) over the last 50 years, whereas the red line represents expected composition under an exponential mixing model (EMM) and the orange line forms an envelope of all possible mixtures of water).

Carbon isotopes

Figure 4-34 displays the stable (^{13}C) and radioactive (^{14}C) carbon isotope composition measured for 50 groundwater samples from aquifers in four different hydrogeological units. The stable isotopic composition for all groundwater samples expressed as $\delta^{13}C$ relative to the Pee Dee Belemnite (PDB) standard ranges from –15.6 to –5‰ PDB. While the radioactive carbon isotope composition for all groundwater samples expressed as ^{14}C concentrations in percent modern carbon (pmC) ranges from 42.6 to 114.5 pmC. The samples with the highest concentrations of ^{14}C come from bores in the northern part of the province, while the samples with the lowest concentration come from bores further south and away from the ranges. While there is a clear decrease in ^{14}C concentrations for samples from the alluvial/colluvial and bedrock aquifers, the samples with the lowest ^{14}C in most cases also have the highest (i.e. to less negative) $\delta^{13}C$ concentration. While this trend is not unexpected as radioactive decay is associated with increased MRT in the aquifers, it may suggest some mineral weathering occurring in parts of the aquifers where higher or less negative $\delta^{13}C$ is associated with carbonate formations.

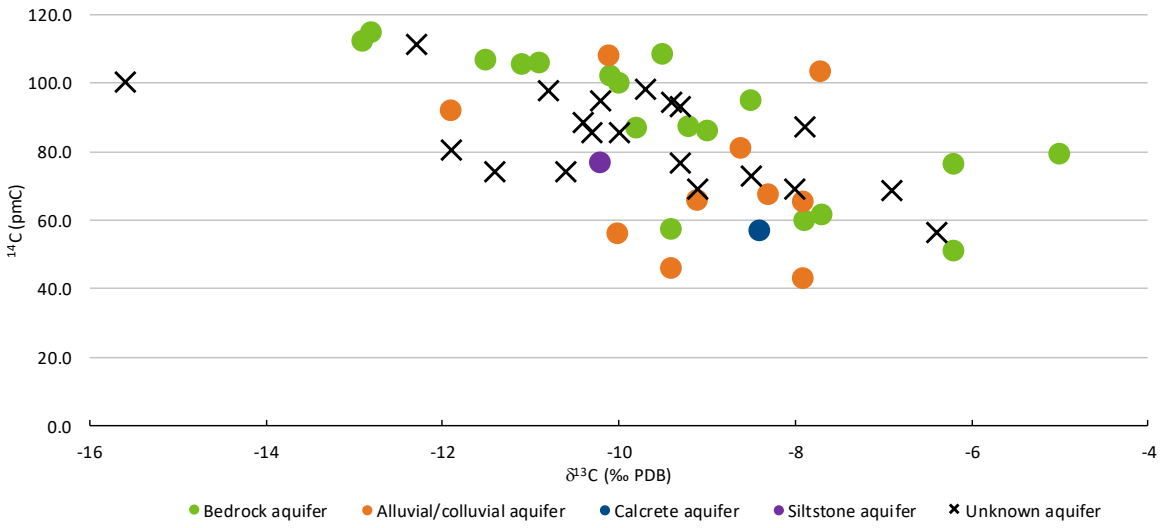

Figure 4-34. Measured ^{13}C and ^{14}C compositions for groundwater from aquifers within four different hydrogeological units. Data collated from Dodds et al. (2001); Craven (2012); Custance (2012); Leaney et al. (2013) and Kretschmer and Wohling (2014).

Regardless of aquifer, the raw or 'uncorrected' ^{14}C concentrations for the 50 groundwater samples corresponds to 'potential' MRTs for groundwater flow in the aquifer ranging between 0 and 7500 years (Table 4-2). However, in some cases groundwater samples contained both radioactively decayed ^{14}C but also measurable CFCs suggesting a mixture of young and old water (Figure 4-35). Therefore, further investigation or careful interpretation is required before assuming a given MRT and using this for estimating groundwater flow velocities or recharge rates. In addition, it is important to ensure the concentration of ^{14}C in the aquifer has not been geochemically altered through hydrogeological processes.

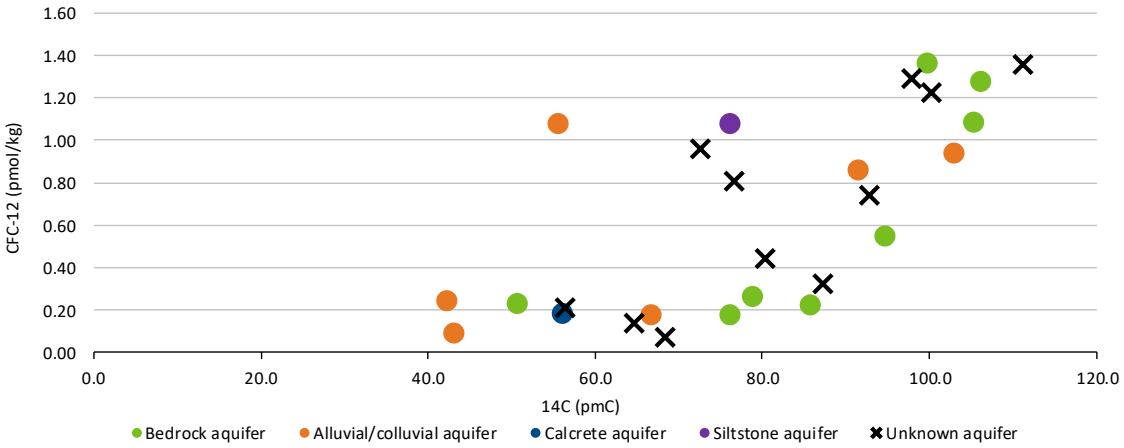

Figure 4-35. Measured ^{14}C and CFC-12 composition of groundwater from aquifers within four different hydrogeological units. Data collated from Leaney et al. (2013) and Kretschmer and Wohling (2014).

Further investigation of the geochemistry of each sample was conducted where possible to account for the possibility of the addition of 'dead' carbon to the TDIC pool of each sample by carbonate mineral weathering in the aquifers. Where possible, field measurements of pH and alkalinity were combined with laboratory chemistry and used as input parameters for geochemical modelling using PHREEQC. The outputs from PREEQC such as calculations of aqueous CO^2 and aqueous HCO_3 concentrations for each sample were then used as input parameters for four MRT corrections schemes (see Section 3.5.3).

Table 4-2: Mean residence times estimated using the raw ^{14}C concentrations for groundwater samples from aquifers in four different hydrogeological units. Data collated from Dodds et al. (2001); Craven (2012); Custance (2012); Leaney et al. (2013) and Kretschmer and Wohling (2014).

UNIT NUMBER	AQUIFER	RAW ^{14}C (pmC)	UNCORRECTED MEAN RESIDENCE TIME (YEARS)
484400002	Alluvial/colluvial aquifer	65.3	4000
494300007	Alluvial/colluvial aquifer	42.6	7500
524300010	Alluvial/colluvial aquifer	45.4	7000
534400018	Alluvial/colluvial aquifer	67.0	3500
534400060	Alluvial/colluvial aquifer	55.9	5000
534400064	Alluvial/colluvial aquifer	64.8	4000
534500021	Alluvial/colluvial aquifer	103.2	0
534500080	Alluvial/colluvial aquifer	107.7	0
534500154	Alluvial/colluvial aquifer	91.8	1000
554500016	Alluvial/colluvial aquifer	80.67	2000
484300012	Bedrock aquifer	57.3	5000
514500109	Bedrock aquifer	101.9	0
524400018	Bedrock aquifer	86.0	1500
524400021	Bedrock aquifer	86.9	1500
534400031	Bedrock aquifer	61.2	4500
534400035	Bedrock aquifer	50.9	6000
534400047	Bedrock aquifer	59.7	4500
534500033	Bedrock aquifer	112.0	0
534500067	Bedrock aquifer	105.5	0
534500068	Bedrock aquifer	106.5	0
534500079	Bedrock aquifer	108.3	0
534500084	Bedrock aquifer	114.5	0
534500120	Bedrock aquifer	105.9	0
544300025	Bedrock aquifer	79.0	2000
544300028	Bedrock aquifer	76.3	2500
544400015	Bedrock aquifer	94.9	1000
554400176	Bedrock aquifer	100.0	500
554500051	Bedrock aquifer	87.38	1500
514300006	Calcrete aquifer	56.4	5000
544400064	Siltstone aquifer	76.3	2500
524400017	Unknown	76.7	2500

534300002	Unknown	87.3	1500
534400008	Unknown	56.5	5000
534400050	Unknown	80.5	2000
534400051	Unknown	68.4	3500
534400071	Unknown	92.9	1000
534500024	Unknown	111.3	0
544400001	Unknown	100.3	500
544400007	Unknown	98.0	500
544400008	Unknown	72.7	3000
554400062	Unknown	85.58	1500
554400108	Unknown	88.32	1500
554400113	Unknown	85.46	1500
554400116	Unknown	74.19	3000
554500020	Unknown	94.53	1000
554500023	Unknown	94.69	1000
554500026	Unknown	97.6	500
554500027	Unknown	69.01	3500
–	Unknown	73.97	3000
–	Unknown	68.9	3500

Of the 50 groundwater samples measured for carbon isotopes, only 14 samples had measurements of field pH and field alkalinity combined with ion chemistry results returning a CBE of <20 %. This simply reflects the different nature of field sampling techniques, field processing of groundwater chemistry samples and difference in analytical facilities used in the different groundwater studies across the Musgrave Province. Of the 14 groundwater samples corrected, the difference between uncorrected and corrected MRT (see Table 4-3: Mean residence times (MRT) for groundwater samples estimated with four different correction schemes that account for the addition of dead carbon and isotope exchange) ranges from 500 years to 5500 years. The corrections are not aquifer specific with samples from the alluvial/colluvial, bedrock and unknown aquifers all indicating the presence of some dead carbon. The range in corrected MRT for the 14 groundwater samples is from 0 to 3000 years. The oldest groundwater samples come from groundwater bores at least 30 km south of the outcropping Musgrave Ranges. This analysis further highlights the importance of accounting for mineral weathering when using carbon isotopes in aquifers such as calcrete that contain carbonate sources. Furthermore, it also highlights the importance of field pH measurements, careful ion chemistry sampling and field alkalinity measurements when sampling for ^{14}C in groundwater.

Table 4-3: Mean residence times (MRT) for groundwater samples estimated with four different correction schemes that account for the addition of dead carbon and isotope exchange.

UNIT NUMBER	AQUIFER	FIELD pH	FIELD ALKALINITY AS HCO_3 (meq/L)	UNCORRECTED MEAN RESIDENCE TIME (YRS)	TAMERS MEAN RESIDENCE TIME (YRS)	PEARSON MEAN RESIDENCE TIME (YRS)	FONTES GARNIER MEAN RESIDENCE TIME (YRS)	MOOK MEAN RESIDENCE TIME (YRS)
534400018	Alluvial/colluvial aquifer	7.1	5.80	4500	0	1500	1000	1000
534500021	Alluvial/colluvial aquifer	7.6	6.60	1000	0	0	0	0
524400018	Bedrock aquifer	7.4	5.60	2500	0	25	0	0
534400035	Bedrock aquifer	7.4	3.40	6500	1500	1500	1500	1500
544300028	Bedrock aquifer	7.7	3.96	3500	0	0	0	0
544300025	Bedrock aquifer	7.4	4.20	3000	0	0	0	0
544300028	Bedrock aquifer	7.7	3.96	3500	0	0	0	0
544400015	Bedrock aquifer	7.4	7.60	1500	0	0	0	0
554500051	Bedrock aquifer	8.4	6.30	2500	0	0	0	0
534300002	Unknown aquifer	7.5	2.20	2500	0	0	0	0
534400008	Unknown aquifer	7.6	4.66	6000	500	500	500	500
534400050	Unknown aquifer	7.1	3.44	3000	0	3000	2000	1000
534400071	Unknown aquifer	7.6	6.60	2000	0	0	0	0

Noble gases

Table 4-4 summarises the noble gas data for 33 groundwater samples from aquifers in four different hydrogeological units. Noble gas concentration is expressed in cubic centimetre of gas per gram at standard temperature and pressure (STP) (i.e. cc(STP)/g). Regardless of aquifer, the range in helium-4 (^{4}He) span over two and a half orders of magnitude ranging from 2.9E–08 to 6.9E–06 cc(STP)/g. Ten of the 33 groundwater samples are close to atmospheric equilibrium (~4.04E–08 cc(STP)/g), while of the remaining 23 samples, 20 samples are about one to one and a half orders of magnitude above atmospheric equilibrium and three samples are about two orders of magnitude higher. Three of the groundwater samples with a ^{4}He concentration an order or two magnitude higher than atmospheric equilibrium also have ^{14}C concentrations albeit uncorrected of <80 pmC (Figure 4-36a). Furthermore, they are either devoid of measurable CFCs or have concentrations close to the detection limit with the exception of one sample below (Figure 4-36b). These three samples are collected from groundwater bores that are all well south of the outcropping ranges (i.e. >80 km). Concentrations of neon-20 (^{20}Ne) for all samples range from 8.8E–08 to 9.3E–07 cc(STP)/g. While concentrations of argon-40 (^{40}Ar) for all samples range from 3.0E–04 to 1.2E–03 cc(STP)/g. Both ^{20}Ne and ^{40}Ar concentrations in groundwater were used by Leaney et al. (2013) and Kretschmer and Wohling (2014) to determine the excess air entrapped in groundwater as a result of localised recharge. Both studies reported a range in excess air of 0.001 to 0.015 cc(STP)/g.

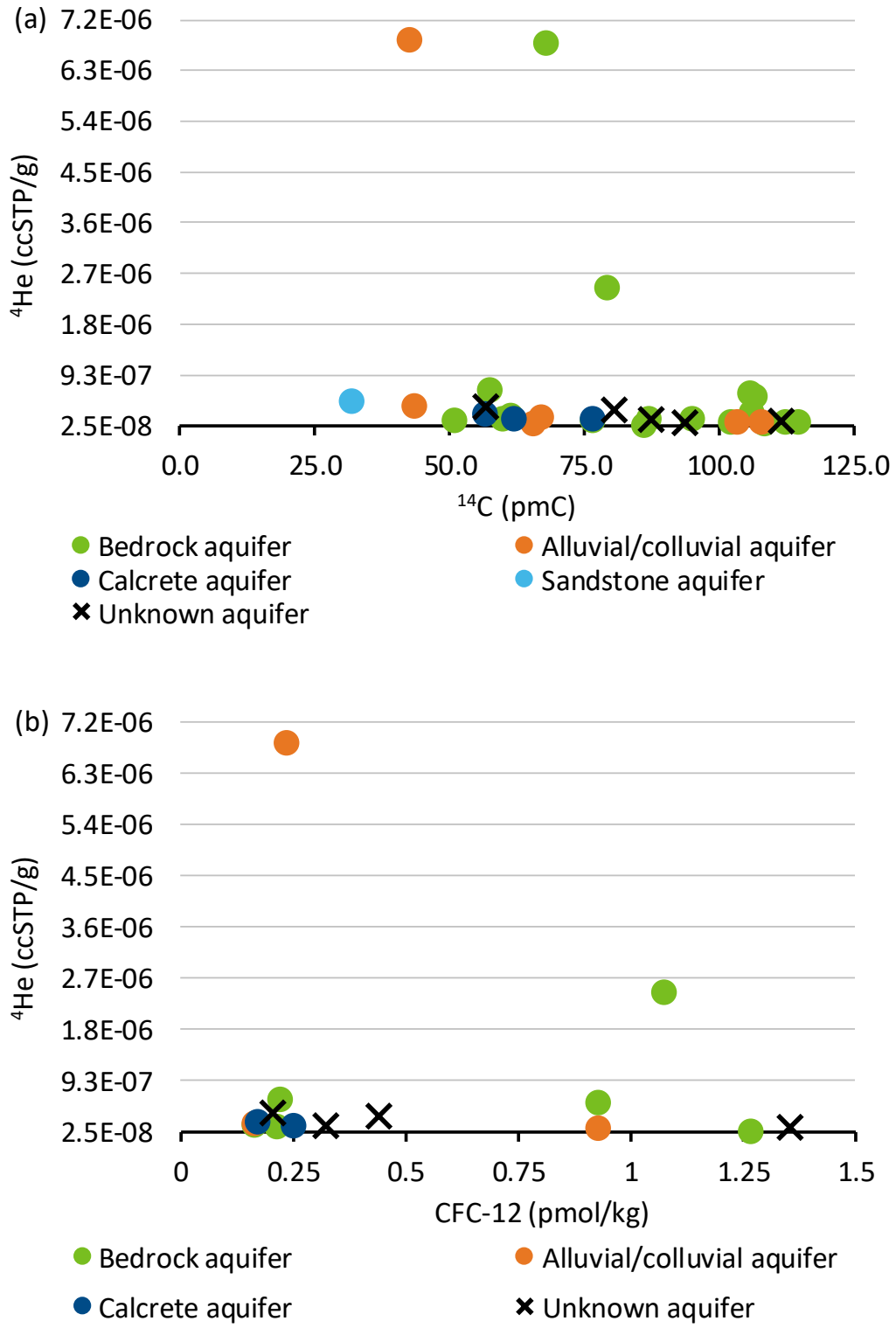

Figure 4-36. Measured ^{14}C versus ^{4}He (a) and measured CFC-12 versus ^{4}He (b) compositions of groundwater from aquifers within four different hydrogeological units. Data collated from Leaney et al. (2013) and Kretschmer and Wohling (2014).

Table 4-4: Summary of noble gas data for groundwater samples from aquifers in four different hydrogeological units. Data collated from Leaney et al. (2013) and Kretschmer and Wohling (2014).

UNIT NUMBER	AQUIFER	^{4}He concentration (cc(STP)/g)	^{20}Ne concentration (cc(STP)/g)	^{40}Ar concentration (cc(STP)/g)	Ae concentration (cc(STP)/g)
534500080	Alluvial/colluvial aquifer	7.28E-08	2.90E-07	4.18E-04	9.86E-03
524300010	Alluvial/colluvial aquifer	3.49E-07	2.22E-07	5.19E-04	5.27E-03
484400002	Alluvial/colluvial aquifer	5.79E-08	1.90E-07	6.20E-04	3.14E-03
494300007	Alluvial/colluvial aquifer	6.86E-06	9.25E-07	1.23E-03	5.23E-02
524300010	Alluvial/colluvial aquifer	3.49E-07	2.22E-07	5.19E-04	5.27E-03
534400018	Alluvial/colluvial aquifer	1.51E-07	2.23E-07	5.12E-04	1.84E-02
534500021	Alluvial/colluvial aquifer	9.19E-08	3.60E-07	3.59E-04	1.91E-02
534500079	Bedrock aquifer	6.01E-08	2.23E-07	5.56E-04	5.33E-03
534400031	Bedrock aquifer	1.89E-07	2.17E-07	5.00E-04	4.97E-03
534400047	Bedrock aquifer	1.30E-07	1.91E-07	3.17E-04	3.23E-03
534500033	Bedrock aquifer	8.53E-08	2.54E-07	8.41E-04	7.43E-03
534500084	Bedrock aquifer	8.05E-08	2.95E-07	5.35E-04	1.02E-02
534500068	Bedrock aquifer	5.37E-07	2.65E-07	3.95E-04	8.17E-03
534500120	Bedrock aquifer	2.53E-07	2.74E-07	7.60E-04	8.74E-03
484300012	Bedrock aquifer	6.52E-07	2.00E-07	5.75E-04	3.80E-03
484400003	Bedrock aquifer	6.82E-06	2.15E-07	3.77E-04	4.81E-03
514500109	Bedrock aquifer	8.53E-08	3.65E-07	8.14E-04	1.49E-02
524400021	Bedrock aquifer	1.22E-07	2.75E-07	8.12E-04	8.87E-03
524400018	Bedrock aquifer	2.94E-08	8.81E-08	4.94E-04	2.04E-02
534400035	Bedrock aquifer	1.16E-07	2.26E-07	3.54E-04	1.68E-02
534500067	Bedrock aquifer	5.92E-07	1.97E-07	5.57E-04	1.84E-02
544300025	Bedrock aquifer	2.47E-06	2.56E-07	5.31E-04	1.47E-02
544300028	Bedrock aquifer	1.14E-07	2.54E-07	3.38E-04	1.61E-02
544400015	Bedrock aquifer	1.40E-07	2.16E-07	4.84E-04	1.95E-02
514300006	Calcrete aquifer	2.06E-07	1.77E-07	3.04E-04	2.30E-03
474400010	Calcrete aquifer	1.41E-07	1.86E-07	6.66E-04	2.86E-03
474500096	Calcrete aquifer	1.38E-07	2.14E-07	3.85E-04	4.79E-03
554400101	Sandstone aquifer	4.46E-07	2.39E-07	4.62E-04	6.41E-03
534500024	Unknown	8.93E-08	3.48E-07	8.25E-04	1.37E-02
514500084	Unknown	6.15E-08	2.97E-07	7.31E-04	1.03E-02
534300002	Unknown	1.27E-07	2.97E-07	4.37E-04	1.91E-02
534400008	Unknown	3.36E-07	2.33E-07	4.02E-04	1.52E-02
534400050	Unknown	2.82E-07	6.42E-07	6.87E-04	3.03E-02

4.7 Groundwater recharge

4.7.1 CHLORIDE MASS BALANCE

Of the 135 groundwater bores with groundwater chloride measurements, a standing water level measurement and available bore construction details, 34 groundwater samples were identified for use in estimating recharge by CMB. As stated in Section 3.5.2, all 34 samples were collected at a depth of <10 m below the water table. By aquifer type, the alluvial/colluvial aquifer has much higher chloride concentrations compared to the bedrock aquifer (Table 4-5). The chloride in groundwater for the alluvial colluvial aquifer (n=7) ranges from 77 to 557 mg/L. For the bedrock aquifer (n=5), chloride in groundwater ranges from 36 to 173 mg/L. However, it must be noted that 20 groundwater bores used in the analysis did not have lithology records and therefore could not be attributed to an aquifer but had chloride in groundwater concentrations ranging up to 3560 mg/L.

Table 4-5 summarises the recharge rates for all samples, where recharge rates range between 0.1 to 7.3 mm/yr. The mean and median annual recharge rates are 1.7 and 1.2 mm/yr respectively. For the alluvial/colluvial aquifer recharge rates range from 0.4 to 3 mm/yr, with a mean and median recharge rate of 1.5 and 1.6 mm/yr respectively. For the bedrock aquifer, recharge rates range from 1.2 to 6.4 mm/yr, with a mean and median recharge rate of 3.2 and 1.7 mm/yr respectively. There was only one sample from each of the calcrete and sandstone aquifers, with the recharge rate calculated for both being 1.1 mm/yr.

Table 4-5: Summary of recharge rates estimated using chloride mass balance. Chloride in groundwater data and standing water level (SWL data) were collated from WaterConnect (DEW, 2018). The chloride deposition data was collated from Davies and Crosbie (2014).

UNIT NUMBER	STANDING WATER LEVEL (SWL)	Cl^- DEPOSITION (kg/ha/yr)	AQUIFER	DEPTH BELOW WATER TABLE (DBWT) (m)	Cl^- (mg/L)	R (mm/yr)
474500003	27.1	2.1	Alluvial/colluvial aquifer	2.4	87.8	2.4
534500017	13.3	2.3	Alluvial/colluvial aquifer	3.3	77.0	3.0
524500012	5.2	2.3	Alluvial/colluvial aquifer	3.7	557.0	0.4
514500027	21.8	2.6	Alluvial/colluvial aquifer	7.3	300.0	0.9
534500021	9.2	2.5	Alluvial/colluvial aquifer	7.9	140.0	1.8
534500022	7.9	2.4	Alluvial/colluvial aquifer	9.1	194.0	1.2
474500086	14.5	2.2	Alluvial/colluvial aquifer	9.3	148.0	1.5
474500079	12.3	2.2	Bedrock aquifer	1.0	150.0	1.5
474500077	12.9	2.1	Bedrock aquifer	4.2	173.0	1.2
534500006	6.1	2.3	Bedrock aquifer	9.1	36.2	6.4
474500032	13.5	2.2	Bedrock aquifer	9.3	130.0	1.7
504500007	32.8	2.5	Bedrock aquifer	9.8	48.1	5.2
474500036	21.5	2.1	Calcrete aquifer	9.7	185.0	1.2
524400014	27.0	2.9	Sandstone aquifer	0.1	253.0	1.2
514500069	3.9	2.6	Unknown	1.0	120.0	2.1
534300015	6.5	3.1	Unknown	1.8	660.0	0.5
534500035	13.0	2.2	Unknown	2.5	30.0	7.4
494500009	25.1	2.4	Unknown	2.7	129.0	1.8
524400015	7.3	2.6	Unknown	3.3	437.0	0.6
534300014	17.0	3.3	Unknown	3.6	380.0	0.9
534400049	5.0	2.8	Unknown	4.1	216.0	1.3
514500066	7.9	2.5	Unknown	4.1	318.0	0.8
514500070	7.6	2.7	Unknown	4.2	2180.0	0.1
534400032	9.2	3.0	Unknown	4.5	1490.0	0.2
514300002	24.9	3.0	Unknown	5.6	306.0	1.0
534500033	7.1	2.3	Unknown	6.1	91.0	2.5
494400009	33.0	2.4	Unknown	6.8	747.0	0.3
534400035	18.7	2.7	Unknown	6.8	330.0	0.8
514500060	18.0	2.8	Unknown	7.0	226.0	1.2
524300004	28.4	3.2	Unknown	7.1	3560.0	0.1
534400034	6.8	3.0	Unknown	7.1	672.0	0.4
514500073	16.0	2.6	Unknown	9.5	104.0	2.5
534400033	8.3	2.8	Unknown	9.6	500.0	0.6
504500018	11.2	2.4	Unknown	9.8	140.0	1.7

Depth below water table (DBWT)

4.7.2 CHLOROFLUOROCARBONS

Of the 27 groundwater samples with CFCs measured in groundwater, 12 groundwater samples had concentrations sufficient to use in estimating recharge while also having a standing water level and bore construction details required to estimate recharge (Table 4-6). Depending on the depth of sampling below the watertable both a PFM and EMM were used to estimate recharge rates. Overall, recharge rates estimated using CFCs range from approximately 4 to 198 mm/yr, with an average error of ±8 mm. The mean and median annual recharge rates are 39 and 15 mm/yr respectively. By aquifer, recharge rates for the alluvial/colluvial aquifer (n=4) range from 9 to 198 mm/yr, with a mean and median recharge rate of 77 and 50 mm/yr. For the bedrock aquifer (n=7), recharge rates range from 4 to 60 mm/yr, with a mean and median recharge rate of 20 and 11 mm/yr respectively. There was only one sample that could be used to calculate recharge to the calcrete aquifer, resulting in a recharge rate of 23 mm/yr. While the recharge rates estimated using CFCs are higher than those estimated with CMB (see Section 4.7.1) both methods have different assumptions and estimate recharge over different temporal scales. In addition, it should be noted that for some bores with measurable CFCs, groundwater samples also contained radioactively decayed ^{14}C indicating a mixture of young and old water. It appears evident that the concentration of CFs in bores 534400060 and 534500154 may have been compromised due to atmospheric exposure during sampling (i.e. the recharge rates are not plausible given the low rainfall and high evapotranspiration across the province). Both of these samples are from the alluvial/colluvial aquifer and if emitted would reduce the range in recharge for this aquifer to between 9 and 13 mm/yr, with a mean recharge rate of 11 mm/yr.

Table 4-6: Mean residence times (MRT) and recharge rates determined using CFC-12 concentrations in groundwater from aquifers in four different hydrogeological units. Recharge rates were estimated using both a piston flow model (samples <10 m depth below water table (DBWT) n=3) or an exponential mixing model (samples >10 m DBWT n= 10) assuming a recharge temperature of 20°C. Porosities were assumed as follows: (i) 5% - bedrock aquifer, (ii) 20% - alluvial/colluvial and sandstone aquifers and (iii) 30% - calcrete aquifer.

UNIT NUMBER	DEPTH BELOW WATER TABLE (DBWT) (m)	AQUIFER	MEAN RESIDENCE TIME (yrs)	RECHARGE RATE (mm/yr)	ERROR (mm/yr)
494300007	11.59	Alluvial/colluvial aquifer	250	9	±3
534400018	22.6	Alluvial/colluvial aquifer	350	13	–
534400060	15.93	Alluvial/colluvial aquifer	40	88	±13
534500154	51.4	Alluvial/colluvial aquifer	50	198	±16
534500068	18.84	Bedrock aquifer	30	35	±8
524400018	46.32	Bedrock aquifer	270	9	±1
534400035	9.65	Bedrock aquifer	45	11	–
534500067	9.6	Bedrock aquifer	30	16	±2
544300025	17.91	Bedrock aquifer	230	4	–
544400015	14.02	Bedrock aquifer	95	7	±1
554400176	27.55	Bedrock aquifer	25	60	±13
514300006	5.4	Calcrete aquifer	45	23	–

Depth below water table (DBWT)

4.7.3 CARBON ISOTOPES

Of the 80 groundwater samples collected containing measurable ^{14}C, less than half of the samples (n=33) could be used to estimate recharge as the sampling at these sites had a standing water level, bore construction details and radioactively decayed ^{14}C required to estimate recharge. Recharge rates were estimated using both a PFM and EMM depending on the depth of sampling below the watertable. Overall, recharge rates estimated with ^{14}C range from 0.1 to 13.7 mm/yr. The mean and median annual recharge rates are 1.5 and 0.7 mm/yr respectively. For the alluvial/colluvial aquifer (n=14), recharge rates range from 0.3 to 13.4 mm/yr, with a mean and median recharge rate of 2.5 and 0.9 mm/yr respectively. For the bedrock aquifer (n=11), recharge rates range from 0.1 to 1.8 mm/yr with a mean and median recharge rate of 0.6 and 0.5 mm/yr respectively. There were three samples collected from the calcrete aquifer where recharge ranged from 0.7 to 2.4 mm/yr. There were also two samples collected from the sandstone aquifer and one from a siltstone aquifer. Recharge rates estimates for the sandstone aquifer were 1.4 and 2.0 mm/yr and for the siltstone aquifer 0.3 mm/yr. These recharge rates are similar to those estimated with the CMB method, but generally an order of magnitude lower than those estimated with CFCs. This is not surprising as recharge rates estimated with ^{14}C are both spatially averaged and cover a temporal scale spanning from hundreds to thousands of years, compared to tens of years with CFCs.

Table 4-7: Summary of recharge rates derived using ^{14}C mean residence times. Recharge rates were estimated using both a PFM (samples <10 m depth below water table (DBWT) (n=5)) or an exponential mixing model (EMM) (samples >10 m DBWT (n= 28)). Porosities were assumed as follows: (i) 5% - bedrock aquifer, (ii) 20% - alluvial/colluvial and sandstone aquifers and (iii) 30% - calcrete aquifer.

UNIT NUMBER	Z – DEPTH BELOW WATER TABLE (DBWT) (m)	AQUIFER	AQUIFER THICKNESS PARAMETER USED IN EMM (H in m)	RECHARGE RATE (mm/yr)
474500038	17.8	Alluvial/colluvial aquifer	50	0.9
474500085	16.8	Alluvial/colluvial aquifer	50	1.4
484300020	25.5	Alluvial/colluvial aquifer	50	0.9
484400002	16.6	Alluvial/colluvial aquifer	50	0.3
494300007	11.6	Alluvial/colluvial aquifer	50	1.0
494500021	22.6	Alluvial/colluvial aquifer	50	0.4
524300010	12.2	Alluvial/colluvial aquifer	50	0.3
524300010	11.7	Alluvial/colluvial aquifer	50	1.3
534400018	22.6	Alluvial/colluvial aquifer	50	0.6
534400060	15.9	Alluvial/colluvial aquifer	50	0.9
534400064	17.0	Alluvial/colluvial aquifer	50	13.7
534500103	3.1	Alluvial/colluvial aquifer	50	3.5
534500154	51.4	Alluvial/colluvial aquifer	50	0.6
484400003	12.9	Alluvium/Calcrete	75	8.7
474500094	18.0	Bedrock aquifer	50	0.7
494500034	13.6	Bedrock aquifer	75	0.3

524400018	46.3	Bedrock aquifer	75	0.3
524400021	6.7	Bedrock aquifer	75	1.8
534400031	31.9	Bedrock aquifer	75	1.4
534400031	31.5	Bedrock aquifer	50	0.1
534400035	6.8	Bedrock aquifer	50	0.5
544300025	18.6	Bedrock aquifer	50	0.5
544300025	17.9	Bedrock aquifer	50	0.1
544400015	14.0	Bedrock aquifer	25	0.4
554400176	27.6	Bedrock aquifer	50	1.0
474400010	37.2	Calcrete aquifer	50	1.3
474500096	12.3	Calcrete aquifer	50	2.4
514300006	5.4	Calcrete aquifer	50	0.7
554400132	31.5	Sandstone aquifer	50	2.0
554400158	38.9	Sandstone aquifer	50	1.4
544400064	14.7	Siltstone aquifer	50	0.3
514500084	18.4	Unkown	50	0.4
554400108	3.8	Unkown	50	0.5

4.7.4 RECHARGE BY HYDROGEOLOGICAL UNIT

The mean annual recharge rates calculated using both CMB and ^{14}C were applied to the total area of fractured bedrock alluvium/colluvium units to estimate recharge volumes for these two important hydrogeological units. Recharge estimates derived using both CMB and ^{14}C provided the greatest number of estimates by aquifer and combine both point estimates with those that are spatially averaged across both aquifers. The areas estimated for each of the aquifers come from the updated hydrogeology map for the entire province refined using the interpretation of new and existing AEM surveys (Figure 5 1). In total, the fractured bedrock unit outcrops over an area of approximately is 8818 km^2, while the alluvial/colluvial unit which covers bedrock and palaeovalleys occupies an area of 75,900 km^2 across the Musgrave Province. When using a conservative mean annual recharge estimate of ~2 mm/yr and the cumulative area of each hydrogeological unit, this results in a mean annual recharge volume for the fractured bedrock and alluvium/colluvium of approximately 18 and 149 GL/yr respectively.

5 Discussion and conclusions

This report summarises the acquisition and interpretation of new geophysical data (airborne, near-surface and borehole), which is combined with existing data sets. This has assisted the mapping and hydrogeological conceptualisation across almost the entire South Australian Musgrave Province. The regional AEM coverage has contributed significantly to determining the extent of the palaeovalley aquifer systems that define the Province.

This interpretation of these geophysical data has been combined with the collation and review of existing groundwater salinity, groundwater yield, groundwater level and groundwater environmental tracer and chemistry data to improve current estimates of interpolated groundwater levels and groundwater recharge and flow across the province. The integration of these datasets underpinned the development of:

1. a revised hydrogeological framework for the province,
2. a refined conceptual model of groundwater recharge and flow, and
3. a revised recharge component of the water balance for key aquifers across the province.

5.1.1 HYDROGEOLOGICAL FRAMEWORK

A revised hydrogeological framework map is a key output from the G-Flows Stage-3 Project. The inverted AEM survey data reveals the extent and geometry of the palaeovalley network in detail (Figure 5-1). This figure shows the deepest part of the palaeovalley network (thalweg; indicated as black lines) which provide a key target for water resource exploration. These areas of deeper palaeoalley fill are also shown in Figure 5-2 which is an updated version of the framework origonally developed in G-Flows 1. The western portion of the South Australian Musgrave province remains relatively undersampled from an AEM perspective, although finer scale surveys covering some parts of the area are available (see Figure 5-1). The opportunity remians to extend the interpreted deep palaeovalley sedimentary sequences to the west and this will form part of an ongoing mapping activity once the AEM data have been inverted.

5.1.2 GROUNDWATER RECHARGE AND FLOW

The review and reinterpretation of groundwater level, chemistry and environmental tracers from previous studies integrated with the geological modelling and findings from the interpretation of new and existing geophysical data has proved invaluable for confirming and refining knowledge of groundwater flow processes. The collation and reinterpretation of environmental tracer data with more stringent constraints (i.e. accounting for sampling depths and aquifer geometry) compared with previous work (Dodds et al., 2001; Craven, 2012; Custance, 2012; Leaney et al., 2013; and Kretschmer and Wohling, 2014) has helped confirm some previous characterisation of groundwater recharge and flow processes as well as refine them and also refine groundwater recharge estimates for aquifers in key hydrogeological units.

The collation and re-interpretation of chemistry data (with a CBE of <20%) has confirmed spatial trends in groundwater chemistry associated with recharge, throughflow and discharge. Groundwater from bedrock aquifers and alluvial/colluvial aquifers in the north of the province in and around the ranges where recharge predominantly occurs is of a calcium-magnesium-bicarbonate composition and low salinity. Whereas, groundwater from alluvial/colluvial and bedrock aquifers further south of the ranges in the Great Victoria Desert progressively develops a sodium-chloride composition and salinity gradually becomes brackish. Groundwater from fractured and highly weathered bedrock aquifers around Indulkana Range and Mount Chandler in the south-east of the province on the geological boundary with the Great Artesian Basin is both highly variable in composition and salinity reflecting the complex hydrogeology. The ionic composition and salinity changes from calcium-magnesium-bicarbonate to sodium-chloride and fresh to saline over relatively short distance (a few km). Some groundwater samples in recharge and throughflow areas are enriched in calcium and bicarbonate due to long-term mineral weathering of patchy pedogenic calcrete horizons as a result of subtle groundwater flow.

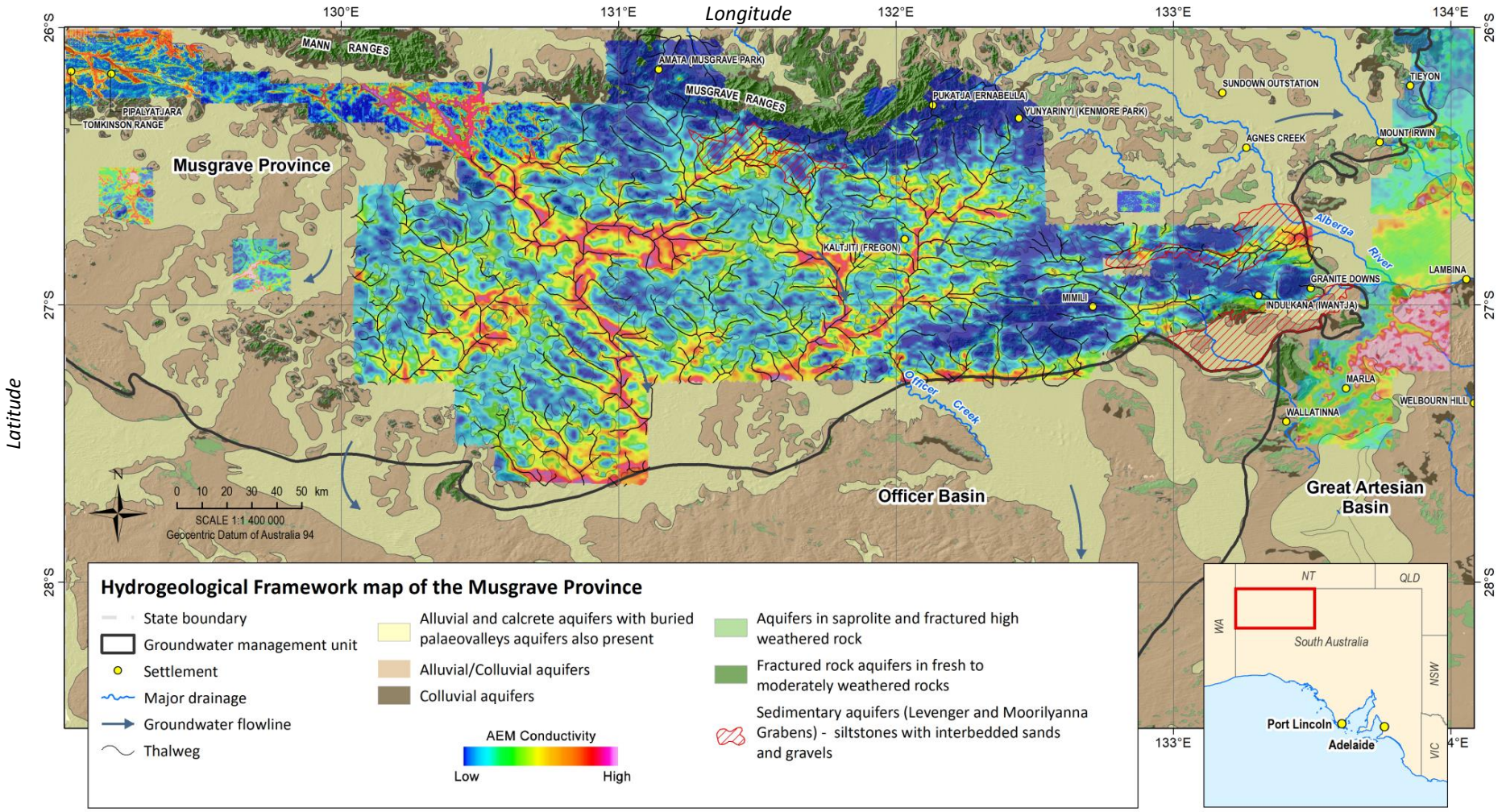

Figure 5-1. Hydrogeological framework map of the Musgrave Province, with pseudocoloured airborne electromagnetic interval conductivity images overlain.

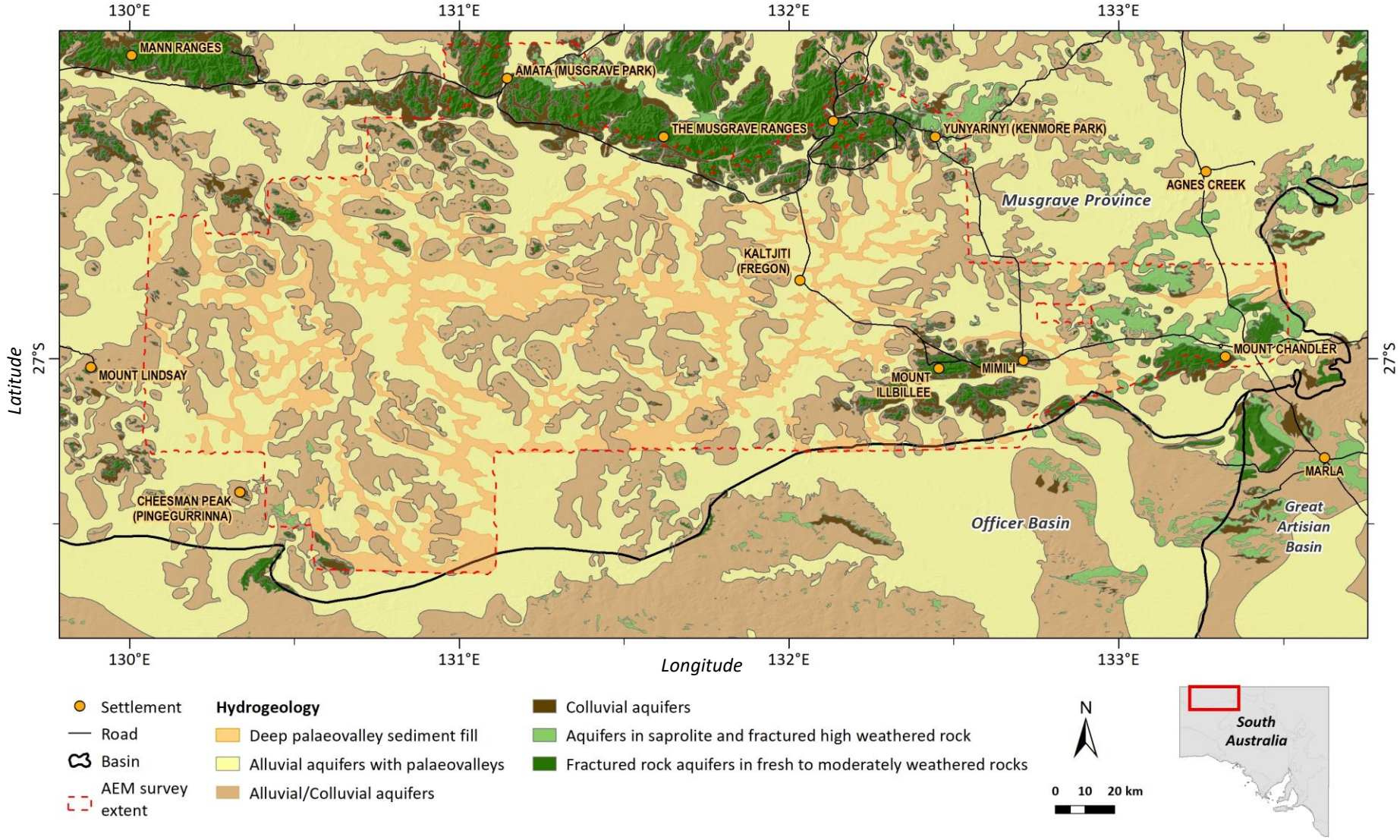

Figure 5-2. Revised hydrogeological framework map for the eastern part of the Musgrave Province with presence of deeper palaeovalley fill indicated in areas of alluvial cover.

Sodium-chloride type waters in discharge areas away from outcropping basement and have developed due to evapoconcentration of salts in the vadose zone that are leached to the watertable during highly episodic recharge events. This is also evidenced by the slightly elevated electrical conductivities observed in the AEM and ground TDEM data at or near the present day water levels in sediments overlying the palaeovalley systems.

Groundwater chloride data was used in the CMB method to refine previous estimates of groundwater recharge by Craven (2012), Custance (2012), Leaney et al. (2013) and Kretschmer and Wohling (2014). Compared with previous estimates of recharge using CMB, in this study any groundwater chloride sampled from a depth greater than 10 m below the water table was excluded from the estimates. This was to adhere more stringently to the assumptions of the CMB method by excluding any chloride at depth that may have accumulated due to lateral groundwater flow upgradient of the sampling point. Overall, the mean annual recharge rate using CMB is very low for all aquifers (<2 mm/yr) which is not surprising given the arid nature of the Musgrave Province. Higher recharge rates (up to 7 mm/yr) were estimated for bores in outcropping bedrock aquifers where vertical recharge occurs directly to saprolite, fractures, joints and faults. Overall and despite more stringent conceptual assumptions using CMB, the recharge rates estimated are similar to those reported by Craven (2012), Custance (2012), Leaney et al. (2013) and Kretschmer and Wohling (2014).

The analysis and interpretation of groundwater level data in this study has confirmed previous interpretations by Varma (2012) and Keppel et al. (2019) of the scale and directions of groundwater flow in the province. In general, groundwater flow is from north to south-south-east. Temporal groundwater level data is sparse and there are large unpopulated areas across the Great Victoria Desert where groundwater exploration has not occurred and therefore no data exists. Nevertheless, the change in static groundwater level from north to south-south-east is ~350 m over a distance of 150 km resulting in a hydraulic gradient of ~0.002. Recharge rates and fluxes are very low (i.e. <2 mm/yr) and groundwater residence times are long (i.e. a few thousand years). Furthermore, geological modelling and interpretation of AEM measurements have highlighted the heterogeneity of both bedrock topography and potential compartmentalisation of surficial cover by structure and possibly neotectonic activity. Together these would contribute to the development of rather complex or tortuous paths of groundwater flow in both the alluvial/colluvial and underlying palaeovalley cover. Neotectonism, involving the reactivation of basement fault systems perpendicular to primary orientation of the main trunk valleys, may also form hydraulic barriers within the pre-existing cover sediments, thereby adding complexity to the groundwater story.

A comparison of ^{2}H and ^{18}O data from groundwater, with that of Alice Springs precipitation, indicates that groundwater is depleted in recharge areas in the north of the province in and around outcropping crystalline basement and enriched with increasing distance to the south and south-east in discharge areas. The depleted isotopic composition confirms localised recharge as the dominant recharge process to bedrock and alluvial/colluvial aquifers in and around outcropping crystalline basement. A comparison of the isotopic composition to the amount-weighted mean monthly isotopic composition of Alice Springs precipitation, indicates that at least 40 mm of rainfall in a given month is required to overcome soil moisture deficits in this arid zone and generate groundwater recharge predominantly in outcropping bedrock and sandstone aquifers. However, at least 60 mm of rainfall in a given month is required to recharge the majority of the bedrock and alluvial/colluvial aquifers across the Musgrave Province.

Chlorofluorocarbons are only present in groundwater from recharge areas including bores in outcropping bedrock aquifers and bores in alluvial/colluvial aquifers either adjacent outcropping bedrock or along or near ephemeral drainage lines. Some groundwater from the alluvial/colluvial aquifers contains both measurable CFCs and radioactively decayed ^{14}C indicating a mixture of young and old water. These bores occur in the valleys and plains adjacent outcropping crystalline basement confirming the hydrological connectivity between the two aquifers as a result of localised discharge from bedrock aquifers into adjacent alluvial/colluvial aquifers. The mean annual recharge rate estimates derived from CFCs for both bedrock and alluvial/colluvial aquifers is an order of magnitude higher than estimates derived with both CMB and ^{14}C (alluvial/colluvial aquifer mean (11 mm/yr) and bedrock aquifer mean 20 mm/yr). This is not surprising given the short temporal scale (tens of years) that CFCs account for and the fact that they only represent the portion of recharge that comes from larger localised flood events in aquifer outcrops and near ephemeral

drainage features, as opposed to long-term diffuse recharge out on the plains. However, the recharge rates estimated here using CFCs are consistent with those estimated for the northern Musgrave Province by Cresswell et al. (2002) when excluding two samples likely contaminated during field sampling.

Radiocarbon has been the most prominently sampled tracer in the Musgrave Province with a total of 80 bores sampled, though ^{13}C data was only available for 50 of these sites. Uncorrected mean residence time (MRT) for groundwater regardless of aquifer ranges from 0 to 16,000 years (± 500 years), though most samples range from 0 to 10,000 years with only three sites >10,000 years. The alluvial/colluvial aquifer has the largest range in MRT and highest median MRT of ~3,500 years which is not surprising given the extensive cover of alluvial/colluvial material spanning an area of approximately 75,900 km^2. Mean residence times for both bedrock aquifers and alluvial/colluvial aquifers in recharge areas in the north of the province near the ranges have low MRTs ranging up to 500 years. Geochemical corrections were undertaken on the data from 14 groundwater sites, which resulted in several sites in recharge areas having much shorter MRT (0 to 500 years) though a number of samples further south in throughflow and discharge areas still having corrected MRT ranging up to 3000 years. Given the patchy nature of pedogenic calcrete horizons throughout the province, the lack of appropriate field and laboratory chemistry required to correct ^{14}C MRTs and no systematic trend in field pH corrections to the large number of ^{14}C measurements was not possible. However, it is conclusive that where corrections were appropriate not enough mineral weathering has taken place given the patchy nature of the calcrete that groundwater with a MRT of several thousand years still occurs in throughflow and discharge areas. This finding is further confirmed by the presence of ^{4}He concentrations in groundwater above atmospheric equilibrium in the same throughflow and discharge areas (see below). Given that geochemical modelling demonstrated that not all ^{14}C require geochemical correction, uncorrected ^{14}C MRTs were used to derive the long-term (several thousand years) annual recharge rates for each aquifer.

Regardless of aquifer the mean annual recharge rate derived using ^{14}C is very low (<2 mm/yr) though recharge rates for individual bores were higher (up to 14 mm/yr) in alluvial/colluvial aquifers adjacent outcropping crystalline basement. Overall, the recharge rates derived with uncorrected ^{14}C MRTs correlate well with those derived using CMB. Both the CMB and ^{14}C derived recharge rates are better suited for understanding the long-term annual recharge rates for aquifers and appear conceptually correct for an arid zone with a mean annual rainfall of <250 mm/yr and annual areal potential evapotranspiration >3,000 mm/yr. In addition, the recharge rates derived with ^{14}C are an order of magnitude higher than those using the same method reported by Craven (2012) and Custance (2012). However, this study had access to a much larger number of samples collected from multiple aquifers over a much larger geographical area unlike the very low (<1 mm/yr) localised estimates derived by Craven (2012) and Custance (2012) which are also likely to be affected by diffusion.

Helium-4 concentrations in groundwater span over two and a half orders of magnitude with a large proportion of the samples (~60%) having concentrations about one to one and a half orders of magnitude above atmospheric equilibrium. The highest concentrations of ^{4}He in groundwater occur well south of the ranges in discharge areas which are also samples with the lowest ^{14}C. Most of the samples with a ^{4}He concentration in groundwater at or close to atmospheric equilibrium occur in the recharge areas in the north of the province in and around the ranges. The noble gas sampling by both Leaney et al. (2013) and Kretschmer and Wohling (2014) was very useful for validating the ^{14}C data and thereby confirming the spatial trends in recharge and discharge areas.

The mean annual volume of recharge estimated for the two most important hydrogeological units in the Musgrave Province (fractured bedrock and alluvium/colluvium) is similar to those published by Kretschmer and Wohling (2014). Estimates derived in this study are slightly higher due to a combination of using a more stringent conceptual assumption with CMB as well as deriving estimates with ^{14}C which are spatially averaged recharge rates, a method not employed by Kretschmer and Wohling (2014). Regardless of the recharge volumes estimated, groundwater discharge estimates are currently unknown and would require further modelling to estimate. Nevertheless, recharge rates are very low across the province and long-term (decadal) groundwater extraction will have to be very carefully managed to ensure groundwater from aquifers is not mined.

5.1.3 HYDROGEOLOGICAL CONCEPTUAL MODEL

The combined geophysics and groundwater hydrology work in G-Flows Stage-3 builds on the earlier work outlined above, and confirms, in broad terms, some of the previous conceptual understanding of aquifers in the arid Musgrave Province. The conceptualisation of both the geology and hydrogeology have been previously presented in conceptual schematics by Munday et al. (2013) and more recently by Gogoll (2016). In this study we have also considered findings from some localised work by Parsekian et al. (2014), and more recently by Munday et al. (2016), Krapf et al. (2019), and Costar et al. (2019), and then coupled them with findings in this study to subsequently adapt and refine conceptual schematics from Munday et al. (2013) and Gogoll (2016) as shown in Figure 5-3.

The key hydrogeological processes include:

- Highly episodic runoff from the outcropping Musgrave, Mann, Tomkinson and Everard Ranges;
- Highly episodic groundwater recharge predominantly at the ranges, where bedrock aquifers outcrop, but episodic recharge fluxes are also possible through ephemeral drainage lines traversing surficial alluvium and colluvium away from the ranges;
- Alluvial/colluvial and bedrock aquifers are hydraulically interconnected via localised bedrock discharge recharging the alluvium/colluvium surrounding the ranges and via throughflow from the alluvium/colluvium recharging underlying palaeovalley and compartmentialised bedrock aquifers;
- Intermediate to regional groundwater flow is ‘generally’ from north to south in both alluvial/colluvial and palaeovalley aquifers;
- Groundwater flow is controlled by highly episodic and low recharge fluxes occurring predominantly around the Musgrave and Mann ranges in the north of the province with flow proceeding and diminishing south towards the Officer Basin given very low hydraulic gradients;
- Intermediate to regional groundwater flow in alluvial/colluvial and palaeovally aquifers is also controlled by bedrock topography where small outcrops and shallow subcrops of crystalline basement sporadically interupt and create more tortuous flow paths from north to south;
- Structure compartmentalises the alluvial/colluvial fill in the palaeovalleys which may also influence the groundwater flow paths;
- The flow paths may also be interrupted by neotectonic activity resulting from the reactivation of basement structures and the formation of hydraulic barriers in the overlying sediment package;
- Groundwater discharge in alluvial/colluvial aquifers occurs via a combination of evapotranspiration and throughflow to both underlying palaeovally and bedrock aquifers, as well as southerly flow towards the Officer Basin;
- Groundwater discharge in bedrock aquifers occurs as evapotranspiration in aquifer outcrops and throughflow to adjacent alluvial/colluvial aquifers at the foot of the ranges;
- There is no hydraulic or hydrogeochemical evidence to support a hypothesis for intermediate to regional groundwater flow in bedrock aquifers in such a data sparse region. Evidence from airborne geophysics, lithological and stratigraphic logs, geological modelling, regional magnetics and high variability in both bore yields and groundwater salinity suggests the bedrock aquifers are highly compartmentalised but hydraulically interconnected at locations where they are overlain with palaeovalley and alluvial/colluvial aquifers.

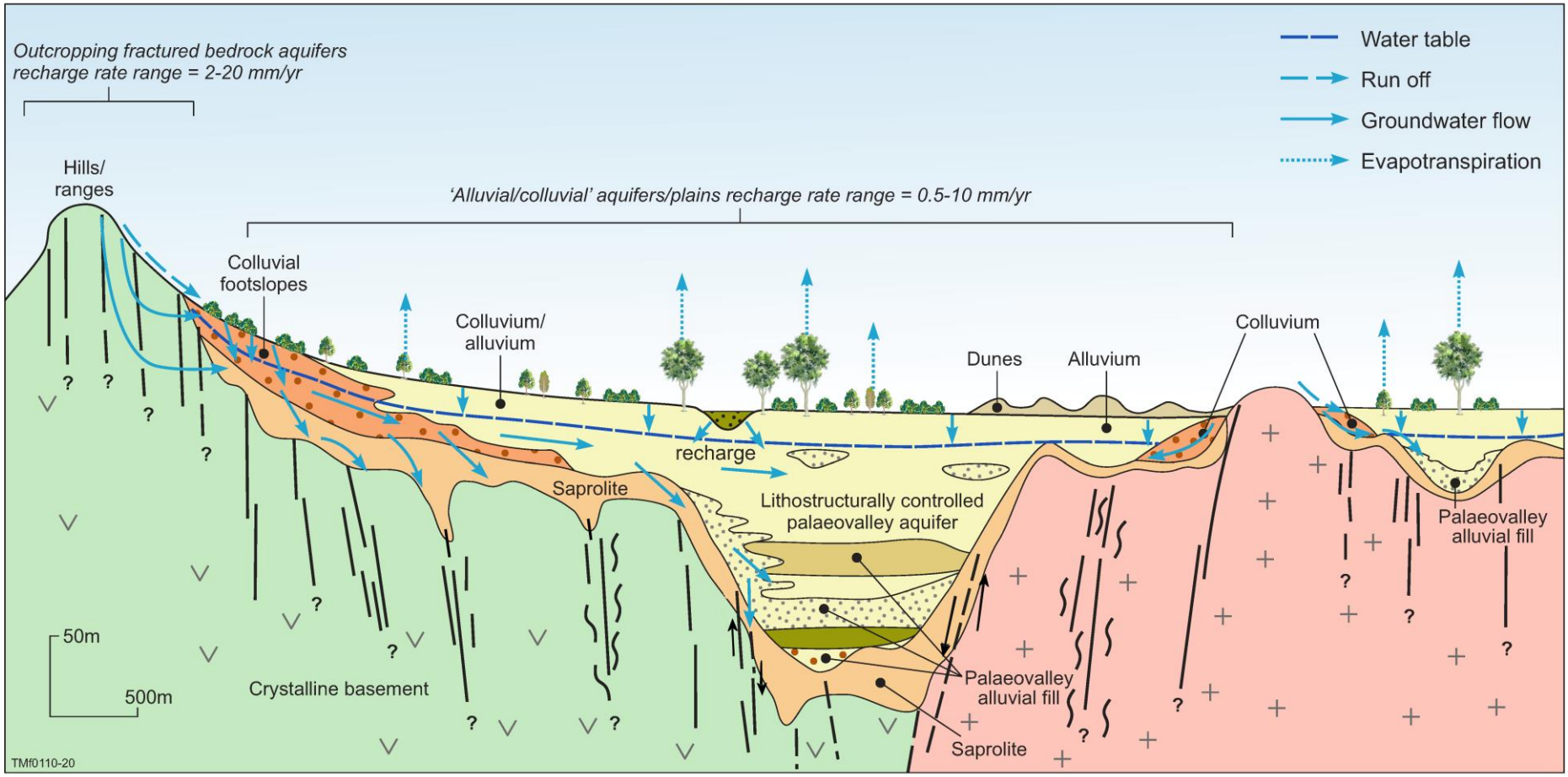

Figure 5-3. Schematic hydrogeological conceptual model showing a typical palaeovalley drainage system in the Musgraves. Figure adapted from Munday et al. (2013, 2020) and Gogoll (2016).

5.1.4 PALAEOVALLEY ARCHITECTURE

Palaeovalley architecture is an important aspect of understanding the water resources they contain. The drilling program in G-Flows Stage-3 provided an opportunity to obtain information on the materials and hydrologic properties down through a large palaeovalley. Drilling in the Lindsay East Palaeovalley (at Site DH1) has provided detail information at this location. Along the length of the palaeovalley some change along the course is expected, but the fill materials are likely to be consistent. The availability of AEM data across many of the main palaeovalley systems as associated buried tributary valleys provides information on the geometry and thickness of the fill sequences.

The well lithology information (Keppel et al., 2019) provides information to help support the AEM interpretation. There are large clay units at depth in the palaeovalley which are associated with estuarine/marginal marine settings. These sediments have higher electrical conductivities (red) but contain less mobile water (see Figure 5-4). The recognition of marginal marine conditions extending well into the APY Lands, coupled with the geometry and depth of the palaeovalley system has allowed predictive models to be derived for the sedimentary fill sequences when linked with existing bore lithology logs.

Borehole Nuclear Magnetic Resonance (BNMR) has provided measurements of how available-water varies with depth as you get deeper in the palaeovalley (capillary and mobile, compared to clay-bound water components in Figure 5-4). The measured BNMR responses and modelled hydraulic properties of the sedimentary fill sequences are highly variable indicative of a complex aquifer system, with zones of higher yielding materials that have potentially good connection with the broader aquifer package.

The BNMR data also suggest that shallower parts of the palaeovalley sediment package at DH1 may be more prospective for water, with a static water level around 8 m below the land surface. Shallow wells (20-40 m) may provide an effective target in this area, as opposed to going very deep (80-100 m). Pumping smaller amounts from distributed multiple shallow bores could be a helpful strategy, although further work is required to assess this option.

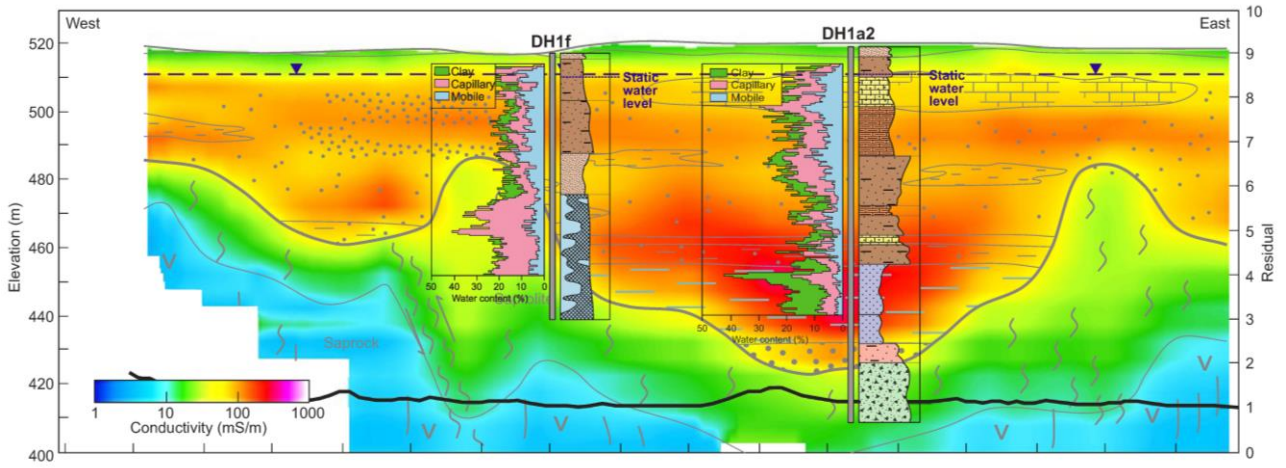

Figure 5-4. Cross-section of Lindsay East Palaeovalley at DH1 (East of Kaltjiti/Fregon). Coloured background is the electrical conductivity determined from the inverted airborne electromagnetic data. Interpreted geology is overlain as grey linework. Well lithology (Keppel et al., 2019), and water content from the borehole nuclear magnetic resonance are superimposed.

References

AGT (2003) Anangu Pitjantjatjara Lands – Review of Sustainability of Community Water Supplies. A report prepared for South Australian Water Corporation by Australian Groundwater Technologies, June 2003. AGT Report No. 2003/18.

AGT (2008) Sustainability of water resources in Anangu Pitjantjatjara Yankunytjatjara Lands, Maralinga Tjarutja Lands & Aboriginal Lands Trust Lands, South Australia. Prepared for Department of Water, Land and Biodiversity Conservation (DWLBC) and South Australian Water Corporation (SA Water) AGT Report No. 2008/31. 03/11/2008- 358.

Aitken ARA and Betts PG (2008). High-resolution aeromagnetic data over Central Australia assist Grenville-era (1300–1100 Ma) Rodinia reconstructions. *Geophysical Research Letters* 35: L01306.

Aitken ARA, Betts PG, Ailleres L (2009). The architecture, kinematics, and lithospheric processes of a compressional intraplate orogen occurring under Gondwana assembly: The Petermann orogeny, central Australia. Lithosphere 1(6): 343–357. doi: https://doi.org/10.1130/L39.1

APYWMC (2002) The Anangu Pitjantjatjara Yankunytjatjara Water Management Plan. A report prepared for: Anangu Pitjantjatjara Yankunytjatjara and the Member Communities, Bureau of Rural Sciences, Arid Area Catchment Water Management Board and the Aboriginal and Torres Strait Islander Commission.

Auken E and Christiansen AV (2004) Layered and laterally constrained 2D inversion of resistivity data. *Geophysics* 69: 752-761.

Auken E, Christiansen AV, Jacobsen BoH, Foged N and Sørensen KI (2005) Piecewise 1D laterally constrained inversion of resistivity data. *Geophysical Prospecting* 53: 497–506.

Auken E, Christiansen AV, Kirkegaard C, Fiandaca G, Schamper C, Behroozmand AA, Binley A, Nielsen E, Effersø F, Christensen NB, Sørensen K, Foged N and Vignoli G (2015) An overview of a highly versatile forward and stable inverse algorithm for airborne, ground-based and borehole electromagnetic and electric data. *Exploration Geophysics* 46: 223–235.

Calf GE, McDonald PS and Jacobson G (1991) Recharge mechanism and groundwater age in the Ti-Tree Basin, Northern Territory. *Australian Journal of Earth Sciences* 38: 299–306.

Clarke J (2009) Palaeovalley, Palaeodrainage, and Palaeochannel – What's the difference and why does it Matter? *Transactions of the Royal Society of South Australia* 133: 57-61, DOI: 10.1080/03721426.2009.10887111

Close DF, Edgoose CJ and Scrimgeour IR (2003) Hull and Bloods Range Special, Northern Territory, 1:100 000 Geological Map Series Explanatory Notes, 4748, 4848. Northern Territory Geological Survey, Darwin.

Coats RP (1962) The geology of the Alberga 4-Mile Military Sheet, Report of Investigations 22. Geological Survey of South Australia, Adelaide.

Conor CHH (2004) The geology of the Eateringinna 1:100 000 sheet area, eastern Musgrave Block, South Australia, Report Book 2003/00016. Primary Industry and Resources South Australia, Adelaide.

Cook PG and Böhlke J-K (2000) Determining Timescales for Groundwater Flow and Solute Transport. In: Cook P and Herczeg AL (eds) Environmental Tracers in Subsurface Hydrology. Kluwer Academic, Boston, 1–30.

Costar A, Love A, Krapf C, Keppel M, Munday T, Inverarity K, Wallis I and Soerensen C (2019) Hidden water in remote areas – using innovative exploration to uncover the past in the Anangu Pitjantjatjara Yankunytjatjara Lands. *MESA Journal* 90: 23–35.

Cotton TB, Scardigno MF and Hibburt JE (2006) The petroleum geology of South Australia. Vol. 2: Eromanga Basin. Petroleum Geology of South Australia Series. Department of Primary Industries and Resources, South Australia.

Craven CB (2012) Sustainability of regolith hosted aquifers in the Musgrave Province: Northern South Australia. Honours Thesis. Flinders University of South Australia.

Cresswell R, Wischusen J, Jacobson G and Fifield K (1999) Assessment of recharge to groundwater systems in the arid southwestern part of Northern Territory, Australia, using chlorine-36. *Hydrogeology Journal* 7: 393–404.

Cresswell RG, Hostetler S, Jacobson G and Fifield LK (2002) Rapid, episodic recharge in the arid north of South Australia. Proceedings of International Association of Hydrogeologists Groundwater Conference "Balancing the Groundwater Budget", May 14-17 2002, Darwin.

Crosbie RS, Jolly ID, Leaney FW, Petheram C and Wohling D (2010) Review of Australian groundwater recharge studies, CSIRO Water for a Healthy Country National Research Flagship Report, Canberra.

Crosbie RS, Pollock DW, Mpelasoka FS, Barron OV, Charles SP and Donn MJ (2012) Changes in Köppen-Geiger climate types under a future climate for Australia: hydrological implications. *Hydrology and Earth System Sciences* 16(9): 3341–3349.

Custance HE (2012) Hydrochemistry of shallow regolith hosted aquifers in the eastern Musgrave Province of South Australia. Honours Thesis. Flinders University of South Australia.

Davies PJ and Crosbie RS (2014) Australian chloride deposition rate. v4. CSIRO. Data Collection. https://doi.org/10.4225/08/545BEE54CD4FC

Davies PJ and Crosbie RS (2017) Mapping the spatial distribution of chloride deposition across Australia. Submitted to Journal of Hydrology. Volume 561, 2018, Pages 76-88, ISSN 0022-1694.

DEW (2018) WaterConnect is South Australia's online water information portal containing a wide range of information and data relating to groundwater and surface water available under a Creative Commons Attribution (CC-By) license. Data viewed and collated, March 2019. https://www.waterconnect.sa.gov.au/Pages/Home.aspx

Dodds S and Clarke D (2003) Groundwater Investigations at Fregon and Mimili Communities, Anangu Pitjantjatjara Lands, South Australia. DWLBC Report 2003/01, Department of Water, Land and Biodiversity Conservation, South Australia.

Dodds S and Sampson L (2000) The Sustainability of Water Resources in the Anangu Pitjantjatjara Lands, South Australia. Department for Water Resources, PIRSA RB 2000/00027, Adelaide.

Dodds AR, Hostetler S and Jacobson G (2001) Community Water Supplies in the Anangu Pitjantjatjara Lands, South Australia: Sustainability of Groundwater Resources. Bureau of Rural Sciences, Canberra.

Edgoose CJ, Scrimgeour IR and Close DF (2004) Geology of the Musgrave Block, Northern Territory, Report 15. Northern Territory Geological Survey, Darwin.

Evins PM, Smithies RH, Howard HM, Kirkland CL, Wingate MTD and Bodorkos S (2010) Devil in the detail; The 1150–1000 Ma magmatic and structural evolution of the Ngaanyatjarra Rift, west Musgrave Province, Central Australia. *Precambrian Research* 183: 572-588.

Fitzgerald J, Cunliffe D, Dodds S, Hostetler S, Rainow S and Jacobson G (2000) Groundwater Quality and Environmental Health Implications, Anangu Pitjantjatjara Lands, South Australia. Bureau of Rural Sciences, Canberra.

Fontes J-C and Garnier J-M (1979) Determination of the initial ^{14}C activity of the total dissolved carbon: A review of the existing models and a new approach. *Water Resources Research* 15: 399–413.

Gallant JC and Dowling TI (2003) A multiresolution index of valley bottom flatness for mapping depositional areas. *Water Resources Research* 39: 1347.

Glikson AY, Ballhaus C, Clarke GL, Sheraton JW, Stewart AJ and Sun S-S (1995) Geological framework and crustal evolution of the Giles mafic-ultramafic complex and environs, western Musgrave Block, central Australia. *AGSO Journal of Australian Geology and Geophysics* 16: 41–67.

Glikson AY, Stewart AJ, Ballhaus CG, Clarke GL, Feeken EHJ, Leven JH, Sheraton JW and Sun S-S (1996) Geology of the western Musgrave Block, Central Australia, with particular reference to the maficultramafic Giles Complex, Bulletin 239. Australian Geological Survey Organisation, Canberra.

Gogoll, M. (2016) Challenges targeting potable groundwater in the APY Lands, SA. Presentation at SA-NRM Science Conference 2016, University of Adelaide 13-15 April 2016. Day 3 Session 8.

Gulbrandsen ML, Cordua KS, Bach T, Hansen TM (2017) Smart Interpretation – automatic geological interpretations based on supervised statistical models. *Computational Geosciences* 21: 427–440.

Harrington GA, Herczeg AL and Cook PG (1999) Groundwater Sustainability and water Quality in the Ti-Tree Basin, Central Australia. CSIRO Land and Water Technical Report 53/99, Adelaide.

Hou B, Frakes LA, Alley NF and Clarke JDA (2003a) Characteristics and evolution of the Tertiary palaeovalleys in the NW Gawler Craton, South Australia. *Australian Journal of Earth Sciences* 50: 215–230.

Hou B, Frakes LA, Alley NF, Gammon P and Clarke JDA (2003b) Facies and sequence stratigraphy of Eocene valley fills in Eocene palaeovalleys, the eastern Eucla Basin, South Australia. *Sedimentary Geology* 163: 111–130.

Hou B, Frakes LA and Alley NF (2007) Palaeochannel evolution, northwestern Gawler Craton, South Australia. In Anand RR and de Broekert, P. (eds.) 'Regolith landscape evolution across Australia; a compilation of regolith landscape case studies with regolith landscape evolution models', Cooperative Research Centre for Landscape Environments and Mineral Exploration (CRC LEME), Bentley, WA, Australia. pp.116–229.

Howard HM, Werner M, Smithies RH, Evins PM, Kirkland CL, Kelsey DE, Hand M, Collins A, Pirajno F, Wingate MTD, Maier WD and Raimondo T (2011) The geology of the West Musgrave Province and the Bentley Supergroup — a field guide. Record 2011/04. Geological Survey of Western Australia, Perth.

Howles S, Gogoll M and Vasilic N (2017) APY Lands and Yalata water search 2015-17, DEWNR Technical note 2017/15, Government of South Australia, Department of Environment, Water and Natural Resources, Adelaide.

IAEA/WMO (2019) Global Network of Isotopes in Precipitation. The GNIP Database. Accessible at: https://nucleus.iaea.org/wiser

Ingerson E and Pearson FJ (1964) Estimation of age and rate of motion of groundwater by the 14C-method. In *Recent researches in the fields of atmosphere, hydrosphere and nuclear geochemistry* (Eds. Y Miyake and T Koyama), pp.263-283, Marusan, Tokyo.

Jacobson G, Calf GE, Jankowski J, McDonald PS (1989) Groundwater chemistry and palaeorecharge in the Amadeus Basin, central Australia. *Journal of Hydrology* 109: 237–266.

Keppel M, Costar A, Krapf C and Love A (2019) G-FLOWS Stage 3 - APY Lands Drilling Program, north-western South Australia. Technical Report Series 19/39, Goyder Institute for Water Research, Adelaide.

Korsch RJ and Kositcin N (eds) (2010) *GOMA (Gawler Craton-Officer Basin - Musgrave Province - Amadeus Basin) Seismic and MT Workshop 2010*. Record 2010/39. Geoscience Australia, Canberra.

Krapf CBE, Irvine JA and Cowley WM (2012) Compilation of the 1:2 000 000 State Regolith Map of South Australia – a summary, Report Book 2012/00016. Department for Manufacturing, Innovation, Trade, Resources and Energy, South Australia, Adelaide.

Krapf C, Costar A, Stoian L, Keppel M, Gordon G, Inverarity L, Love A and Munday T (2019) A sniff of the ocean in the Miocene at the foothills of the Musgrave Ranges – unravelling the evolution of the Lindsay East Palaeovalley. *MESA Journal* 90: 4–2.

Kretschmer P, Wohling D (2014) Groundwater recharge in the Anangu Pitjantjatjara Yankunytjatjara Lands, South Australia. DEWNR Technical Report 2014/06, Government of South Australia, through the Department of Environment, Water and Natural Resources, Adelaide.

Krieg GW and Rogers PA (1995) Eromanga Basin: stratigraphy – marine succession. In *The Geology of South Australia. Vol. 2, The Phanerozoic* (eds. JF Drexel, and VP Preiss), pp 112-123, Bulletin 54, Geological Survey of South Australia.

Lawrie K, Brodie RS, Christensen NB, Gibson D, Halas L, Symington N, Tan KP, Sandiford M, Ziramov S, Urosevic M, Grunewald E and Hayes P (2016) Neotectonic intra-plate fault zone mapping and hydrogeology in floodplain sediments: an inter-disciplinary approach, ASEG Extended Abstracts, 2016:1, 1-9, DOI:10.1071/ASEG2016ab400.

Leaney FW, Taylor AR, Jolly ID, and Davies PJ (2013) Facilitating Long Term Out-Back Water Solutions (G-FLOWS) Task 6: Groundwater recharge characteristics across key priority areas, Goyder Institute for Water Research Technical Report Series No. 13/6, Adelaide, South Australia.

Lewis SJ, English PM, Wischusen JDH, Woodgate MF, Gow LJ, Hanna AL and Kilgour PL (2010) The Palaeovalley Groundwater Project: Operational Update on Demonstration Study Sites July 2009 to April 2010. Milestone 5 Report by Geoscience Australia for the National Water Commission, April 2010, 302p.

Ley-Cooper AY and Munday TJ (2013) Groundwater Assessment and Aquifer Characterization in the Musgrave Province, South Australia: Interpretation of SPECTREM Airborne Electromagnetic Data, Goyder Institute for Water Research Technical Report Series No. 13/7, Adelaide, South Australia.

Magee JW (2009) Palaeovalley Groundwater Resources in Arid and Semi-Arid Australia – A Literature Review. Geoscience Australia Record 2009/03. 224 pp.

Major RB and Conor CHH (1993) 'Musgrave Province', in Drexel, JF & Preiss, WV (eds), The Geology of South Australia, Vol. 1, The Precambrian, Bulletin 54, Geological Survey, Adelaide, pp.156–167.

Mook WG (1980) Carbon-14 in hydrogeological studies, in *Handbook of Environmental Isotope Geochemistry. Vol. 1.* eds. Fritz P and Fontes J.Ch., Elsevier, pp 449-474.

Munday TJ (2008) Regolith Geophysics. In *Regolith Science*. (Eds. Scott K and Pain C). Berlin, Springer.

Munday TJ (2013) The role of airborne geophysics in facilitating long-term outback water solutions to support mining in South Australia: 23rd Geophysical Conference, ASEG, Extended Abstracts, http://dx.doi.org/10.1071/ASEG2013ab189.

Munday TJ, Macnae J, Bishop J and Sattel, D, (2001) A Geological Interpretation of Observed Electrical Structures in the Regolith: Lawlers, Western Australia, Exploration Geophysics, 32:1, 36-47, DOI: 10.1071/EG01036

Munday TJ, Abdat T, Ley Y and Gilfedder M (2013) Facilitating long-term outback water solutions (G-FLOWS-1): Hydrogeological framework. Adelaide: Goyder Institute for Water Research.

Munday TJ, Cahill K, Sorensen C, Davis A, and Ibrahimi, T (2016) Uncovering the Musgraves – a different perspective on an old landscape, GSSA Discovery Day, Adelaide, December 2016.

Munday TJ, Sørensen C and Gulbrandsen ML (2018) Peeling back the cover on an ancient landscape – AEM in the Musgrave Province, South Australia; Extended Abstract, The 7th International Workshop on Airborne Electromagnetics. June 17-20, Kolding, Denmark.

Parkhurst DL and Appelo C (2013) Description of input and examples for PHREEQC version 3: a computer program for speciation, batch-reaction, one-dimensional transport, and inverse geochemical calculations. US Geological Survey.

Parsekian A, Grombacher D, Davis A, Flinchum B, Munday TJ and Cahill K (2014) Near-surface geophysics for informed water-management decisions in the Anangu Pitjantjatjara Yankunytjatjara (APY) lands of South Australia. The Leading Edge. 2014; 33(12):1342-1347. https://doi.org/10.1190/tle33121342.1

Pawley MJ and Krapf CBE (2016) Investigating the potential for bedrock aquifers in the APY Lands. Report Book 2016/00021. Department of State Development, South Australia, Adelaide.

Pawley MJ, Dutch RA, Werner M, and Krapf CBE (2014) Repeated failure: long-lived faults in the eastern Musgrave Province. *MESA Journal* 75(4): 45–55.

Rankin LR and Newton CA (2002) Musgrave Block, Central Australia: Regional geology from interpretation of airborne magnetic data. Report Book 2002/031 Primary Industries & Resources SA.

Rogers PA (1995) Hamilton Basin. In JF Drexel and WV Preiss eds, The geology of South Australia, Volume 2, The Phanerozoic, Bulletin 54. Geological Survey of South Australia, Adelaide, p. 198.

Rutherford J, Munday T, Meyers J and Cooper M (2001) Relationship between regolith materials, petrophysical properties, hydrogeology and mineralisation at the Cawse Ni laterite deposits, Western Australia—Implications for exploring with airborne EM. *Exploration Geophysics* 32: 160–170.

Scanlon BR, Keese KE, Flint AL, Flint LE, Gaye CB, Edmunds WM and Simmers I (2006) Global synthesis of groundwater recharge in semiarid and arid regions. *Hydrological Processes* 20(15): 3335–3370.

Smithies RH, Howard HM, Evins P and Kirkland C (2010) Geochemistry, geochronology and petrogenesis of Mesoproterozoic felsic rocks in the western Musgrave Province of central Australia, and implication for the Mesoproterozoic tectonic evolution of the region, Report 106. Geological Survey of Western Australia, Perth, Western Australia.

Smithies RH, Howard HM, Evins PM, Kirkland CL, Kelsey DE, Hand M, Wingate MTD, Collins AS and Belousova E (2011) High-temperature granite magmatism, crust–mantle interaction and the Mesoproterozoic intracontinental evolution of the Musgrave Province, Central Australia. *Journal of Petrology* 52: 931–958.

Soerensen CC, Munday TJ, Ibrahimi T, Cahill K and Gilfedder M (2018). Musgrave Province, South Australia: Processing and inversion of airborne electromagnetic (AEM) data: preliminary results. Technical Report Series 18/06. Goyder Institute for Water Research, Adelaide.

Tamers MA (1967) Radiocarbon Ages of Groundwater in an Arid Zone Unconfined Aquifer. in *Isotope Techniques in the Hydrologic Cycle*, Volume 11, (Ed. Stout GE)).

Tewkesbury P and Dodds AR (1997) An Appraisal of the Water Resources of the Musgrave Province, South Australia. Department of Mines and Energy Resources, South Australia Report Book No. 97/22, Adelaide.

Varma S (2012) Hydrogeological review of the Musgrave Province, South Australia. Goyder Institute for Water Research Technical Report Series No. 12/8, Goyder Institute for Water Research, Adelaide.

Viezzoli A, Auken E and Munday TJ (2009) Spatially constrained inversion for quasi 3D modelling of airborne electromagnetic data – an application for environmental assessment in the Lower Murray Region of South Australia. *Exploration Geophysics* 40: 173–183.

Vignoli G, Sapia V, Menghini A. and Viezzoli A (2017) Examples of improved inversion of different airborne electromagnetic datasets via sharp regularization. *Journal of Environmental and Engineering Geophysics* 22(1): 51–61.

Vogel JC (1967) Investigation of groundwater flow with radiocarbon: Isotopes in Hydrology, International Atomic Energy Agency, Vienna, pp 355–369.

Wade BP, Barovich KM, Hand M, Scrimgeour IR and Close DF (2006) Evidence for early Mesoproterozoic arc magmatism in the Musgrave Block, central Australia: implications for Proterozoic crustal growth and tectonic reconstructions of Australia. *Journal of Geology* 114(1): 43–63.

Wade BP, Kelsey DE, Hand M and Barovich KM (2008) The Musgrave Province: Stitching north, west and south Australia. *Precambrian Research* 166: 370–386.

Watt EL and Berens V (2011) Non-prescribed groundwater resources assessment – Alinytjara Wilurara Natural Resources Management Region. Phase 1 – Literature and Data Review, DFW Technical Report 2011/18, Government of South Australia, through Department for Water, Adelaide.

Wightman W (1973) Ernabella Resistivity Survey in Department of Mines South Australia Mineral Resources Review No. 138 pp. 51-55.

Wood WW (1999) Use and Misuse of the Chloride-Mass Balance Method in Estimating Ground Water Recharge. *Groundwater* 37(1): 2–3.

Woodhouse AJ and Gum JC (2003) Musgrave Province —geological summary and exploration history, Report Book 2003/00021. Department of Primary Industries and Resources South Australia, Adelaide.

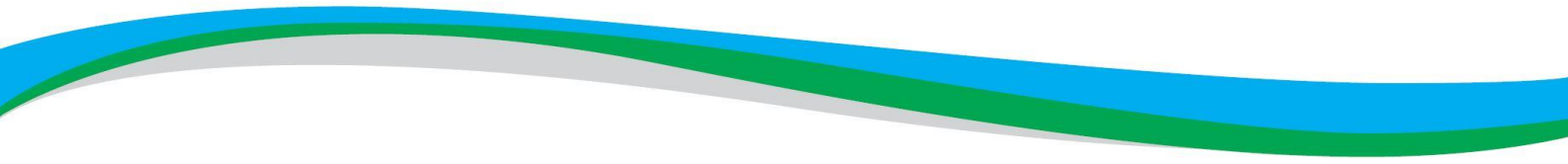

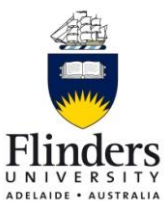

The Goyder Institute for Water Research is a partnership between the South Australian Government through the Department for Environment and Water, CSIRO, Flinders University, the University of Adelaide, and the University of South Australia.